2004-05-03

Development of an Instrumented Dynamic Mannequin Test to Rate the Protection Provided by Protective Clothing

Joel Edwards Sipe
Worcester Polytechnic Institute

Development of an Instrumented Dynamic Mannequin Test to Rate the Thermal Protection Provided by Protective Clothing

A Thesis
Submitted to the Faculty
of the
WORCESTER POLYTECHNIC INSTITUTE
in partial fulfillment of the requirements for the
Degree of Master of Science
in
Fire Protection Engineering
April 2004
By:

Joel Edwards Sipe

Approved:

Dr. Jonathan R. Barnett, Advisor

Bob Hall, Navy, NCTRF, Reader

Professor David A. Lucht, Director:
Center for Firesafety Studies

Abstract

A dynamic mannequin testing facility has been constructed to test the thermal protective properties of Navy uniforms and protective clothing. The existing facility consists of a traversing mannequin mechanism that passes through a fire that has been spatially characterized by temperature and heat flux measurements. The fire is provided by 8 propane sand burners in a modified ISO 9705 room. The current project is a continuation of work done by WPI Students over the last 5 years. A copper disk surface heat flux transducer has been designed and calibrated in the WPI Cone Calorimeter. The mannequin has been instrumented with 40 of these transducers for the acquisition of heat flux data during fire exposures. Heat Flux data was collected with the bare mannequin and through protective clothing for a range of exposure times. A finite difference method approach is used to model the skins temperature response at the epidermis-dermis interface. This temperature is used to predict 1^{st} and 2^{nd} degree skin burns using Henrique's burn damage integral. The percent total body area (%TBA) affected by burns can be calculated by this method. The facility is now capable of providing comparative data on the relative thermal protection provided by different clothing.

Acknowledgements

First and foremost I would like to thank Professor Jonathan Barnett, my advisor. His guidance and endless patience throughout the course of this project have helped me to learn so much. I have never met a teacher that devotes so much time and effort to his profession. His teaching style is far from orthodox, but it has helped me to become a better student and team leader because of it. A big thanks is due to Professor Nicholas Dembsey, whose advice, input, and immense body of knowledge were invaluable to the sensor design and skin burn calculations. Also I would like to thank the representatives from the Navy Clothing and Textile Research Facility. Without the continued support and input from Bob Hall, Harry Winer, and Richard Wojtaszek this project could not have ever been completed. A very special thanks is also in order for the Major Qualifying Project group that assisted in collecting data at the Fire Testing Facility in Holden. Without these 6 seniors the project would have not gotten anywhere. The bulk of the work and time spent on this project was completed by Melissa Barter, David Hartman, Jason Kramarczyk, Jonathan Martin, Marc Moseley, and Aaron Vanney. I am very much indebted to them for all their help. Also I must thank Randy Harris in the WPI Fire Science Lab for his endless help and patience while running tests in the cone calorimeter.

Table of Contents

List of Tables

List of Figures

Nomenclature

c_p	Specific heat (constant pressure)
ΔE	Activation energy
Fo	Fourier number
Gr	Grashof number
H	Heat transfer coefficient
k	Thermal conductivity (W/mC)
P	Pre exponential constant (s^{-1})
q”	Heat flux (kW/m^2)
Q	Heat (joules)
T	Time (seconds)
T	Temperature (Kelvin or deg C)
x	Skin depth or length (meters)
α	Thermal diffusivity (J^2/m^4C^2s)
ε	Emissivity
ρ	Density (kg/m^3)
τ	Duration of heat flux exposure (seconds)
Ω	Burn Damage

Subscripts

∞	Ambient
i	Time step
j	Node #

1. Introduction

In 2001 there were 102 firefighter fatalities that were not associated with the terrorist attacks on the World Trade Center. Of these fatalities, 4 were caused by burn injuries (FEMA, 2002). Between the years 1993 and 1997, 3,255 fire ground injuries were attributed to burns (Woodward, 2003), this number represents 7.5 % of all fire ground injuries. While it is not the leading cause of firefighter injuries and fatalities, it is still a large problem. Burn injuries are one of the worst possible kinds of injuries. Burn injuries are very difficult to treat and take a long time to heal (Torvi, 1997).

Work on the current project was begun in 1996 by the Navy Clothing and Textile Research Facility. The first WPI involvement came from David LeBlanc. LeBlanc analyzed the most likely fire scenarios to occur on Navy ships. He found that jet fires from flammable liquids, pool fires, and cellulosic fires were the most likely to occur. The construction of the present facility was overseen by Terry Fay, and began in 1999 (Fay, 2002). The fire environment was characterized with spatial temperature and heat flux measurements by Andrew Woodward (Woodward, 2003). The current focus is on developing a method to measure the amount of heat transferred through the clothing and formulate a rating system, whereby the comparative protection provided by clothing can be rated. The completed product sought by the Navy is a test method that allows for testing the protection provided by clothing when exposed to accurate simulations of real fires that would be expected on board Navy ships. While the exact fires cannot be reproduced by the current facility, the effects on the mannequin are very comparable. This test apparatus now allows a wide variety of different scenarios to be reproduced.

2. Literature Review

2.1 The Prediction of Skin Burns from Thermal Radiation

2.1.1 The Skin

Skin represents approximately 15% of an average adult's body weight and is the largest organ in the human body (SFPE Guide). The skin serves many purposes, and is a very complex organ. In order to understand the physiology of a skin burn, a basic understanding of the skin is required. The components of the skin can be divided into three primary layers: the epidermis, the dermis, and the hypodermis (SFPE Guide).

- The *epidermis* is approximately 75 - 150 μm (except in the palms and soles where it is 0.4 - 0.6 mm) and is the outermost layer of the skin.
- The *dermis* (also called the corium) is directly below the epidermis and is between 1 to 4 mm thick.
- The *hypodermis* (also called the subcutaneous fatty tissue) consists of fat followed by muscle. The thickness of fat varies from almost none in certain areas to 1.5 - 2.0 cm in others. The thickness of this fat layer is affected by individual and anatomical differences. These differences can be very large and can play a role in determining the degree of injury in a severe burn.

The three regions of the skin are shown in figure 1 (Majchrzak and Janinski, 2001)

Figure 1- The Skin

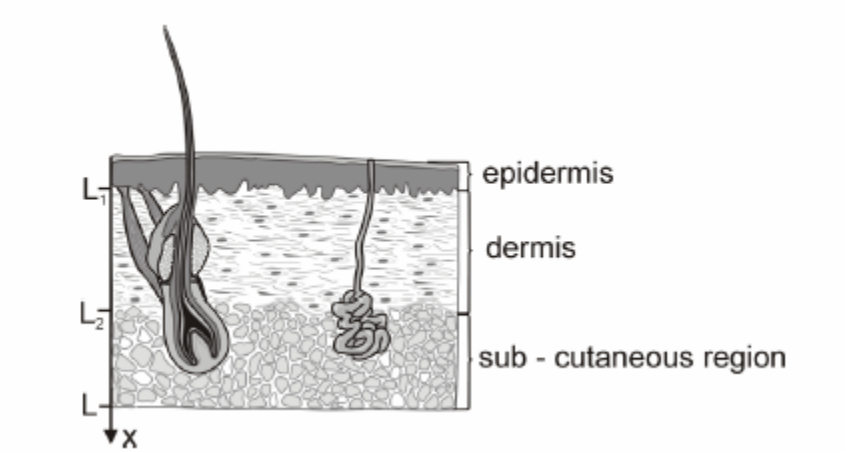

2.1.2. Classifying Burns

The traditional ranking system of burns is based on the depth of damage to the tissue and level of necrosis. Critics of this system point to the lack of correlation between the initial appearance and the depth of injury. The latter is considered the most accurate indication of the severity of a burn (SFPE Guide).

- First-degree burns are superficial burns, and only involve the epidermis. The skin will become red and painful but blistering will not occur. Severe sunburns are the most common form of first-degree burns.
- Second-degree burns occur when the entire epidermis is destroyed. Second-degree burns can be sub-divided into superficial and deep classifications. A superficial second-degree burn involves no damage to the dermis. The skin will be blistered, red, and painful, with a moist look to it. If there is some damage to the dermis, then it is considered a deep second-degree burn. The skin will be blistered with a pale white color under the blisters.

- Third-degree burns involve complete destruction of the dermis, with necrosis possibly extending into the subcutaneous tissue. The skin will not blister, but instead be dry, gray and possibly leathery. There is usually no feeling, and little to no possibility for regeneration.
- "Fourth-degree burns require skin grafts. Fifth and sixth-degree burns involve destruction of muscles and or bones respectively" (SFPE Guide).

2.1.3. The Process of Skin Burns

Once the effects of skin burns are fairly well understood, then the process by which they occur must may be understood and hopefully predicted. Available methods for predicting the onset and severity of skin burns use empirical correlations of experimental data rather than a type of approach derived from first principles. The experimental set-ups used for each study varied, as do the resulting correlations. In general, the experiments involved applying a heat source, usually radiation, to a section of skin. The skin could be human skin on the volar surface of the forearm of test subjects, or for more intense exposures pigs and rats were used. (Takata, 1974)(Stoll and Greene, 1959)(Stoll and Chianta, 1969). In some tests the skin was blackened to absorb almost all of the incident radiation. If the skin is not blackened for the tests, then a lower absorbtivity of the skin must be used when calculating the incident flux (Takata, 1974). The effect of the initial temperature of the skin can be very significant, and a small change of even 1^{o} C can alter the results. Normal human skin is 32.5^{o} C (SFPE Guide).

Damage will begin to occur to the skin when the temperature of the basal layer reaches 44^{o} C. The basal layer is at the base of the epidermis and is approximately 80 μm below the skin surface (Stoll and Chianta, 1971). The rate at which damage to the skin occurs will increase logarithmically with a linear increase in temperature. Stoll and Chianta illustrate this effect with the example that "damage occurs a hundred times faster at 50^{o} C than at 45^{o} C" (Stoll and Chianta, 1971). At a temperature of 72^{o} C the skin is destroyed almost instantaneously (Stoll and Chianta, 1971). Therefore the amount of damage done to the skin is a function of the skin temperature as well as the amount of time that the skin is above 44^{o} C. This means that the burn occurs during the heating and cooling phase of the exposure. At lower intensity exposures 90% of the damage is done during the heating phase, while at higher intensity exposures 65% of the damage can be done during the heating phase (SFPE Guide). This does not seem so strange when considered from a practical viewpoint. The rapid application of ice to an exposed area can prevent a blister by eliminating about one third of the burn damage.

2.1.4. Predicting Pain

Also useful to the study of skin burns is the prediction of the elapsed time until the pain threshold is reached. When pain is felt by an individual in a fire situation it may be too late to remove protective clothing in time to prevent a burn. This is perhaps part of the reason many experienced firefighters refuse to wear protective hoods that cover their ears. Traditionally the ears were used by firefighters as in indicator of dangerously high temperatures. While there are advantages to protecting the face, neck,

and ears, extra caution must also be exercised. The extra protection can also allow a firefighter to enter a room that is dangerously hot, and remain there for too long. By the time pain is felt, it is often too late to avoid a burn in such a situation. Simple empirical correlations have been developed that allow the prediction of the time until pain is felt. Equation 1 relates the radiation incident on the skin to the time to pain (SFPE Guide).

$$t_p = \left(\frac{35000}{\dot{q}''} \right)^{1.33} \qquad \text{(Eq. 1)}$$

It is recommended that equation 1 be used with a factor of safety of 2 or 4. For incident heat fluxes less than or equal to 6000 W/m^2 a factor of 2 is appropriate, whereas for fluxes above 6000 W/m^2 a factor of 4 is more appropriate. At heat fluxes below 1.7 kW/m^2 pain is not felt no matter how long the exposure duration (SFPE Guide).

2.1.5. Predicting Blisters

Blisters begin to form at the base of the basal layer, approximately 80 μm below the skin surface, and can be defined as the separation of the epidermis from the dermis. Equation 2 is a curve fit to experimental data on time to blister.

$$t_b = 300 \left(\frac{\dot{q}''}{1000} \right)^{-1.46} \qquad \text{(Eq. 2)}$$

It is recommended that equation 2 be used with a factor of safety of 1.5. It should be noted that due to the lack of any data on burns caused by a transient heat flux, equations 1 and 2 are only applicable to cases of constant heat flux.

2.1.6. Predicting Skin Temperature

The SFPE Guide to Predicting 1st and 2nd Degree Skin Burns from Thermal Radiation presents four algorithms for predicting the temperature of skin exposed to thermal radiation. Each model uses a square wave input of radiant energy. The first algorithm does not include the cooling phase, and can only be used to predict the onset of pain. This occurs when the basal layer (at a depth of 80 μm) of the skin reaches a temperature of 44°C. The temperature of the skin at a depth x can be predicted with equation 3.

$$T = T_o + \frac{\dot{q}''_r}{k}\left[\frac{2\sqrt{\alpha t}}{\sqrt{\pi}}\exp\left(-\frac{x^2}{4\alpha t}\right) - x\,erfc\left(\frac{x}{2\sqrt{\alpha t}}\right)\right] \qquad \text{(Eq. 3)}$$

When calculating the temperature of the surface of the skin equation 3 reduces to

$$T_s = T_o + \frac{2\dot{q}''_r\sqrt{t}}{\sqrt{\pi k\rho c}} \qquad \text{(Eq. 4)}$$

The remaining three algorithms presented by the Guide all take skin cooling into account. This is important because up to one third of the damage to the skin can be caused after the cessation of the thermal insult (SFPE Guide). The first algorithm is equation 5.

$$T = T_o + \frac{2\dot{q}''_r}{\sqrt{k\rho c}} + \left[\sqrt{\tau}\,ierfc\left(\frac{x}{2\sqrt{\alpha t}}\right) - \sqrt{t-\tau}\,ierfc\left(\frac{x}{2\sqrt{\alpha(t-\tau)}}\right)S(t)\right] \qquad \text{(Eq. 5)}$$

If $(t > \tau)$ then $S(t) = 1$, if $(t < \tau)$ then $S(t) = 0$. By relating the error function to the complimentary error function, and the integral of the complimentary error function using equations 7 and 8, equation 5 can be rearranged to give equation 6.

$$T = T_o + \frac{\dot{q}''_r}{k}\left[\frac{2\sqrt{\alpha t}}{\sqrt{\pi}}\exp\left(-\frac{x^2}{2\alpha t}\right) - x\left(1 - erf\left(\frac{x}{2\sqrt{\alpha t}}\right)\right)\right] -$$
$$\frac{\dot{q}''_r}{k}\left[\frac{2\sqrt{\alpha(t-\tau)}}{\sqrt{\pi}}\exp\left(-\frac{x^2}{2\alpha(t-\tau)}\right) - x\left(1 - erf\left(\frac{x}{2\sqrt{\alpha(t-\tau)}}\right)\right)\right] \quad \text{(Eq. 6)}$$

Error Function Relationships

$$erfc\beta = 1 - erf\beta \quad \text{(Eq. 7)}$$

$$ierfc\beta = \frac{1}{\sqrt{\pi}}e^{-\beta^2} - \beta erfc\beta \quad \text{(Eq. 8)}$$

The third equation using relaxation or cooling of the skin is shown as equation 9.

$$T(t_2) = T_o + \left[T(t_1) - T_o\right]\sqrt{\frac{t_1}{t_1}} + \frac{\left[\dot{q}''_r(t_2) + \dot{q}''_r(t_2)\right](t_2 - t_1)}{2\sqrt{\frac{k\rho c t_2}{\pi}}} \quad \text{(Eq. 9)}$$

Equation 9 can only predict the temperature of the surface of the skin and for that reason it is not recommended that it be used for the prediction of skin burns (SFPE Guide). Skin burns will begin to occur when the basal layer at a depth of 80 μm reaches 44^{o}C (Stoll and Chianta, 1971), so it is important that the temperature at this depth be accurately predicted. These models all assume that the skin is a single layer, opaque, semi-infinite solid, and the effects of it's non homogeneous structure, sweating, and blood profusion are all ignored (SFPE Guide). Also worth mentioning is the temperature dependence of the skins thermal properties. It was found that the thermal conductivity of the skin as well as the thermal diffusivity depended not only on temperature, but also on whether the skin was being heated or cooled (SFPE Guide). The average values shown in table 1 were shown to provide an acceptable fit to the data.

Table 1 Thermal Properties of the Skin (SFPE Guide)

Property	Symbol	Value	Units
Thermal Conductivity (heating)	k_h	0.5878	W/m-K

Thermal Conductivity (cooling)	k_c	0.4518	W/m-K
Volumetric Heat Capacity	ρc	4,186,800	J/m^3-K
Basal Layer Depth	x	0.00008	M
Thermal Diffusivity (heating)	α_h	$1.40 * 10^{-7}$	m^2/s
Thermal Diffusivity (cooling)	α_c	$1.08 * 10^{-7}$	m^2/s

2.1.7. Predicting Skin Burns

The first and currently most widely used model of skin damage was proposed by Henriques and is a single order Arrhenius expression (Henriques, 1947). Equation 10 is the function that he proposed and it shows the rate of epidermal injury can be "modeled as a rate process governed by an activation energy and pre-exponential constant" (Henriques, 1947).

$$\frac{d\Omega}{dt} = P\exp\left(\frac{-\Delta E}{RT}\right) \qquad \text{(Eq. 10)}$$

Equation 10 can be integrated to yield a function that gives the total damage to the skin (SFPE Guide).

$$\Omega = \int_0^t P\exp\left(\frac{-\Delta E}{RT}\right)dt \qquad \text{(Eq. 11)}$$

The severity of the burn is determined by the total damage calculated by equation 11. Henriques gives the injury parameters listed in table 2.

Table 2- Burn Injury Parameters (SFPE Guide)

Injury Parameter Value (Ω)	Level of Injury
0.53	First Degree Burn
1.0	Superficial Second Degree Burn

The calculated total damage to the skin will depend on the activation energy (ΔE), and pre-exponential term (P) used for the burn damage integral. The values given by

Henriques are $6.28*10^8$ j/kmol and $3.1*10^{98}$ 1/sec for the activation energy and the pre-exponential term respectively (Henriques, 1947). Since the original work by Henriques, numerous other studies have been conducted that also use the burn damage integral. These studies have concluded that different values for the input parameters are appropriate. A summary of these parameters is given in the SFPE Guide to Predicting 1st and 2nd Degree Skin Burns.

Table 3- Input Parameters for Burn Damage Integral (SFPE Guide)

Model	Temperature Range ^oC	Activation Energy, ΔE j/kmol	Pre-Exponential, P 1/sec
Weaver and Stoll	$44 \leq T \leq 50$	$7.78*10^8$	$2.185*10^{124}$
	$T>50$	$3.25*10^8$	$1.83*10^{51}$
Fugitt	$44 \leq T \leq 55$	$6.97*10^8$	$3.1*10^{98}$
	$T>55$	$2.96*10^8$	$5.0*10^{45}$
Takata	$44 \leq T \leq 50$	$4.18*10^8$	$4.322*10^{64}$
	$T>50$	$6.69*10^8$	$9.389*10^{104}$
Wu	$44 \leq T \leq 53$	$6.27*10^8$	$3.1*10^{98}$
	$T>53$	$6.27*10^8-5.10*10^5(T-53)$	$3.1*10^{98}$
Henriques	All Temps	$6.27*10^8$	$3.1*10^{98}$
Diller and Klutke	$44 \leq T \leq 52$	$6.04*10^8$	$1.3*10^{95}$
Mehta and Wong	All Temps	$4.68*10^8$	$1.43*10^{72}$
Torvi and Dale	$44 \leq T \leq 50$	$7.82*10^8$	$2.185*10^{124}$
	$T>50$	$3.27*10^8$	$1.83*10^{51}$

The level of deviation between the values given from the different models is indicative of the complexity of the problem, and the difficulty in using a simple model to predict the burn damage. Values for the input parameters vary by many orders of magnitude. The different models give burn times that do not differ by orders of magnitude, but there is significant scatter of the data. Figures 2 and 3 show the scatter in the time to first and superficial second degree burn as predicted by the various burn damage models.

Figure 2- Predicted Time to First Degree Burn

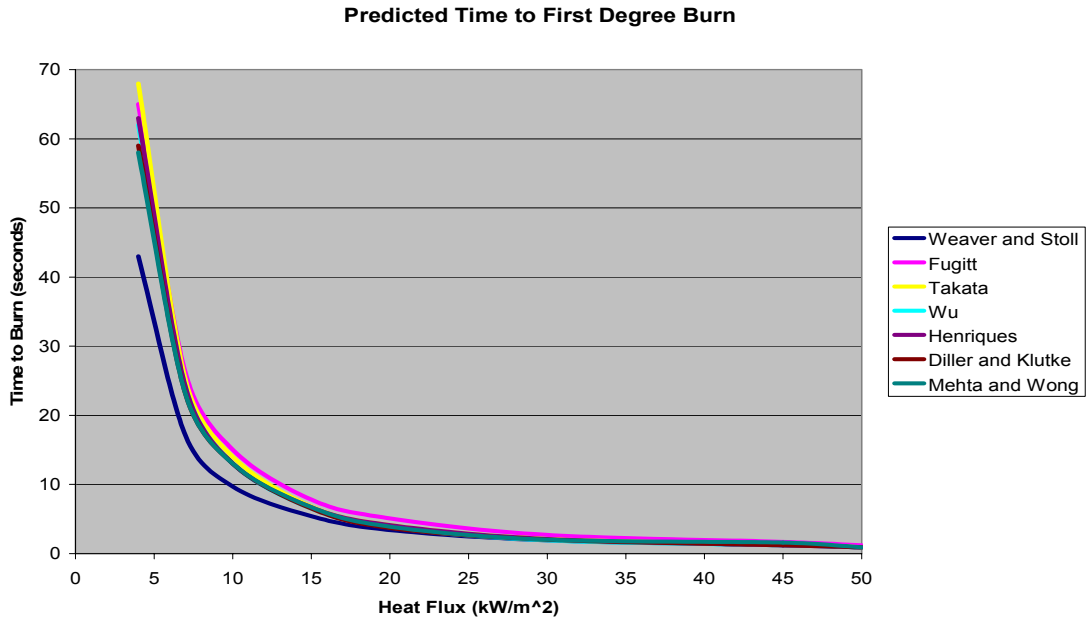

Figure 3- Predicted time to Superficial Second Degree Burn

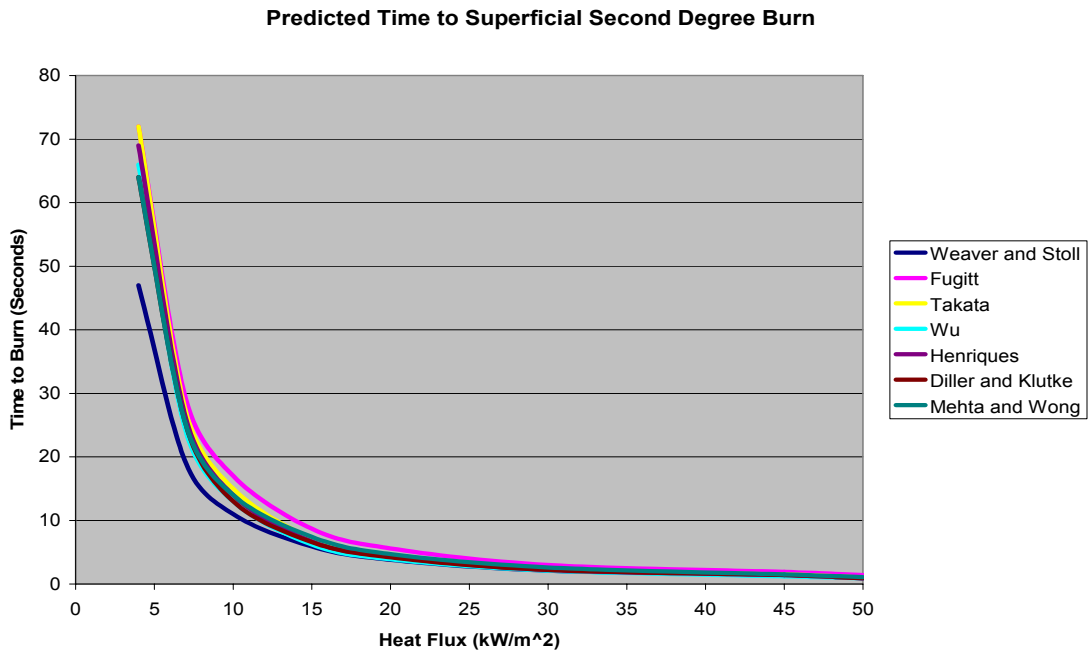

Stoll and Chianta Criterion

Based on experimentally observed times to second degree burn, Stoll and Chianta developed a simplified method of predicting second degree burns (Stoll and Chianta,

1969). By taking a series of heat flux exposures and graphing the equivalent temperature rise of a copper slug calorimeter as defined in ASTM E 457-96, the Stoll and Chianta curve was developed. When a copper slug calorimeter is exposed to a square wave heat flux, if the temperature is graphed with the Stoll and Chianta curve overlaid, the intersection marked point at which a burn would occur. The data from which the curve is created is shown in Table 4.

Table 4- Stoll and Chianta 2nd Degree Burn Criteria.

Time	Heat Flux to Cause 2nd Deg Burn		Total Energy Absorbed		Calorimeter Equivalent Temp Rise	
	cal/cm^2*s	kW/m^2	cal/cm^2	kJ/m^2	Def F	Deg C
1	1.2	50	1.20	50	16.0	8.9
2	0.73	31	1.46	61	19.5	10.8
3	0.55	23	1.65	69	22.0	12.2
4	0.45	19	1.80	75	24.0	13.3
5	0.38	16	1.90	80	25.3	14.1
6	0.34	14	2.04	85	27.2	15.1
7	0.30	13	2.10	88	28.0	15.5
8	0.274	11.5	2.19	92	29.2	16.2
9	0.252	10.6	2.27	95	30.2	16.8
10	0.233	9.8	2.33	98	31.1	17.3
11	0.219	9.2	2.41	101	32.1	17.8
12	0.205	8.6	2.46	103	32.8	18.2
13	0.194	8.1	2.52	106	33.6	18.7
14	0.184	7.7	2.58	108	34.3	19.1
15	0.177	7.4	2.66	111	35.4	19.7
16	0.168	7.0	2.69	113	35.8	19.8
17	0.160	6.7	2.72	114	36.3	20.2
18	0.154	6.4	2.77	116	37.0	20.6
19	0.148	6.2	2.81	118	37.5	20.8
20	0.143	6.0	2.86	120	38.1	21.2
25	0.122	5.1	3.05	128	40.7	22.6
30	0.107	4.5	3.21	134	42.8	23.8

Figure 4- Stoll and Chianta Curve

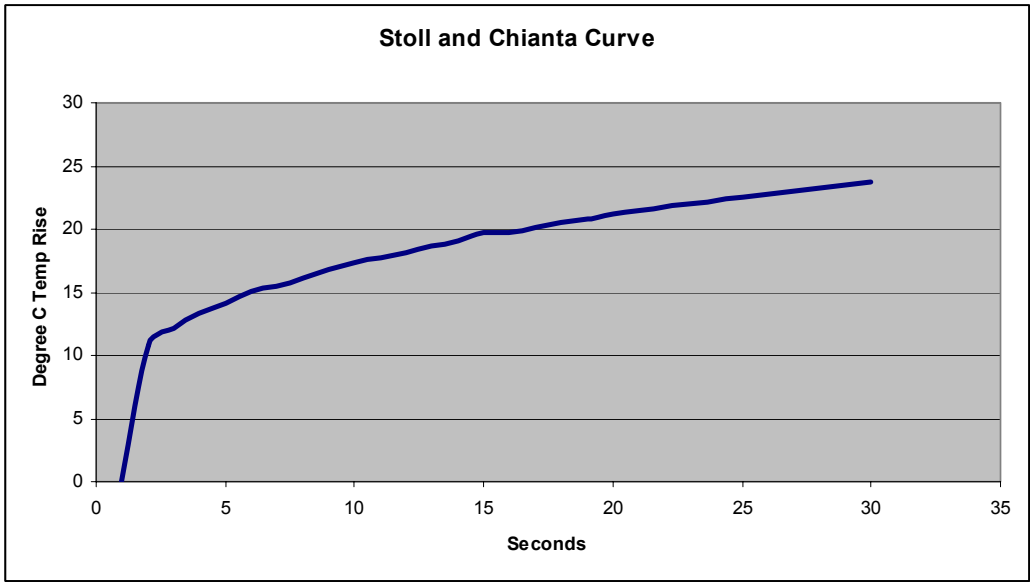

2.2. Current Test Methods

Tests that rate the comparative effectiveness of thermal protective clothing can be grouped into two broad categories: bench scale and full scale. Bench scale testing is carried out on a sample of the material that an ensemble is constructed from. Tests can determine thermal protection characteristics of a material as well as physical characteristics such as durability and strength. Bench scale testing is relatively inexpensive and easy to perform, which makes it desirable for manufacturers. Bench scale testing cannot, however, take things such as stitching, zippers, and hook and loop closures into account. Thus sometimes it is desirable to test entire ensembles, and that is where full-scale instrumented mannequin testing is involved. Not many facilities are equipped to test entire ensembles. It is a very complicated endeavor and can be prohibitively expensive. Three tests for ensembles are the Thermo-Man® test conducted by E. I. du Pont de Nemours and Company, the Pyro Man test conducted at the Textile Protection and Comfort Center (T-PACC) at North Carolina State University, and the Instrumented Mannequin Evaluation of Thermal Protective Clothing performed by the University of Alberta. All three tests are very similar and will be discussed in detail later.

2.2.1. Bench Scale Testing Methods

Three different bench scale tests are reviewed here. They are the ASTM D 4108 test, the NFPA 1971 TPP Test, and the NFPA 1977 RPP test. Each of these standard tests can be conducted at any of a large number of facilities including the Navy Clothing and Textile Research Facility in Natick MA, the sponsor for this current research.

2.2.1.1 ASTM D 4108 Standard Test Method for Thermal Protective Performance of Materials for Clothing by Open Flame Method

Although ASTM D 4108 was removed from publication in 1996 (Gagnon), the method outlined in it is very similar to that used in NFPA 1971 to determine Thermal Protective Performance (TPP) ratings. The test exposes samples of material to a convective heat flux of 84 kW/m^2 (2 cal/cm^2*s) for a short duration. The heat is applied to downward oriented sample from below with a Meker or Fisher burner. The amount of heat transferred through the material is measured with a copper calorimeter, built in accordance with ASTM E 457, mounted on top of the sample. For single layers a 6.4 mm spacer is required to provide an air gap between the sensor and the sample. For multiple layer samples the air gap is not required (ASTM D 4108). The duration of the exposure is controlled by a water cooled shutter. The shutter is water cooled so that it does not allow any heat from the burner to reach the sample until the test begins.

Temperature data from the copper calorimeter is used in conjunction with the curve developed by Stoll and Chianta to predict when a second degree burn would occur. By overlaying the Stoll and Chianta curve on the temperature curve from the copper calorimeter, the intersection can be found. The zero time point of the Stoll and Chianta Curve must be aligned with the start of the exposure (shutter open). The time coordinate of the point at which the two curves intersect is considered the time at which a second degree burn occurs (ASTM D 4108). At first this may seem like a perfectly reasonable criterion when considering that the Stoll and Chianta curve can only be used with a square wave heat flux exposure, just like the one applied to the sample. The not so obvious detail however, is that the heat flux incident on the copper calorimeter is not a

square wave. Figure 5 shows an example of the heat flux reaching a sensor placed behind one layer of clothing. The heat flux reaching the copper disk is roughly rectangular in shape, but does not instantly reach the maximum value and slowly drops off to zero after the exposure is finished. Tests that utilize multiple layers will have an even more attenuated heat flux that is not at all square in shape. This illustrates an inherent uncertainty in this type of criterion for predicting burns. How much effect this has on the results is not certain, but it does however raise questions about the relationship of a predicted burn to an actual burn.

Figure 5- Heat Flux Measured by Skin Simulant Sensor Placed Behind One Layer of Clothing Exposed to 21 kW/m^2 (Gagnon, 2000)

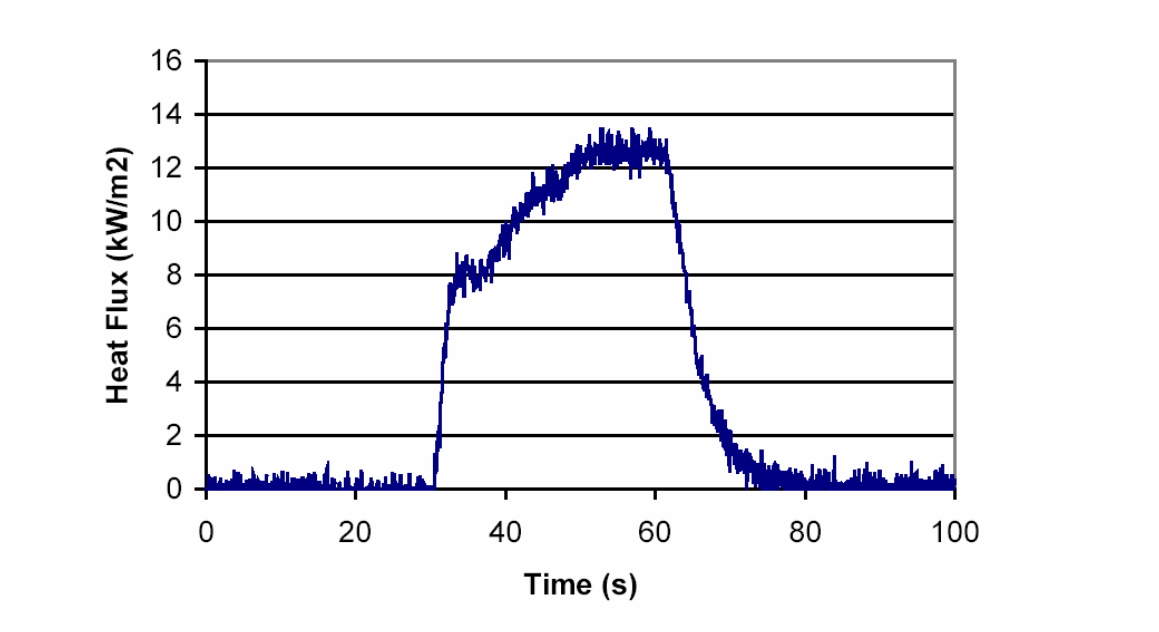

2.2.1.2. NFPA 1971 Protective Ensemble for Structural Firefighting

NFPA 1971 provides design specifications on clothing ensembles worn for structural firefighting. It includes numerous tests to measure the strength of the material as well as the seams, and a TPP test to measure the thermal protection provided. Since NFPA is not a code enforcing agency, protective ensembles are not required to conform to this standard. Protective ensembles that meet the criterion will use compliance with NFPA 1971 as a selling point. It signifies a certain minimum level of durability and thermal protection, and gives some confidence to the consumer. For this literature review the thermal protection requirements are of greater import.

The TPP test used in NFPA 1971 is similar in nature to the ASTM D 4108 test. It uses a combination of a bank of quartz lamps to provide a radiant flux, and a pair of Fisher or Mekker burners to provide a convective heat flux. The total heat flux incident on the sample must be 2.0 cal/cm^2 ±0.1 cal/cm^2 (84 kW/m^2 ±4 kW/m^2) and be checked with a water cooled Gardon type of heat flux transducer. Samples of material measuring 6" by 6" (15.2cm by 15.2 cm) are held on a mounting plate with a 4" by 4" square hole cut out exposing the material. Specimens are oriented horizontally and the heat is applied from below. When a sample of material is tested, the time to second degree burn is determined using the Stoll Criterion. The total Thermal Protective Performance (TPP) rating is determined using equation 12 (NFPA 1971, 2000).

$$TPP = F * T \qquad \text{(Eq. 12)}$$

Where:

F = total heat flux in cal/cm^2

T = time in seconds until the Stoll burn criterion is met

NFPA 1971 requires that ensembles consisting of a moisture barrier, thermal liner, and outer shell have a TPP rating at least 35.0 cal/cm^2 (1450 kJ/m^2) (NFPA 1971, 2000).

Figure 6- Test Procedure Set-Up for TPP testing (NFPA 1971, 2000)

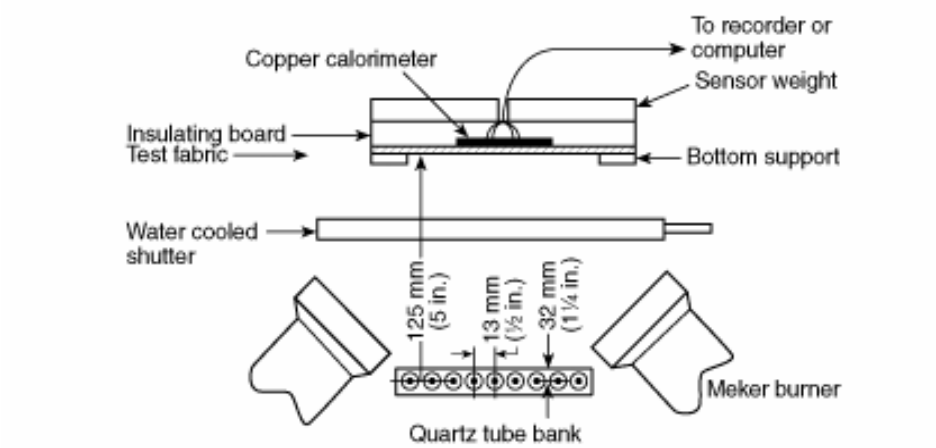

2.2.1.3. NFPA 1977 Standard on Protective Clothing and Equipment for Wildland Fire Fighting

Ensembles and equipment used for fighting wildfires and wildland urban interface fires have different requirements than do their structural firefighting counterparts. NFPA 1977 seeks to address these different needs. Firefighting personnel engaged in fighting outdoor deflagrations typically are moving a great deal and require a lighter ensemble that protects them from radiant exposures. Instead of a TPP test as in NFPA 1971, NFPA 1977 requires a Radiant Protective Performance (RPP) test. In this test a section of material is exposed to a bank of quartz lamps supplying a heat flux of 0.5 cal/cm^2 ±0.1 cal/cm^2 (21 kW/m^2 ±4 kW/m^2). The incident heat flux is determined by exposing the bare copper calorimeter to the radiant panel for 10 seconds. The heat flux can be determined using equation 13 (Gagnon, 2001).

$$q_r = \rho c_p \delta \frac{\Delta T}{\Delta t} \qquad \text{(Eq. 13)}$$

Samples of material used are 3" by 10" (7.6 cm by 25.4 cm), and are held in the vertical orientation by a specimen holder with a 2.5" by 6" (5.7 cm by 14 cm) cutout exposing the material. NFPA 1977 requires that fabrics used for wildland fire fighting have a minimum RPP value of 7.0 cal/cm^2 (290 kJ/m^^{2}) (NFPA 1977, 1998).

Figure 7- Quartz Lamps for NFPA 1977 RPP Test (NFPA 1977, 1998)

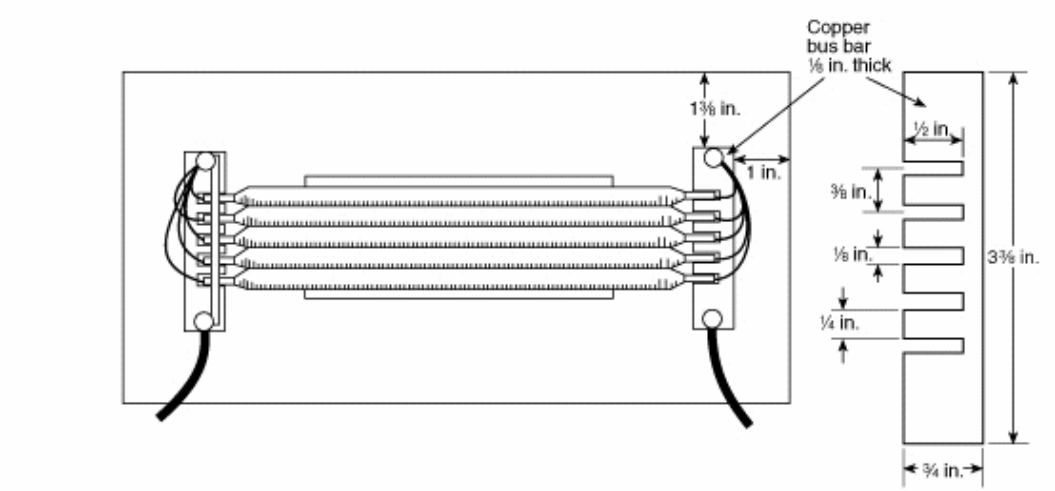

Figure 8- Specimen Holder Assembly for NFPA 1977 RPP Test (NFPA 1977, 1998)

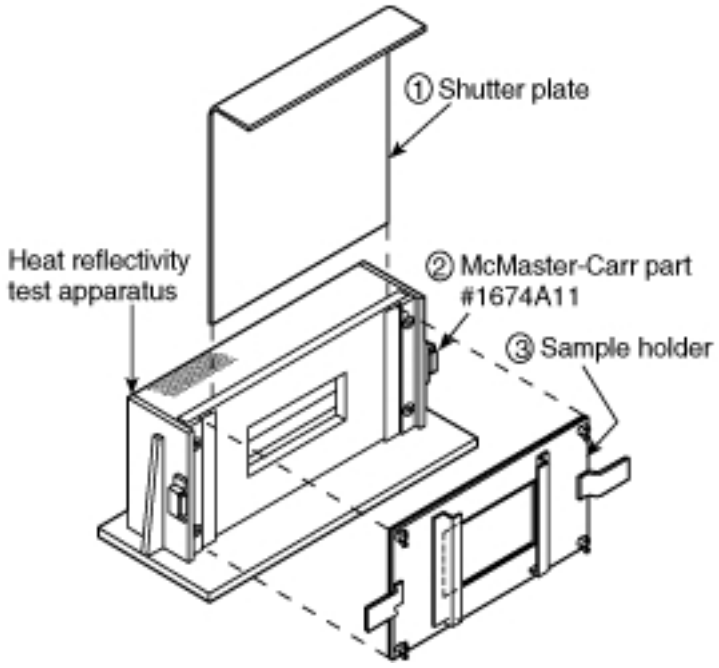

2.2.1.4. Limitations of Bench Scale Tests

Current bench scale test methods only examine small sections of material. Construction elements of the turnout gear such as seams, reflective patches, Velcro, and zippers could have adverse effects on the protection provided, and this is not addressed. The burn criteria presented by Stoll and Chianta is presented for use with square wave heat fluxes only. In their paper (Stoll and Chianta, 1969) they specify that any deviation from a square wave invalidates the burn criterion. Yet this burn criterion is used for both NFPA 1971 and NFPA 1977. Tests were conducted in the Cone Calorimeter at the WPI Center for Firesafety Studies to determine the nature of the heat flux wave that reaches a sensor behind a sample consisting of an outer shell, moisture barrier, and thermal liner. The Cone Calorimeter, shown in figure 9, (ASTM E 1354) is an instrument that heats a 4" by 4" (100 cm by 100 cm) specimen using a conical electrical resistance heater. Once

the material ignites the products of combustion are collected in a hood and the rate of heat release is measured by oxygen consumption calorimetry. The smoke is analyzed for other properties such as optical density and species concentrations (CO and CO_2). The cone heater can be set at a range of different temperatures to give the desired heat flux to the material.

Figure 9- Southwest Research Institute Cone Calorimeter

For this test the heat flux was set at 21 kW/m^2 to simulate an RPP test. The cone heater is slightly different from the quartz lamps used for NFPA 1977. They can both be set to give the same total incident heat flux, but since they operate at different temperatures, the radiation is at different wavelengths. To produce a heat flux of 21 kW/m^2, the cone heater required a temperature of approximately 870 K. To produce the same heat flux, the quartz lamp filaments require a temperature of approximately 1625 K (Gagnon, 2000). A representative graph of the emissive power versus wavelength is shown in figure 10.

Figure 10- Spectral Emissivity of Cone Heater and Quartz Lamps (Gagnon, 2000)

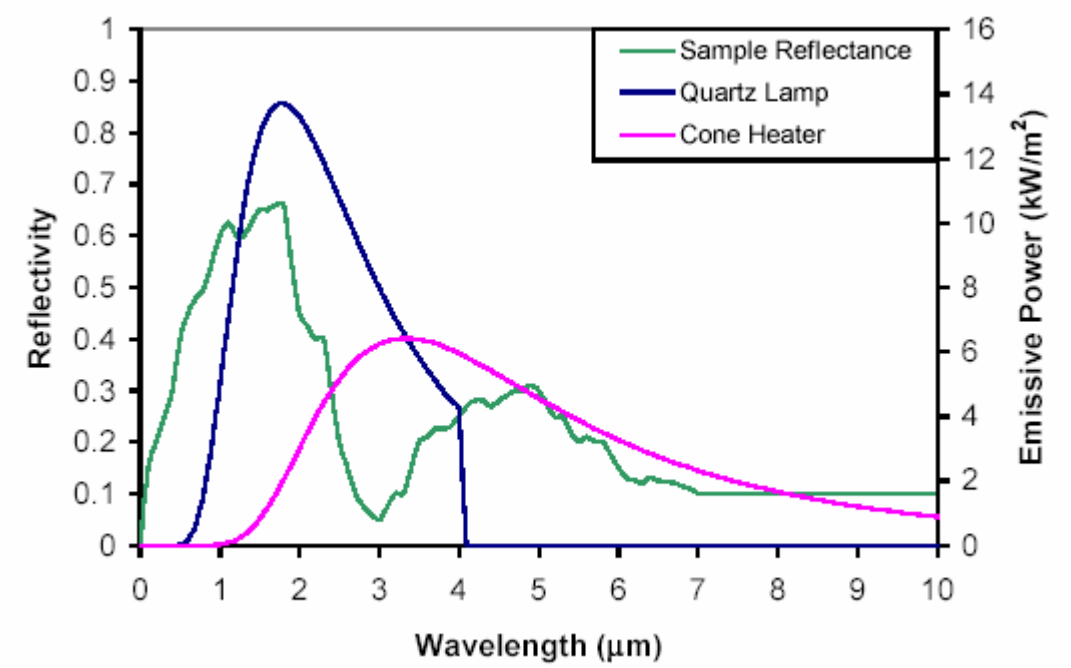

The quartz lamps used in NFPA 1977 produce the most radiant energy near a spectral peak wavelength of 1.8 µm. The cone heater used in the Cone Calorimeter has a spectral peak at 3.5 µm. When compared to the reflectivity of an average material (Quintiere, 1974) used for the shell of firefighter turnout gear, the peak emissive power of the quartz lamps lies at the same wavelength as the peak reflectivity of the material. The peak spectral emissivity of the cone heater lies at the same wavelength (3.5 µm) as the peak absorbtivity, as reported by Quintiere. Temperatures reached in the cone heater (500 - 1100 K) are more representative of temperatures of flames that firefighters would be exposed to. This is not discussed in detail in this thesis, but merely mentioned to illustrate another uncertainty that is inherent in bench scale testing methods.

These shortcomings are not highlighted to expose bench scale tests as irrelevant or outdated. They are pointed out to show some of the complexities associated with the problem of thermal testing of materials. Bench scale tests are very useful and can be used

to comparatively rate the thermal protection offered by protective clothing. It should be kept in mind that these tests do not necessarily have a strong relation to burn times associated with real world fire exposures. They can however provide a useful criterion for comparing different material to each other.

2.2.2. Full Scale Testing Methods

Although much more complex and expensive than bench scale tests, mannequin testing can provide different and sometimes more useful information. There are a handful of organizations and institutions that conduct mannequin thermal testing. In this section three will be discussed: Thermo-Man® conducted by DuPont, PyroMan conducted by North Carolina State University, and the University of Alberta test. Thermo-Leg® is a somewhat full scale instrumented leg test and is also discussed in this section. Full scale testing can give a more accurate assessment of how a protective suit will respond to a fire exposure. Most available mannequin tests try to simulate an "ideal" flash fire exposure of 84 kW/m^2 (2.0 cal/cm^2*s)(Torvi, 1997). This is an estimate of the heat flux that would be experienced if a worker or fire personnel were trapped in an intense flash fire for a short duration (usually less than 5 sec). This value is higher than most firefighters will ever experience, even for short durations. Most everyday firefighting use involves much lower heat fluxes, but several studies have shown that flash fires can actually give a much more severe thermal insult. Several different flash fire exposures and the resulting measured heat fluxes are given in table 5.

Table 5- Heat Fluxes from Flash Fires (Torvi, 1997)

Mine Explosions	**130-330 kW/m^2**
JP-4 Fuel Fires	**167-226 kW/m^2**
Severe Post Flashover Fires	**Up to 180 kW/m^2**
Propane Flash Fire	**160 kW/m^2**

The relevance of these higher heat flux values as well as the practicality of designing a test to simulate such a severe exposure is the topic of much debate. It is mentioned here to point out that the exposures used for existing mannequin tests may not actually be indicative of the scenario that they are simulating (Torvi, 1997). LeBlanc did research for the Navy on possible shipboard fire scenarios. These are the types of design fires that protective clothing worn by Navy personnel will be most likely exposed to (LeBlanc, 1998). LeBlanc determined that the most likely fires to occur on a ship are:

1. Machinery Spaces- Engine spaces, steering gear spaces, generator spaces, auxiliary machine spaces, repair shops, and other machine rooms are most likely candidates for fires. The abundance of flammable liquids in close proximity to ignition sources (sparks, cutting, welding, electrical sources).
2. Supply Areas- Areas such as mess halls, laundry rooms, galleys, and storage areas typically have large amounts of solid fuel sources and limited liquid fuels. Grease fires in these areas are the most common fire occurrence.
3. Habitable Spaces- Crews and officers quarters often contain combustible materials such as mattresses and bedding. Ignition sources are expected to be smoking paraphernalia, arson activities, or faulty wiring.

4. Deck Storage Areas- These areas are difficult to classify due to the dynamic nature of topside activities. The most likely source of fire will be from painting and cleaning activities. The most severe fire source will be from spilled fuel during refueling activities or an aircraft crash.

LeBlanc determined the most severe fire scenarios to be pool and jet fires most likely using flammable liquid such as hydraulic fluid or fuel. Maximum radiative heat fluxes from jet fires were determined to be from 200-8.0 kW/m^2 at distances of 0.5-4.0 m respectively. Radiative heat fluxes from large pool fires were determined to be 80-3.0 kW/m^2 at distances of 5.5-20m.

The impetus for the current research is to design a test that can more accurately replicate these design fires. Little has been done to address the relationship of current full scale tests to real world phenomenon that they are imitating. That being said, there is a lot of useful information that can be gained from full scale mannequin testing that bench scale tests cannot measure. Since the exposure is delivered by means of turbulent diffusion flames provided by gas burners, there is less of a question as to the accuracy of the spectral emissive peak wavelength of the flames. Mannequin tests can also test construction elements of protective suits such as seams, and zippers. Mannequin testing can also tell information about the effects of body geometry. Burn predictions are calculated for each of the sensors to give a map of areas with high burn damage. Each of the three tests uses some form of heat flux transducer to measure the heat transferred through the protective clothing and then convert the heat flux data to skin temperatures. Skin temperatures are then used to calculate skin burns using Henriques burn damage

integral. While many attempts have been made to make mannequin tests indicative of actual real world performance, they are still regarded as for comparative use only. Times to first, second, and possibly third degree burn injury are not generally regarded at absolute times, but rather used as a basis for comparing two protective garments.

2.2.2.1. Thermo-Man®

Thermo-Man® is a test conducted by by E. I. du Pont de Nemours and Company to rate the comparative thermal protection offered by it's protective clothing, namely Nomex® garments. The specifications of the test are described in ASTM F 1930 -00: Standard Test Method for Evaluation of Flame Resistant Clothing for Protection Against Flash Fire Simulations Using an Instrumented Manikin. The mannequin is to be equipped with at least 100 sensors capable of measuring incident heat fluxes of up to 4.0 cal /cm^2 (167 kW/m^2) and have a response time of $\leq$ 0.1 s. The fuel is to be propane and the delivery system must be able to give an exposure of 2.0 cal /cm^2 (84 kW/m^2) for at least 5 seconds (ASTM F 1930-00). Other specifications of the test are given in the standard.

Figure 11- Instrumented Mannequin Set-Up (ASTM F 1930-00)

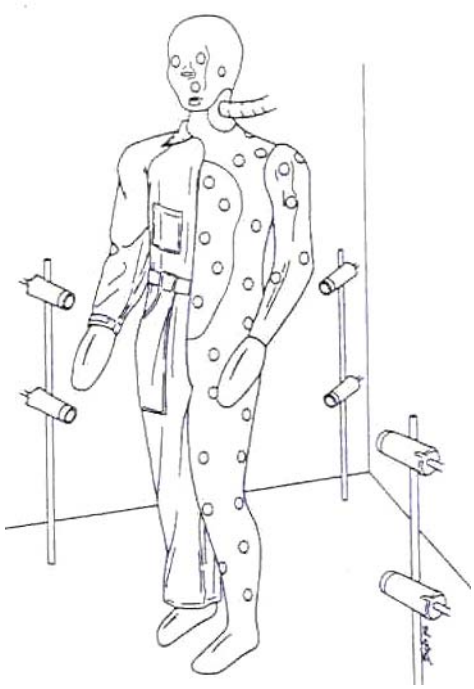

The type of sensors used in the Thermo-Man® are not very well documented, at least in the public domain, and this author was not able to find very much information on their design and construction. What is known is that at one time they were constructed of a thermoset polymer with an imbedded thermocouple just below the surface. The material was designed to have a similar thermal response to that of skin. Incident heat flux was estimated using an inverse method that was prone to error due to a strong sensitivity to the location of the embedded thermocouple (Barker et al, 1999).

Figure 12- Thermo-Man Sensor

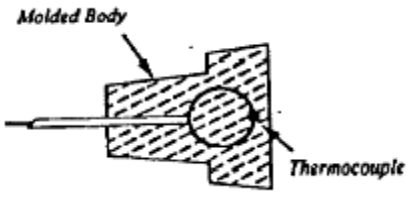

2.2.2.2. Thermo Leg

Similar in nature to the Thermo-Man® test is the Thermo-Leg, conducted by E. I. du Pont de Nemours and Company. The Thermo-Leg test is an instrumented moving leg mechanism that simulates the running motion. Heat is applied to the leg by means of diffusion flames from four large propane torches (Behnke et al, 1992). Average heat fluxes incident on the leg are 2.0 cal /cm^2 (84 kW/m^2). The motion of the leg is designed to simulate the path of the ankle of a running person, with the frequency cycle of the stride. Average running speed of 3-4 m/s is achieved by running the leg at 1.1 cycles per second (Behnke et al, 1992). This gives a running speed of 9.8 feet per second.

Figure 13- Thermo-Let Apparatus

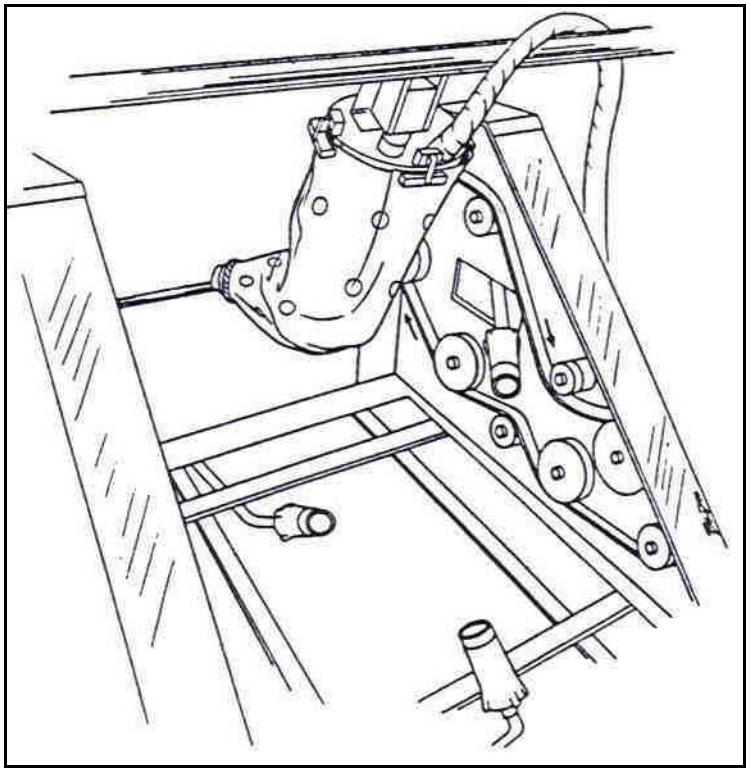

2.2.2.3. Pyro Man

The Center for Research on Textile Protection and Comfort at North Carolina State University conducts an instrumented mannequin test very similar to the Thermo-Man® test. Heat Flux Transducers on the mannequin calculate both the total incident heat flux with and without protective clothing. Heat that is transferred through a garment being tested is measured and used to model the skins response and predict burn damage. Sensors used by the Pyro Man test were formerly embedded thermocouple sensors, but recently a decision was made to switch to copper disk sensors (Barker et al, 1999). Copper sensors designed by Grimes were designed based on an energy balance on a copper disk. The net heat flux was determined to be (Grimes, 1993):

$$\dot{q}'' = \rho c_p dL \frac{dT}{dt} + h\left(T - T_\infty\right) + \dot{q}''_{condlosses} \qquad \text{(Eq. 14)}$$

Figure 14- Copper Slug Sensor Developed by Grimes (Barker et al, 1999)

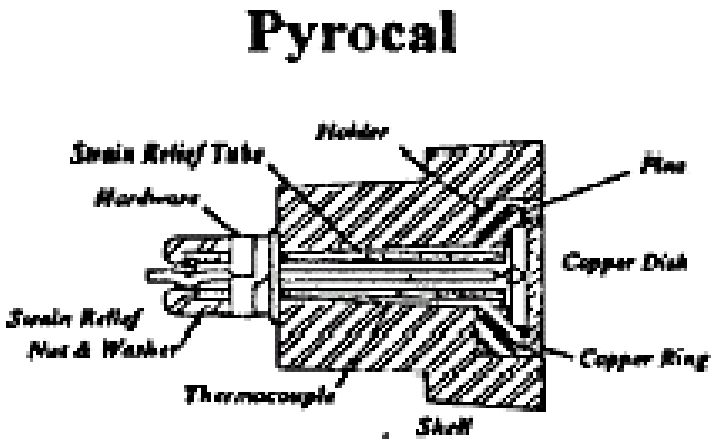

A possible replacement for the copper slug sensor was a water cooled design that operated by measuring the temperature differential of water flowing in and out of the area

under a copper disk. The differential heat balance in equation 15 is used to calculate the total incident flux to the sensor.

$$\frac{dQ}{dt} = \frac{dm_{h20}}{dt} c_p \Delta T \qquad \text{(Eq. 15)}$$

Figure 15- Pyro Man Water Cooled Sensor

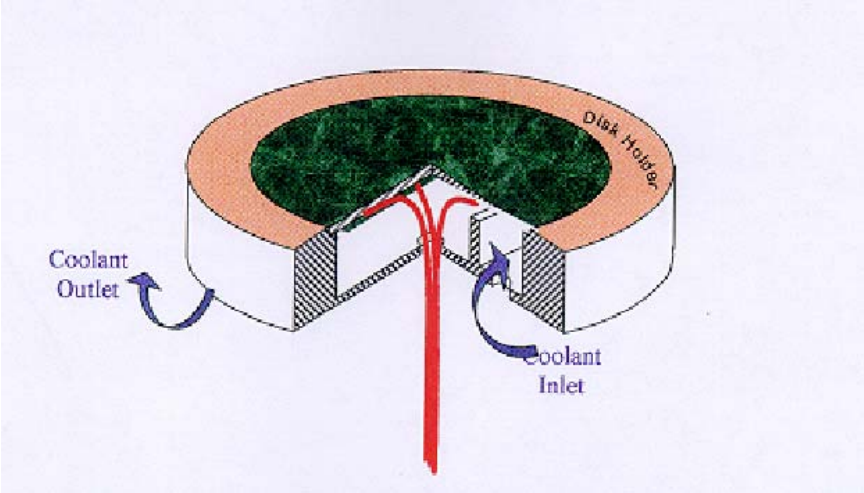

2.2.2.3. University of Alberta Test

The University of Alberta conducts tests with an instrumented size 40 mannequin constructed from fiberglass. Flame exposures typically produce heat fluxes of 67-84 kW/m^2 (1.6-2.0 cal/cm^2*s) for a duration of 3 or 4 seconds. Heat fluxes are recorded by 110 skin simulant sensors. These sensors are made of an inorganic material called "Colorceran" made from calcium, aluminum, silicate, asbestos fibers, and a binder. "Colorceran" is the material that is commonly used to make the top layer of chemistry lab benches. The material does not have similar values for density, thermal conductivity, or specific heat when compared to skin, as can be seen in table 6. The product of the three, the thermal diffusivity, which is more important than any individual value, does however

have a very close value to that of skin. The sensors work by modeling the heat flux into the skin simulant. Temperatures are measured by a flat thermocouple held onto the surface by an epoxy-phenolic adhesive (Dale et al, 1992). The sensors are installed on the mannequin and then the entire mannequin is painted with flat black high temperature paint. Heat fluxes are calculated using a modified form of equation 6. Since the temperature at the "skin" surface and the properties of the simulant are known, the incident heat flux can be calculated. Heat transfer into the skin is modeled based on the skin model of Mehta and Wong (Mehta and Wong, 1973), and burn damage is predicted using Henrique's burn damage integral.

Figure 16- University of Alberta Skin Simulant Sensor

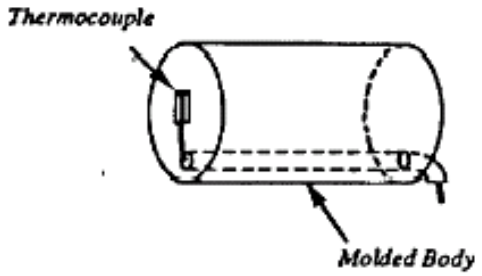

Table 6- Thermal Properties of Skin and Alberta Sensor

Property	Human Skin		Skin Simulant
	Epidermis	Dermis	
k (W/m*K)	0.255	0.523	0.97
ρ (kg/m^3)	1200	1200	1877
c (J/kg*K)	3598	3222	1205
kρc (J^2/m^4*^{o}C^2*s)	1.1*10^6	2.0 *10^6	2.2*10^6
√ kρc (J/m^2*^{o}C*s$^{1/2}$)	1050	1414	1483

2.3. Summary

Many methods exist for predicting the skins response to a thermal insult. Some of them have been outlined in this literature review. Unfortunately all of the methods here rely on constant energy flow so they cannot model transient heat fluxes. This issue will

be addressed in section 3.2.6.. Existing bench scale testing procedures are effective at comparing the relative protection provided by protective clothing materials, but cannot provide detailed information about the final product. Current mannequin testing can provide details about the protection provided by the clothing itself, but cannot replicate different types of fires and may not actually be replicating what it is claiming to. The current test method outlined here seeks to address this issue by replicating expected fires aboard Navy Ships.

3. Dynamic Mannequin Test Apparatus

3.1. Fire Test Facility at Alden Research Labs

A facility has been constructed at Alden Research Labs in Holden MA, to conduct full scale mannequin testing. The project, as it currently exists, is the culmination of a series of theses done by graduate students at WPI. Research into protective garment testing and design fire scenarios was conducted by LeBlanc (LeBlanc, 1998). Contacts at the Navy Clothing and Textile Research Facility (NCTRF) were interested in taking the findings and ideas from LeBlanc's research and developing an instrumented mannequin test. The facility was designed and constructed by Fay (Fay, 2002. The facility contains an apparatus consisting of a modified ISO 9705 standard room. The room is 2.4 m wide by 2.4 m tall by 3.6 m in deep. There are two doors 0.81 m by 2.4 m, one on each of the short walls (the standard room has one door). The remaining wall sections on the short sides of the room are split at a height of 6' and the lower sections are hinged horizontally at the room corners. A traversing chain driven track mechanism is mounted to the ceiling and is capable of moving a mannequin through the room (Bradbury et al, 2001). Recently a variable speed three phase motor was added to the track system (Barter et al, 2004). Fire scenarios are created with flames from eight 30 cm (8") square propane sand burners. The burners can be arranged into four different configurations to simulate different fire scenarios. The temperature and heat flux profiles of the room were mapped by Woodward (Woodward, 2003).

Figure 17- Room with Doors Open

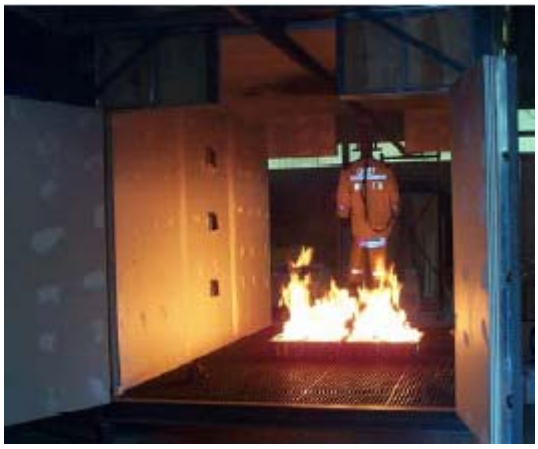

The current work adds an instrumented mannequin to the facility. The Navy provided a mannequin that had previously been used for clothing thermal testing at the NCTRF. The fiberglass body's outer surfaces are coated in a high temperature polymer. The mannequin contains 124 sockets for thermal sensors similar in nature to the Thermo-Man® sensors. A large number of these embedded thermocouple sensors accompanied the mannequin but the sensors were inoperable and suitable replacements were needed.
In addition to the thermal instrumentation of the mannequin, the fire test facility at Alden Research Labs received several other improvements over the course of this work. The traversing mannequin mechanism was outfitted with a 250 V Variable Frequency Drive (VFD) motor. This motor allows different speeds to be dialed in with the newly built controller. The motor controller contains a forward/backward/off switch, and a potentiometer to control the speed of the motor. The effective range of speed available from this motor is shown in figure 18.

Figure 18- Mannequin Speed

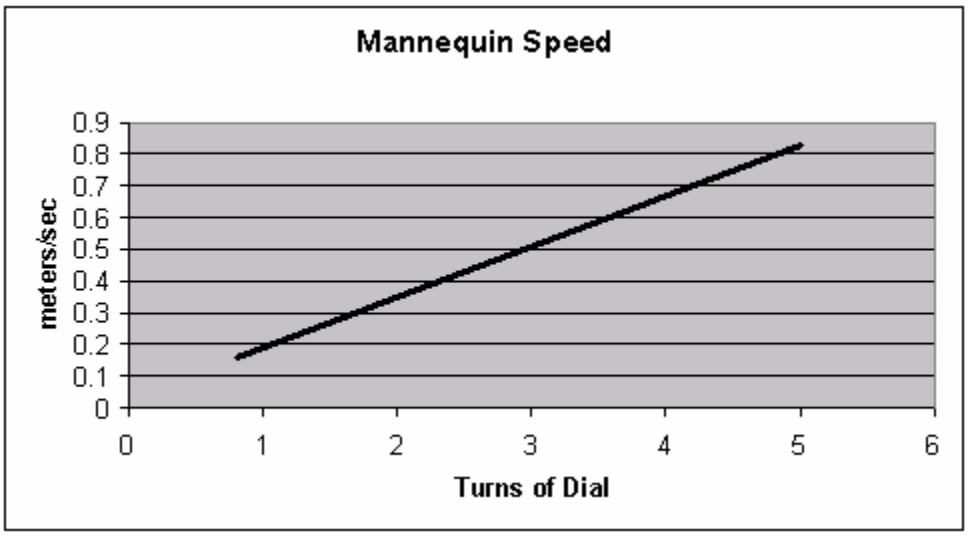

The propane delivery system at the fire test facility was also upgraded to include a mass flow controller to deliver consistent and reproducible fires. The controller selected was a Teledyne Hastings HFC-308 digital mass flow controller. The HFC-308 has a range of 0 – 70 grams/second when flowing propane (the gas for which it is calibrated). This gives an effective fire heat release rate range of 0 – 3.08 MW. However, the pipe friction losses between the flow controller and the burners currently prevents this maximum figure from being attained. Testing has shown that 1.6 MW is the largest fire size that can be supported with the current set up. Slight modifications to the valve system that control the flow of gas to individual burners would increase this value. The HFC-308 mass flow controller is accurate to within 1-3% according to product literature, but it exhibited some fluxuations in the actual mass output displayed. This fluxuation disappeared after about 30 seconds. The HRR data specified in this report is from tests where the fire was allowed to level out and the uncertainty is believed to be less than 3%.

3.2. Mannequin Instrumentation

3.2.1. Sensor Selection

A study was performed to determine the ideal sensor for the mannequin thermal instrumentation. The sensors used for the three mannequin tests described in section 2.2.2., as well as a variety of other sensors, were considered. The ideal sensor would have the following attributes.

1. Inexpensive. The project is operating on a very limited budget.
2. Easy to fabricate, or if purchased they must be readily available.
3. Accurate enough to read total incident heat fluxes within ± 10%.
4. Rugged enough to withstand repeated fire exposures and cleanings.
5. Representative of human skin
6. Have a range of operation of 0 – 100 kW/m^2.

The last requirement is somewhat unlikely if the other criteria are to be met. In order to measure the heat flux through protective clothing it is not necessary to measure 100 kW/m^2. A max range of about 0 - 20 kW/m^2 would be sufficient for most applications. Under ideal circumstances however it would be desired to run the mannequin through the fire to determine the heat flux incident on its bare skin from the flames. This would give a baseline for comparison to other mannequin tests that aim for an average value of 84 kW/m^2 (2 cal/cm^2s). Criteria number five is important, although perhaps not possible to attain on the projects limited budget. Ideally the mannequin would be instrumented with sensors that accept heat at a similar rate to skin. Since the

Navy is interested in developing a comparative test, this is not considered as important when compared to the first four criteria. These first four performance criteria were determined to be the most important in sensor selection. The most likely possible choices, considering the performance criteria are:

1. Surface mounted thermocouple sensors
2. Buried thermocouple sensors (current Navy mannequin sensors)
3. Copper slug sensors
4. Schmidt-Boelter thermopile type transducers
5. Thin foil or Gardon transducers

Attempts were made to construct surface mounted thermocouple sensors using the sensor bodies from the Thermo-Man® sensors. These were unreliable and the exact thermal properties of the thermoset polymer were not known. Also many difficulties were encountered when attempting to glue the thermocouples to the sensor. Therefore this design was abandoned. The current sensors used for the Navy mannequin employ an embedded thermocouple and were determined by the Navy to be excessively inaccurate (Wojtaszek, 2003). These sensors require a stable approximate solution to the inverse heat transfer problem, and as such, it is highly dependant on the exact location of the thermocouple bead (Grimes, 1993). Since this exact location is an uncertainty, this method is by nature inaccurate. Water cooled gauges such as a Schmidt-Boelter or Gardon type transducer were determined to be the most desirable. Schmidt-Boelter gauges operate by measuring the axial temperature differential between the front face of the sensor and a water-cooled copper or aluminum heat sink with a thermopile. Gardon

type gauges measure the radial temperature differential between a constantan disk and a water-cooled copper heat sink. Typically the measuring faces of these gauges are painted black to absorb all incident radiation. Sometimes they can be left unpainted to measure only the convective heat flux. The significant drawback to both of these types of transducers is the cost associated with purchasing and calibrating them. These types of water cooled transducers are available for between $500 to $1,100 US. This is more than the research budget will allow for all of the sensors combined. Therefore it was decided that the final option, the copper slug sensor would be pursued. Although there are problems inherent in a copper disk sensor, namely that it will not absorb heat in a similar fashion to skin. Skin will increase in temperature faster than the copper disk, and this can lead to calculated heat fluxes that may not accurately represent the heat flux into skin for a similar situation. Due to financial restrictions, skin simulant sensors are not an option for this project. Since the Navy is interested in developing a test that can determine the relative protection provided by a particular set of clothing, the copper disc sensors are considered to be accurate enough.

3.2.2. Sensor Design

The design that was used for the sensors is shown in figure 19 along with the energy balance for a radiant exposure. The sensor is basically a copper disk about the size of a penny mounted in the thermoset polymer sensor body from the existing Navy mannequin sensors. The front faces of the sensors were machined on a lathe to add a cylindrical hole to fit the disk. The disk is 1/16” (1.6 mm) thick and ¾” (19 mm) in

diameter. The disks are machined from Copper 110 alloy (ρ=8910 kg/m^3, c_p=0.385 kJ/kg). There is a ¼" air gap behind the sensor insulating the back face.

Figure 19- New Copper Slug Sensor Design

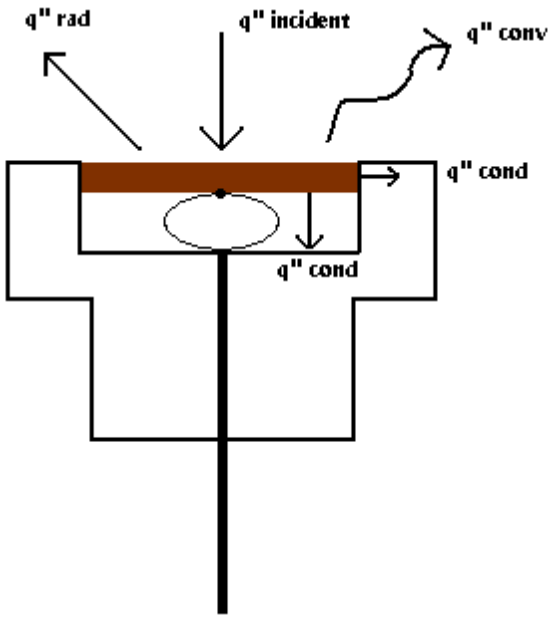

Disk temperature is measured by a 30 gauge type T thermocouple. The thermocouple bead is glued to the back of the mannequin and the glue has been shown to be durable to temperatures up to 100 deg C. Alternative methods of attaching the bead could include intrinsically welding it to the back face, or possibly soldering. Attempts were made to weld the wires to the disk, but the extremely thin diameter of the wire (0.254 mm)(Omega, 2000) prevented a good weld from being made. Solder was judged to add too much mass to the disk and would therefore add thermal inertia and cause the disk to act as if it had a greater thickness.

3.2.3. Sensor Operation

The operation of the sensors is outlined in the following energy balance. If a control volume is placed surrounding the disk. Then conservation of energy tells us that:

$$\varepsilon \dot{q}''_{incident} - \dot{q}''_{conv} - \dot{q}''_{rad} - \dot{q}''_{cond} - \dot{q}''_{storage} = 0 \qquad \text{(Eq. 16)}$$

$$\dot{q}''_{storage} = \rho c_p dL \frac{dT}{dt} \qquad \text{(Eq. 17)}$$

Eq. 16 can be re-arranged to solve for the incident heat flux:

$$\dot{q}''_{incident} = \frac{1}{\varepsilon}\left[\rho c_p dL \frac{dT}{dt} + \dot{q}''_{conv} + \dot{q}''_{rad} + \dot{q}''_{cond}\right] \qquad \text{(Eq. 18)}$$

The convective and radiative losses can be defined as a Newtonian cooling term and a function of temperature to the fourth power respectively:

$$\dot{q}''_{conv} = h(T(t) - T_\infty) \qquad \text{(Eq. 19)}$$

$$\dot{q}''_{rad} = \varepsilon\sigma\left(T(t)^4 - T_\infty{}^4\right) \qquad \text{(Eq. 20)}$$

The conductive losses can actually be broken into two distinct components, as shown in figure 13. There will be a radial and an axial conductive loss. Assuming that there is no contact resistance, these will be governed by equation 20.

$$\dot{q}''_{cond} = kL_{gap}\left(T(t) - T_{air}\right) \qquad \text{(Eq. 21)}$$

This assumes that there is no free convection occurring in the air gap. To justify this assumption a Grashof number can be calculated. Grimes gives a minimum Grashof number of 8000 as the threshold for free convection for vertically inclined surfaces, and a value of 2000 for horizontal surfaces (Grimes, 1993). If a Grashof number is defined as:

$$Gr = \frac{\rho^2 g \beta \Delta T x^3}{\mu^2} \qquad \text{(Eq. 22)}$$

where:

ρ = ambient air density (kg/m^3)

g = acceleration of gravity (m/s^2)

$\beta = T^{-1}$ (K^{-1})

$\Delta T = T_{disk} - T_{\infty}$

x = air gap thickness (m)

μ = viscosity of air

and the following properties are used for the air gap:

$\rho = 0.88$ kg/m^3

$g = 9.8$ m/s^2

$\beta = 1/273$ K^{-1}

$\Delta T = 127$ K

$x = 0.00635$ m

$\mu = 2.286*10^{-6}$

then the Grashof number can be calculated to be 1740. This is below the values of 8000 and 2000 at which free convection will begin on a vertical or a horizontal surface respectively. This indicates that the assumption of conduction into that air is a justified one. Air has a thermal conductivity of $k = 0.0033 W/m*K$ at a temperature of 400 K, higher than the disk is expected to reach. At this temperature the conductive heat flux into the air gap will be 0.0266 W/m^2. Since this is several orders of magnitude lower than the incident fluxes being measured it will be neglected for this analysis. The radial conduction values will be higher than the axial conduction values, but they are assumed to be negligible as well. The reason that they are not calculated is the changing temperature of the sensor body. There will be a temperature gradient in the thermoset polymer so the radial conduction will vary not only with time, but axial location. This

spatial and temporal dependence is outside the scope of this simple energy balance, and for practical reasons it is ignored. The validity of this assumption is addressed later.

3.2.4. Sensor Calibration

3.2.4.1. Sensor Test Apparatus and Cone Calorimeter Modifications

In order to determine the accuracy of the previously described method of calculating the incident heat flux, a calibration was performed in the WPI Cone Calorimeter. The calibration of heat flux transducers is a very complicated undertaking, and much care is needed. The standard procedure is to calibrate them using a known source of radiant energy. Calibration of a heat flux transducer with a convective source is very difficult to perform, and not often practical. The difficulty is in finding a known convective source that will not change over time as the sensor heats up. This time varying temperature will cause changes in the Nusselt number, thus affecting the heat transfer coefficient. Thus the radiant calibration of these copper slug sensors is assumed to be accurate for either a radiant or convective heat source.

The WPI Cone Calorimeter has the ability to produce an effective range of heat fluxes from 0 – 90 kW/m^2. For this research only tests with heat fluxes of up to 21 kW/m^2 were conducted. A test apparatus was constructed to mount one of the new sensors in the cone calorimeter. The apparatus was constructed from a 5” by 5” square plate of ¼” steel, and four 14” long ½” diameter steel tubes that are used as legs. The apparatus has the appearance of a small four legged table 14” in height. A hole was

machined in the middle of the plate to hold a sensor with three set screws. The apparatus also has the ability to mount a 1” water cooled Schmidt Boelter or Gardon Gauge for testing as well.

Before the sensors were tested in the apparatus, modifications to the cone calorimeter were made. The shutter mechanism that controls the duration of the exposure by moving into place and blocking the radiant heat was determined to be in need of an improvement. The shutter is insulated in the exposed side by a thin (1/4”) sheet of Kaowool mineral fiber cloth. This insulation heats up and at high heat flux exposures can radiate a large amount of heat back to the specimen. This gives a non-zero heat flux when the shutter is closed and was determined to be undesirable. A set of replacement shutters were machined from 1/8” copper to have the same dimensions as the original parts. There were only two modifications made to the new shutters. The new shutters were first equipped with traversing 1/8” copper tubes soldered to the unexposed face for cooling water to flow through. Second, a lip was added to the unexposed edge on the inner edge to provide 3/8” of overlap. This prevented some small amount of radiation from penetrating the gap between the shutters when a perfect seal was not made. The new shutters were used for the calibration of the new copper slug sensors, and after several tests they appear to be very effective. At heat fluxes of 5, 10, and 21 kW/m^2, virtually no radiation was measured with the Schmidt-Boelter gauge with the shutter closed. It should be noted here that the heat fluxes are measured at the level that the gauge was to be placed and does not represent the incident heat flux to the shutters themselves.

3.2.4.2. Calibration Results

The calibration procedure went as follows. One of the sensors was placed in the calibration apparatus and exposed to a square wave heat flux using the WPI Cone Calorimeter (ASTM E1354, 1999). The temperature response of the sensor was used to calculate the incident heat flux and this was then compared to the actual heat flux. The heat flux level was determined using a ½" calibrated Schmidt Boelter Transducer. The transducer was used to set the temperature of the cone heater, in order to provide the desired heat flux to the surface of the transducer. Although the uncertainty of the transducer is low, the temperature of the cone heater is not completely constant. To test for transient effects the Schmidt Boelter gauge was exposed for approximately 90 seconds. Over the course of the exposure the heat flux dropped and then rose again. This is most likely due to the cone heater compensating for a drop in temperature. The results of the test are shown in figure 14 and 15. The percent residual heat flux is calculated by taking the difference of the set value and the measured value and dividing it by the set value, 10 kW/m^2 in this case.

Figure 20- Heat Flux Measured by SB Gauge

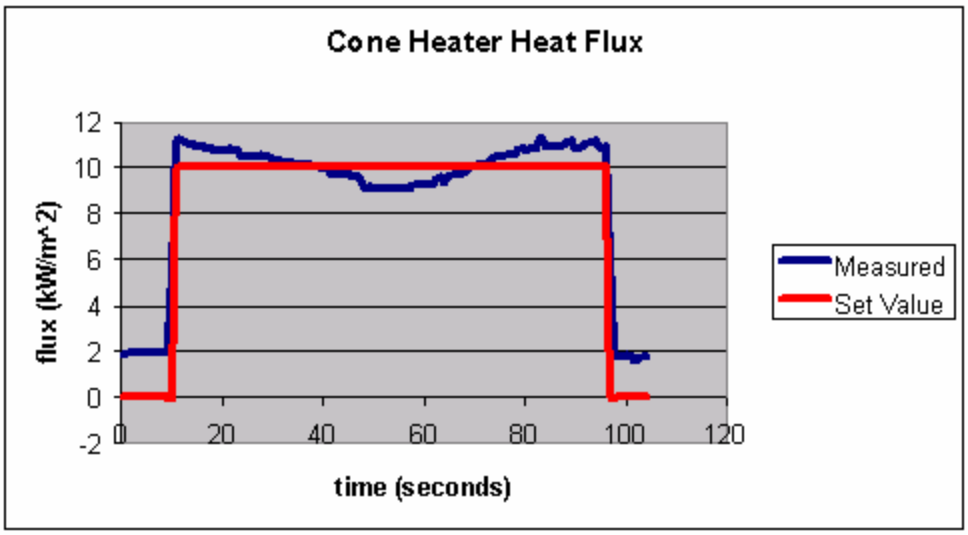

Figure 21- % Residual Heat Flux

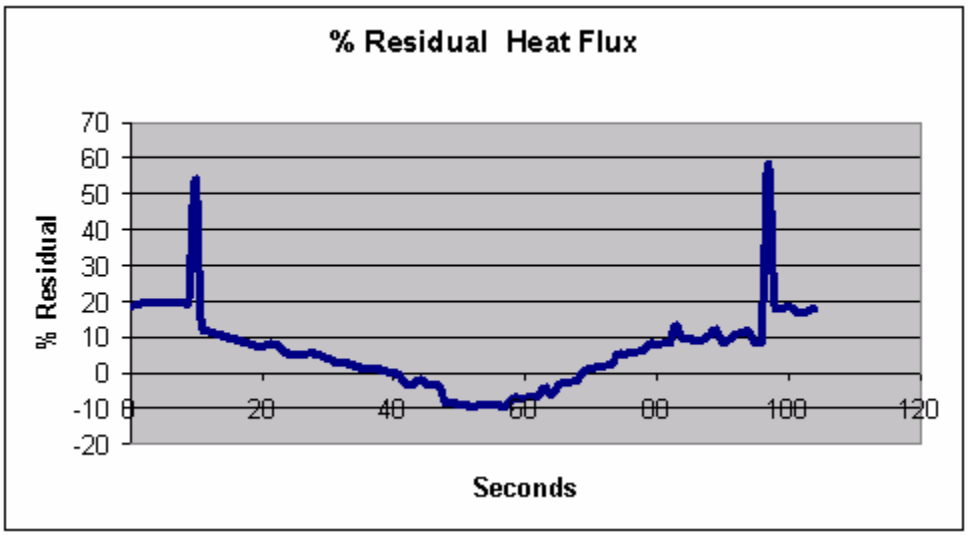

The values of about 20% before and after the exposure are due to radiation from the closed shutters. At the time of this measurement the cone had not been modified to incorporate the water cooled shutters. During the exposure the percent residual is between approximately positive and negative 10 percent. This means that when the cone is used for a radiative heat source the value for incident heat flux has an uncertainty of

about 10 %. The spikes at the beginning and end of the exposure are due to lag time in the shutter/gauge/DAQ system and are considered minor. The shutters are hand operated and do not respond instantaneously. This is most likely the source of the delay in reaching the peak value.

The test apparatus has set screws on the bottom of the legs to set the sensor at the same height as the Schmidt Boelter Gauge. The sensor was exposed to two heat fluxes (5 and 10 kW/m^2) for 30 seconds. The temperature was measured for 30 seconds before and 30 seconds after the exposure. The disk temperatures for the two tests are shown in figures 22 and 23. The water cooled shutters were used for these tests, although for the test at 5 kW/m^2 the shutters were not closed tightly and a small amount of radiation was able to penetrate the seam between the two.

Figure 22- 5 kW/m^2- Sensor Temperature

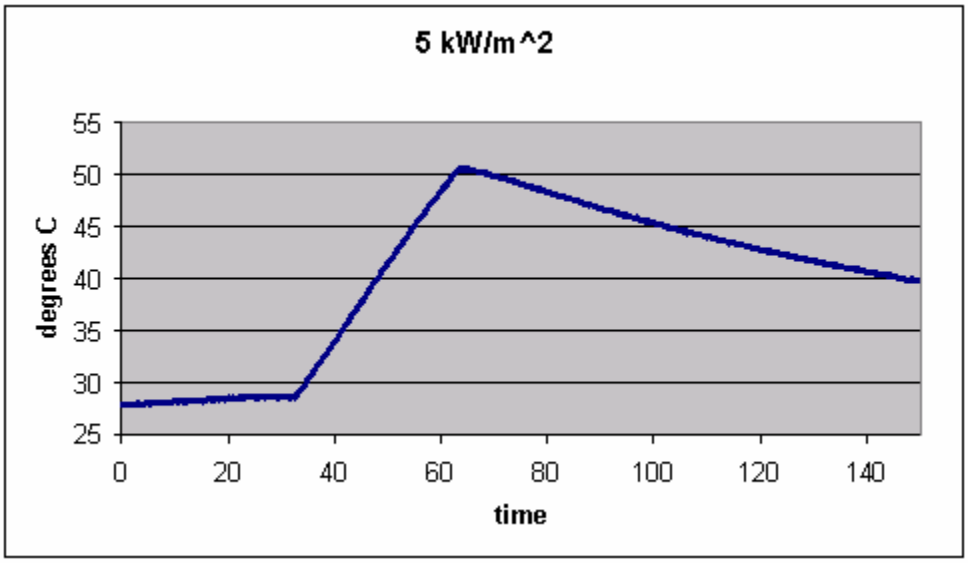

Figure 23- 10 kW/m2- Sensor Temperature

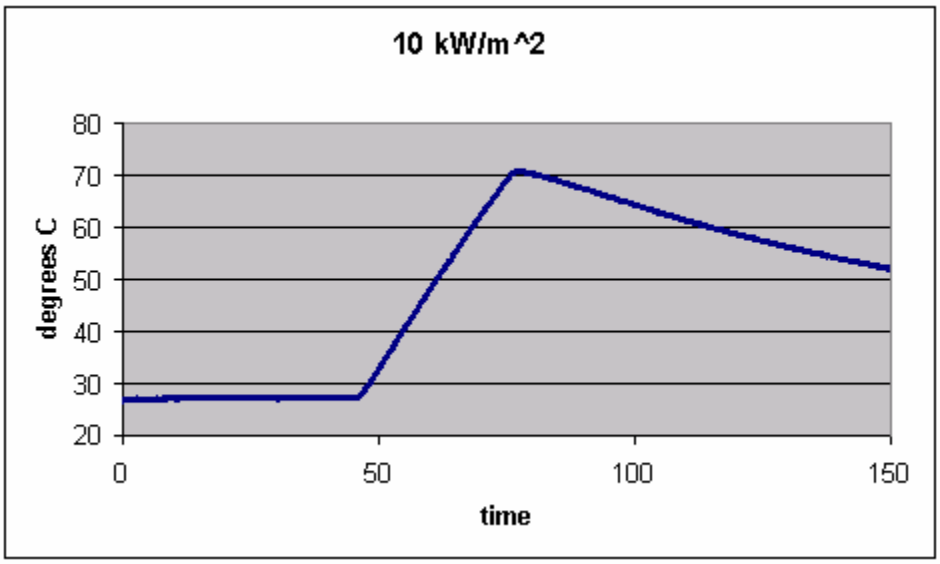

The instantaneous rate of temperature change can be computed numerically by:

$$\frac{dT}{dt} \approx \frac{\delta T}{\delta t} = \frac{T(t_2) - T(t_1)}{t_2 - t_1} \qquad \text{(Eq. 23)}$$

The rates of change of temperature for the two tests are shown in figures 24 and 25.

Figure 24- 5 kW/m^2- dT/dt

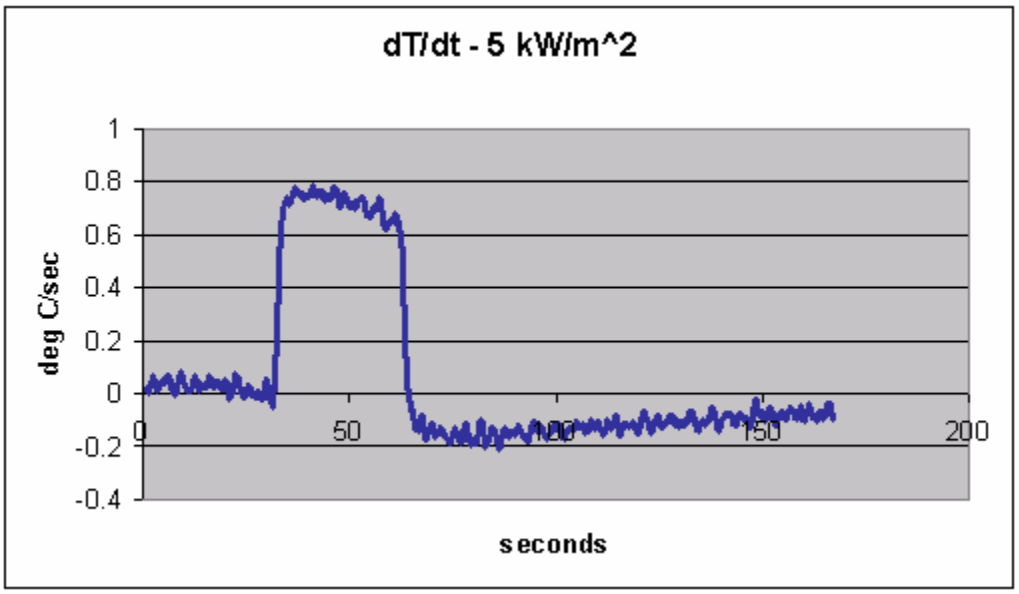

Figure 25- 10 kW/m^2- dT/dt

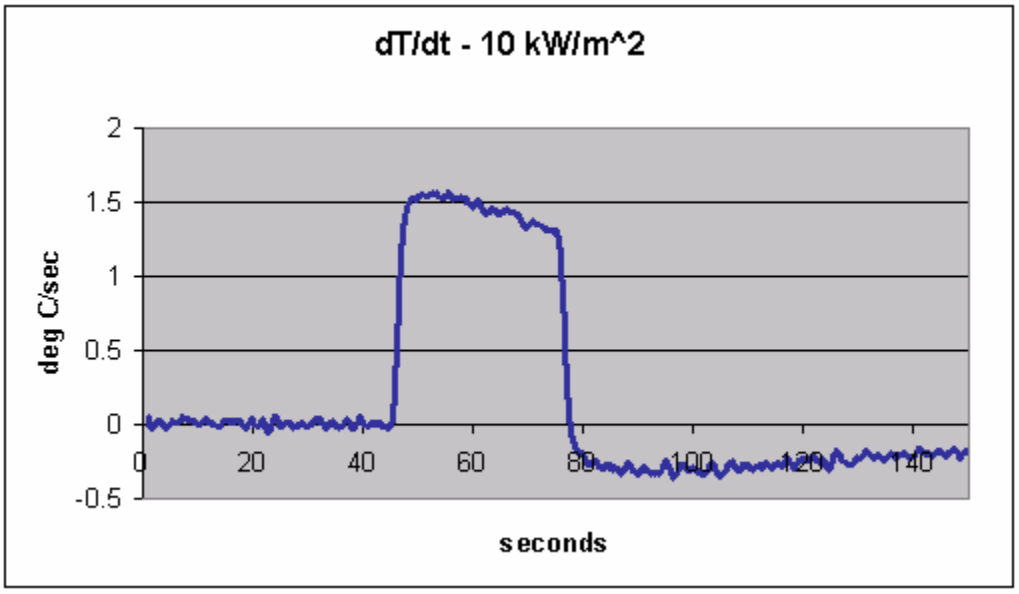

The terms of the energy balance are shown graphically in figures 26 and 27, and the total calculated incident fluxes are shown in figures 28 and 29.

Figure 26- Energy Balance- 5 kW/m^2

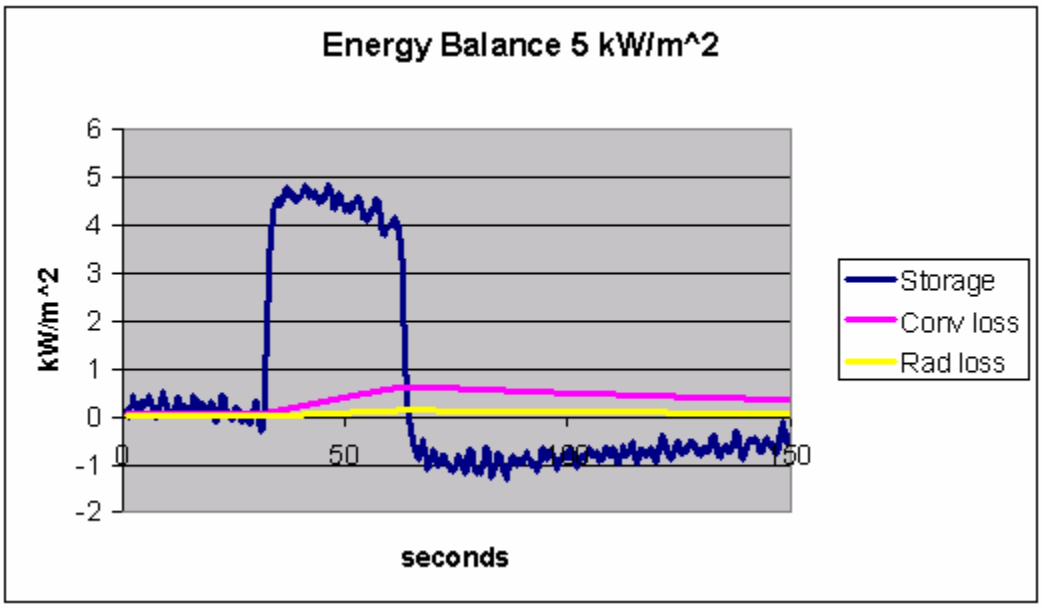

Figure 27- Energy Balance- 10 kW/m^2

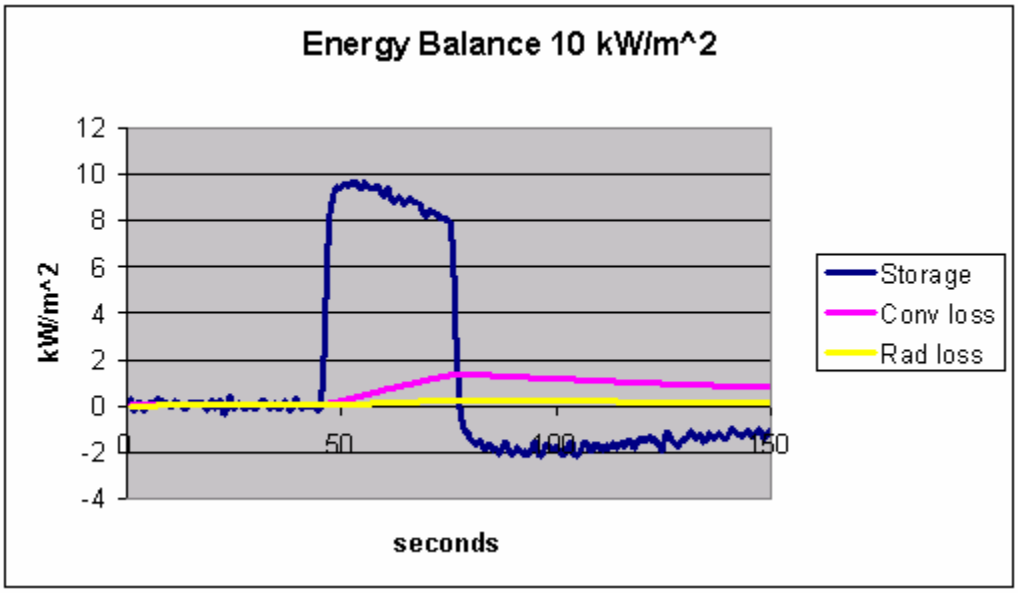

Figure 28- Calculated Incident Flux- 5 kW/m^2

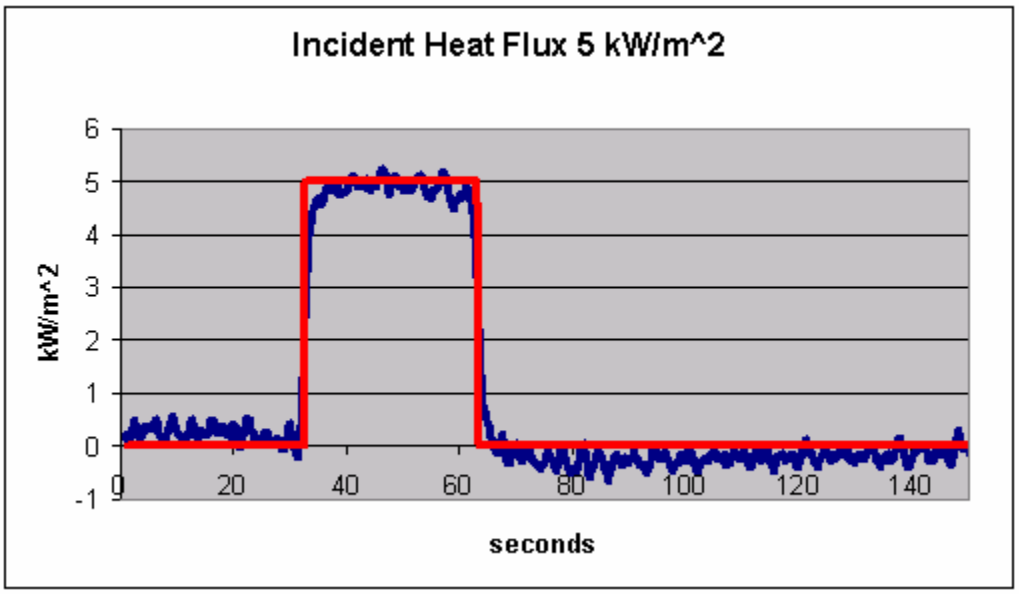

Figure 29- Calculated Incident Flux- 10 kW/m^2

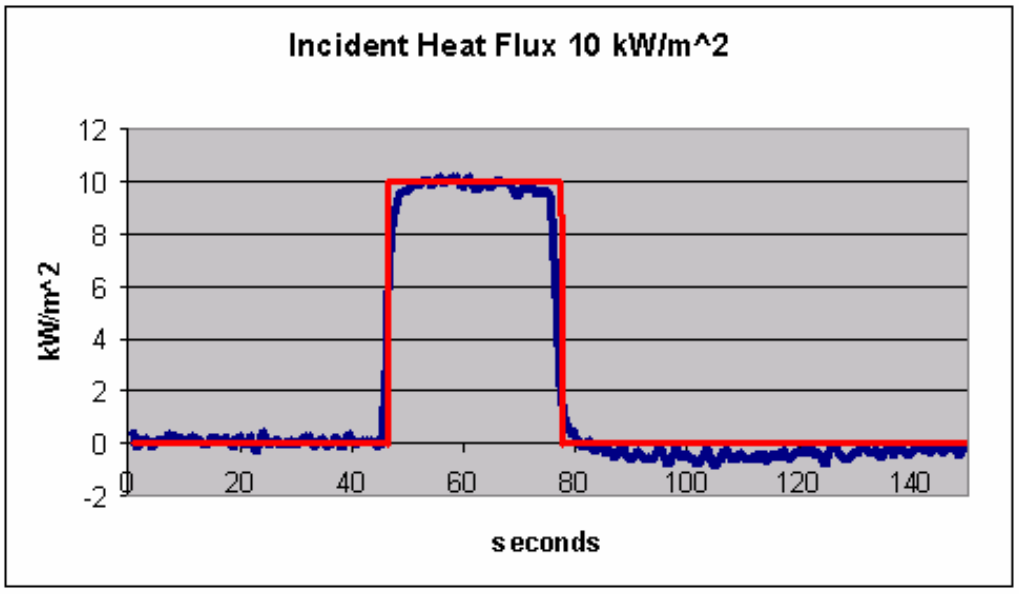

The calculated values appear to show good agreement with the "actual" heat flux as measured by the Schmidt-Boelter gauge. It should be kept in mind that the "actual" heat flux has approximately a 10% uncertainty associated with it. This uncertainty is assumed to be much larger than the uncertainty in the output form the Schmidt-Boelter gauge and as such the gauge uncertainty is ignored. The difference between the cone heat

flux and the value calculated with the copper slug sensor can be graphically illustrated as a residual heat flux. This residual heat flux is shown in figures 30 and 31, and as a percent of the incident heat flux in figures 32 and 33. The values calculated by the copper disk sensor are always within 10% of the exposure heat flux. Since the exposure heat flux has about a 10% uncertainty associated with it, the sensor output falls within that uncertainty band.

Figure 30- Residual Heat Flux- 5kW/m

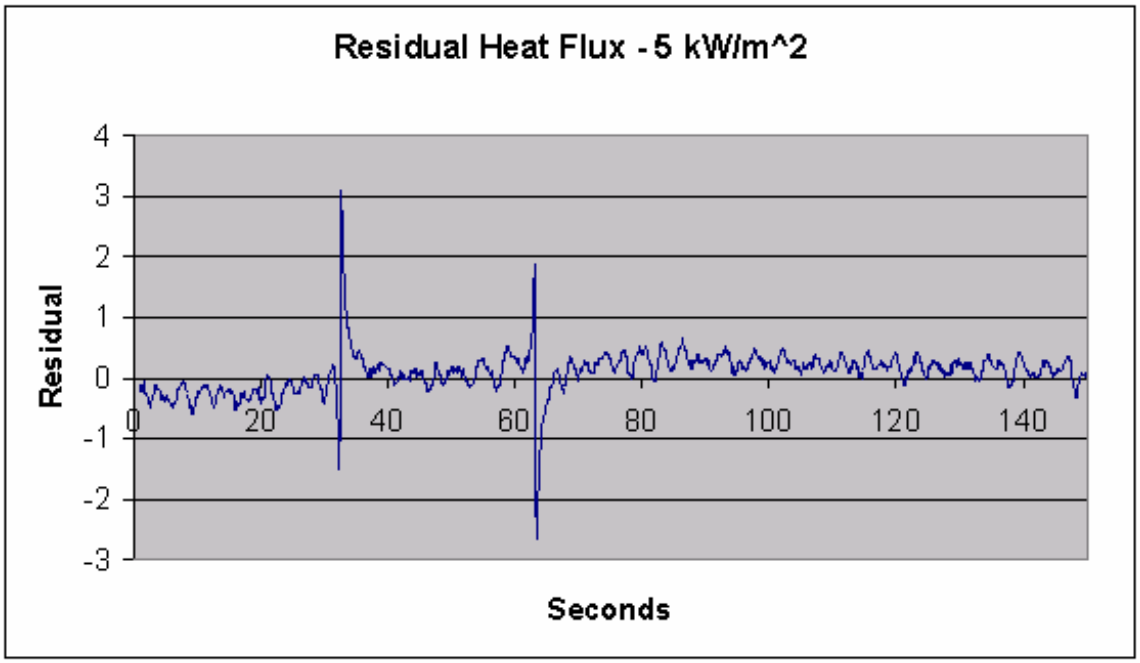

Figure 31- Residual Heat Flux- 10kW/m

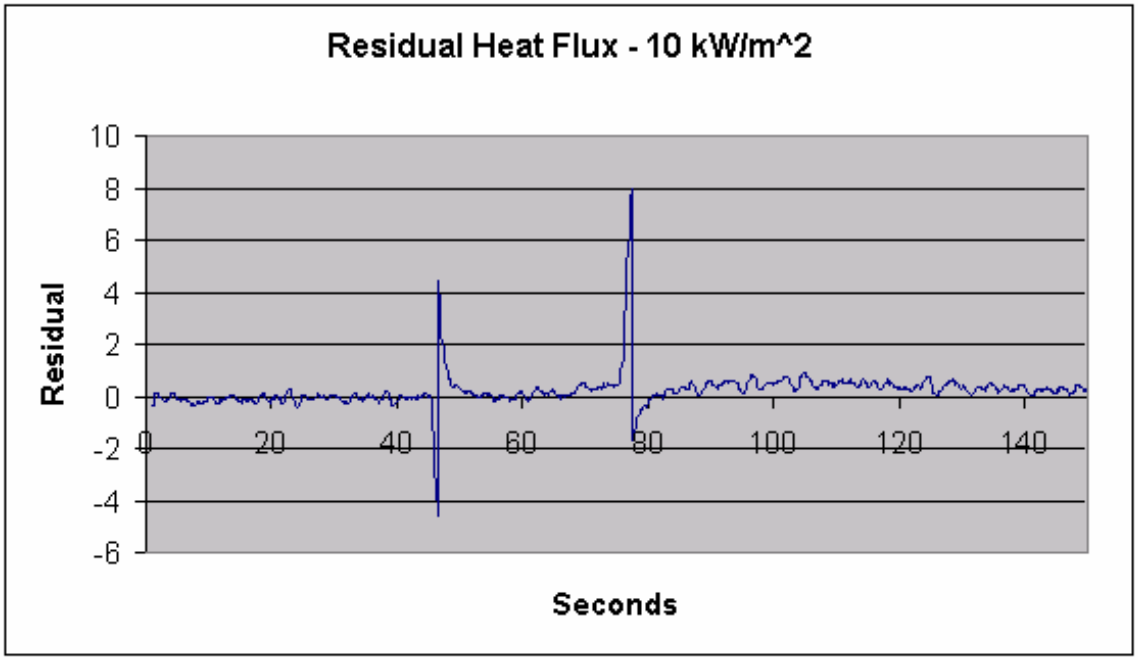

Figure 32- Percent Residual Heat Flux- 5kW/m

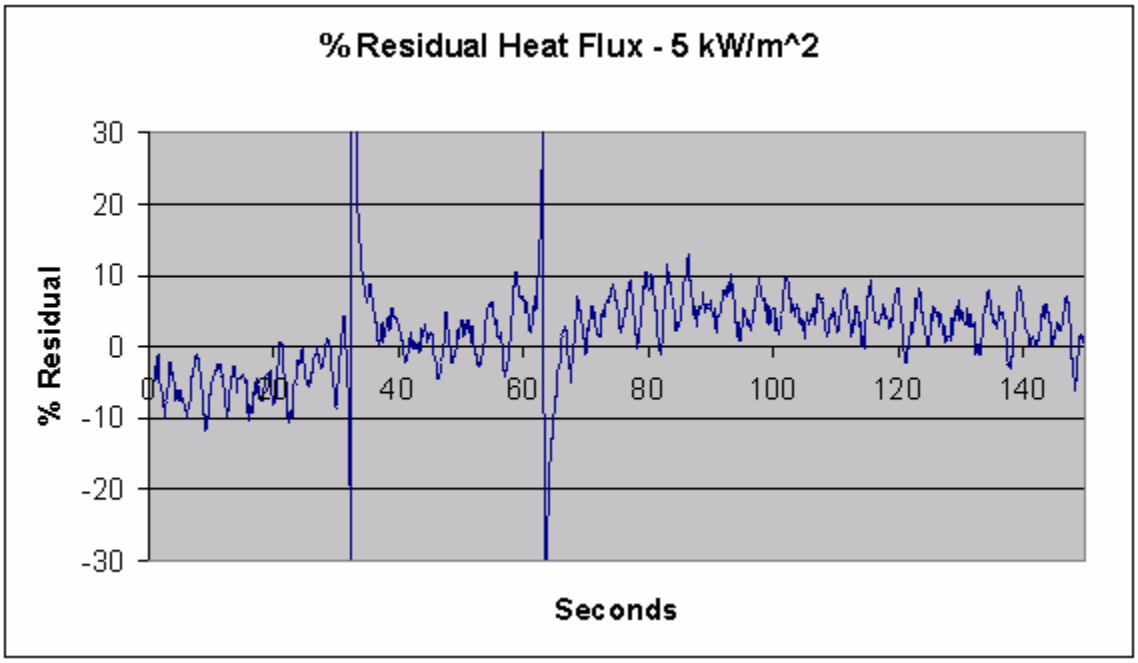

Figure 33- Percent Residual Heat Flux- 10kW/m

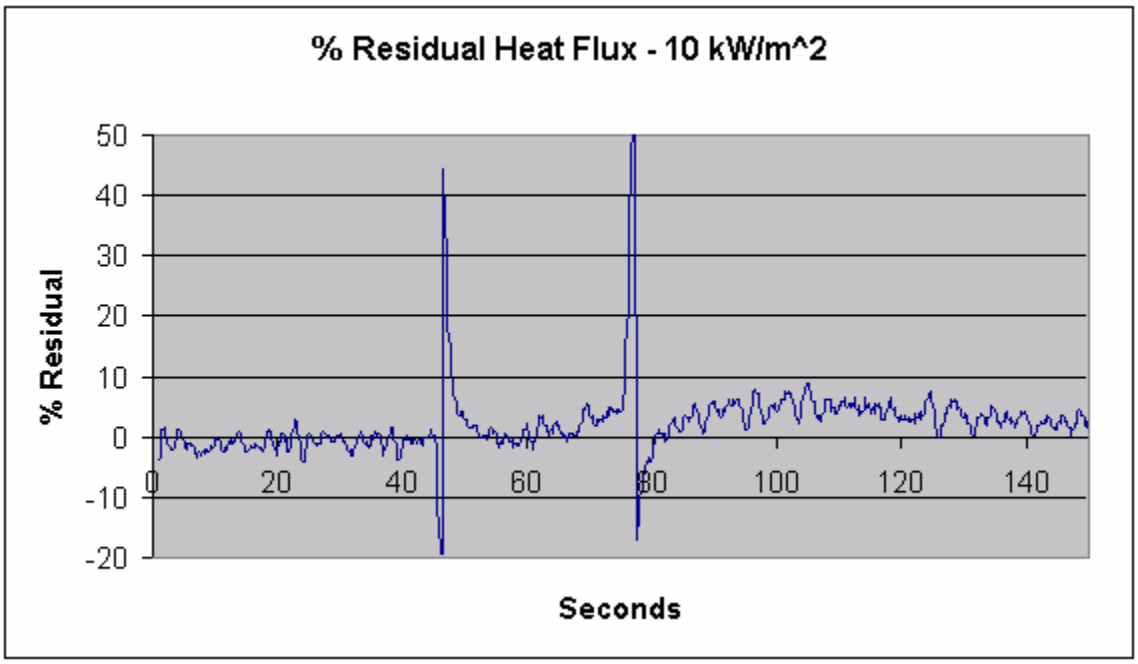

The spikes at 30 and 60 seconds are the points where the shutter was opened and closed. Since there is a lag time associated with the sensors there is not an instantaneous response. This is the reason for the spikes in the residual. It is not a major concern since it is only evident during the brief transient stages where the sensor is rapidly changing. It must be kept in mind however that the sensors do have a lag time associated with them and will not respond instantly. The data from these cone tests was deemed acceptable and the mannequin was instrumented with 40 newly fabricated copper disk sensors.

3.2.5. Mannequin Instrumentation

The mannequin contains sockets for 124 sensors, most of which were occupied with the old style Thermo®-Man buried thermocouple type of sensors when the mannequin was received. The sockets are labeled with etched numbers on the mannequin's surface. Due to financial constraints and limits of the data acquisition hardware only 40 new copper disk sensors were put on the mannequin. The locations of the sensors on the mannequin are shown in tables 7 and 8. Two arrangements of sensors were used. One puts most of the sensors on the front of the mannequin and was used to for test scenarios where the mannequin was placed outside of the room and subjected to a purely radiant exposure. The second arrangement placed the sensors all over the mannequin to give a more complete coverage of the total body area for sending the mannequin through the room.

Table 7- Sensor Locations on Front of Mannequin

Sensor #	Navy #	Description
1	1	Left Shoulder
2	4	Left Bicep
3	6	Left Elbow
4	8	Left Forearm Facing Out
5	9	Left Forearm Facing In
6	15	Right Shoulder
7	16	Right Bicep
8	20	Right Elbow
9	21	Right Forearm Facing Out
10	24	Right Forearm Facing In
11	30	Left Quad
12	34	Left Knee
13	39	Left Upper Shin
14	40	Left Calf Facing Out
15	41	Left Calf Facing In
16	46	Right Quad
17	50	Right Knee
18	52	Right Back of Knee
19	60	Right Lower Calf
20	56	Right Upper Calf Facing Out
21	71	Left Abdomen
22	65	Right Thoracic Region
23	70	Right Stomach
24	63	Right Pectoral
25	78	Right Hip
26	82	Right Quad
27	88	Left Quad
28	90	Right Hip
29	68	Center Stomach
30	66	Left Lower Chest
31	74	Right Clavicle
32	94	Left Clavicle
33	62	Left Upper Chest
34	93	Left Side Chest
35	61	Right Upper Chest
36	79	Right Upper Side Abdomen
37	89	Left Hip Flexor
38	83	Right Quad
39	85	Left Quad
40	84	Lower Abdomen

Table 8- Sensor Locations on Mannequins Entire Body

Sensor #	Navy #	Location
1	1	Left Shoulder
2	2	Left Bicep
3	6	Left Elbow
4	8	Left Forearm Facing Out
5	9	Left Inner Forearm Facing In
6	15	Right Shoulder
7	16	Right Bicep
8	20	Right Elbow
9	21	Right Forearm Facing Out
10	24	Right Forearm Facing In
11	30	Left Quad
12	34	Left Knee
13	39	Left Front Calf
14	40	Left Calf Facing Out
15	41	Left Calf Facing In
16	46	Right Quad
17	50	Right Knee
18	52	Right Rear Knee
19	60	Right Lower Calf
20	56	Right Upper Calf
21	63	Right Pectoral
22	64	Left Pectoral
23	68	Center Abdomen
24	73	Right Upper Shoulder
25	78	Right Hip
26	82	Right Upper Quad
27	89	Left Upper Quad
28	90	Left Hip
29	84	Lower Abdomen
30	95	Left Upper Shoulder
31	108	Left Back
32	97	Left Shoulder Blade
33	99	Right Shoulder Blade
34	101	Left Lower Shoulder Blade
35	105	Right Lower Shoulder Blade
36	107	Center of Back
37	112	Left Upper Butt
38	117	Right Butt
39	121	Left Rear Upper Thigh
40	124	Right Upper Thigh

The sensors have type T thermocouple male connectors at the end of the wire that contains the bead on the back of the disk. These plug into female connectors inside the mannequin. The female connectors are connected to 20 gauge type T wire that exits the mannequin through a square hole in the mannequin's upper back. These wires are type TT-T-20 from Omega Engineering. The insulation is Teflon® and is rated to withstand temperatures up to 260°C (Omega, 2000). Since the room's thermal environment is much greater than 260 °C, the wires are bundled and encased in fiberglass sheathing. The sheathing is then covered with high temperature metal tape. This has consistently been shown to provide adequate protection to the wires and insulation during our testing. The wire is supported by a series of rollers designed and built by a group of WPI students (Bradbury et al, 2001). These rollers follow the mannequin through the room and hold the wires off of the ground and out of the hottest part of the flames. As soon as the mannequin passes through the room, the gas burners are turned down to protect the wires that are still extended through the room. The wires connect to a National Instruments data acquisition system that consists of a SCXI 1000 multiplexer containing three SCXI 1122 modules. The thermocouple wires connect to three 16 channel SCXI 1322 terminal blocks. The modules each have the capability to record data at up to 100 Hz. The data for most tests was collected at 4 Hz per channel, the maximum rate possible for the number of channels being recorded.

3.2.6. Skin Burn Prediction Method

The heat flux data from the mannequin sensors can be used to provide an indication of the response of human skin in several ways. The equations in section 2.1 can be used to predict the onset of pain and calculate temperature. These equations however are only valid for constant energy flow and are not applicable to transient heat fluxes. Since only the radiant heat fluxes from the fire when the mannequin is stationary in the doorway are quasi-steady, another method must be used. Heat fluxes measured through clothing are very transient in nature as well as the heat fluxes measured as the naked mannequin traverses the room. To calculate skin temperature for a transient heat flux a finite difference model of human skin was developed. The model is based on work by Gagnon (Gagnon, 2000), and can calculate skin response to a transient thermal insult. The model divides the first 1.2 cm of the skin into 40 nodes spaced 0.3 mm apart. The model assumes the skin to be homogeneous and have constant spatial thermal properties. Different values for the thermal conductivity are used for the heating and cooling phase of the exposure (see table 1). The heat flux that is absorbed into the skin is defined as the difference between the incident heat flux and the losses:

$$\dot{q}''_{abs} = \dot{q}''_{incident} - \dot{q}''_{conv} - \dot{q}''_{rad} \qquad \text{(Eq. 24)}$$

The energy storage term from the energy balance on the disk is used for this. The temperature of the nodes can be solved for by the following finite difference model:

Surface Node Temperature:

$$T_j^{i+1} = 2Fo\left(T_{j+1}^i + \frac{\dot{q}''_{abs}\,\Delta x}{k}\right) + (1-2Fo)T_j^i \qquad \text{(Eq. 24)}$$

Internal Node Temperature:

$$T_j^{i+1} = Fo\left(T_{j-1}^i + T_{j+1}^i\right) + (1-2Fo)T_j^i \qquad \text{(Eq. 25)}$$

Where:

Time = i, i+1

Depth = j-1, j, j+1 (where positive sign convention indicates direction into the skin)

Fo = $\frac{\alpha \Delta t}{\Delta x^2}$

In order to ensure that the model is in sync with the conduction physics that it is replicating, the following stability criterion must be observed:

$$Fo = \frac{\alpha \Delta t}{\Delta x^2} \leq \frac{1}{2} \qquad \text{(Eq. 26)}$$

Where $\alpha = \frac{k}{\rho c}$

Since the first node is 0.3 mm below the surface of the skin and the basal layer where a burn forms is 0.08 mm below the surface, the basal layer temperature must be interpolated assuming a linear temperature gradient:

$$T^i_{Basal} = T^i_{Surface} - \frac{0.08}{0.3}\left(T^i_{Surface} - T^i_{Node1}\right) \qquad \text{(Eq. 27)}$$

The results of this method were compared to equation 6 to determine the accuracy of both the finite difference model used and the linear interpolation method for finding the basal layer temperature. Since skin temperature data from transient heat flux exposures is practically non-existent, only constant heat flux exposures can be used to validate the model. Equation 6 is from the SFPE Guide to Predicting 1st and 2nd Degree Burns, and has been compared to experimental data and found to show acceptable agreement (SFPE Guide, 2000). The finite difference model predicts very similar temperature responses of both the skin surface and the basal layer for a 5.5 second radiant

exposure of 15.7 kW/m^2. The temperature of the skin surface and basal layer are shown in figures 34 and 35.

Figure 34- Skin Surface Temperature- Equation 6 vs. FDM

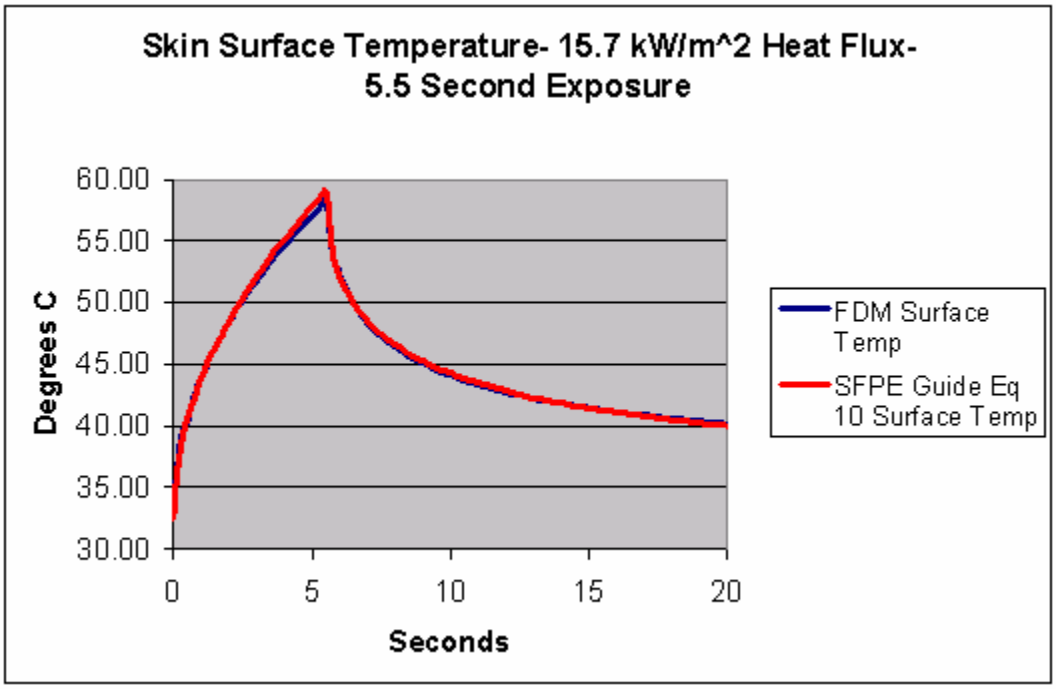

Figure 35- Skin Basal Layer Temperature- Equation 6 vs. FDM

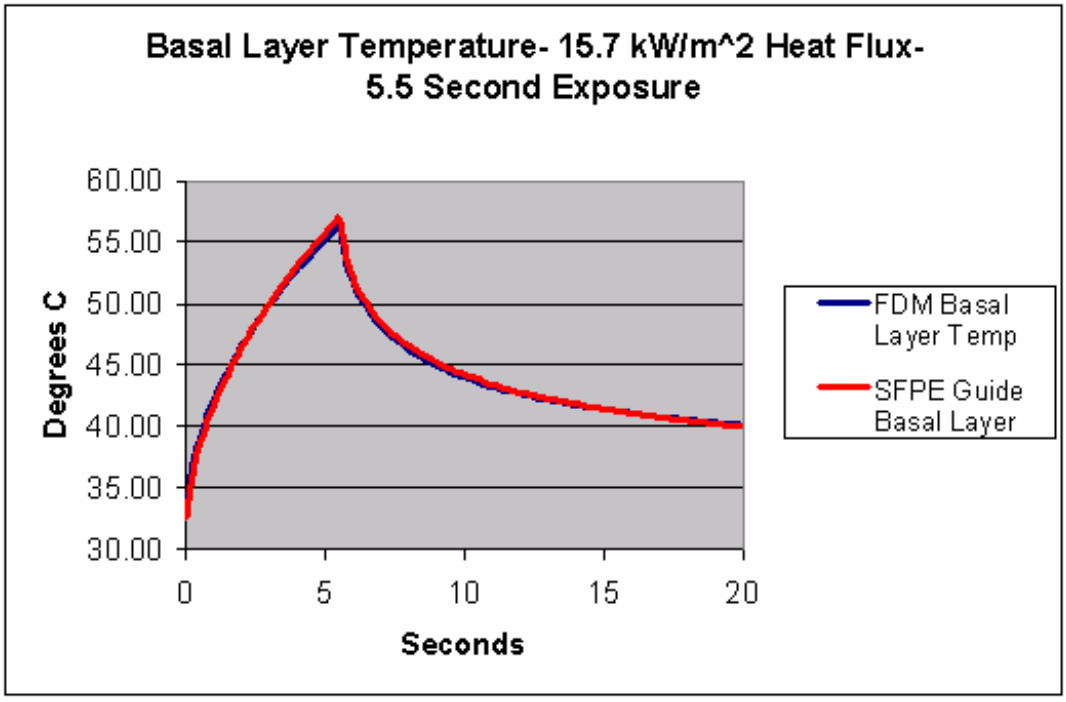

Since the temperature at the basal layer is the critical parameter for skin burn predictions it is most important that it be accurate. The residual temperature difference between the two methods is shown in figure 36.

Figure 36- Residual Temperature Difference- Equation 6 vs. FDM

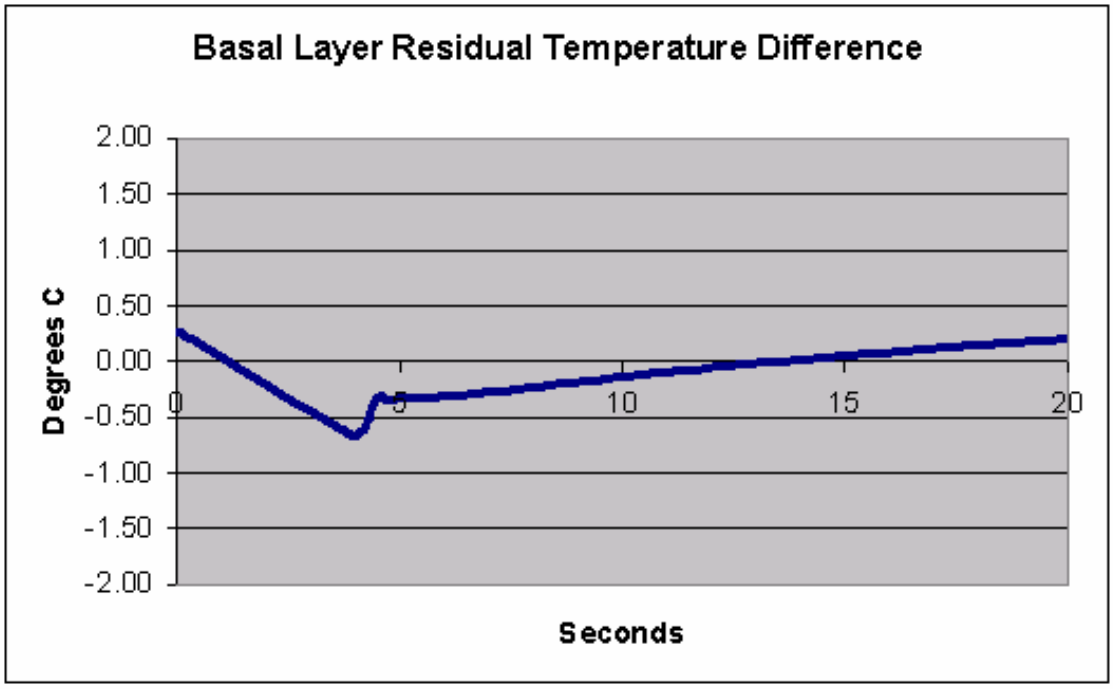

The basal layer temperature difference is never more than 0.7 degrees Celsius, which is acceptable for our purposes. It is assumed that the model is also accurate for highly transient heat fluxes, although validation data is not available.

The basal layer temperature from the finite difference model can then be used to predict skin burns using Henriques Burn Damage Integral (Eq. 10):

$$\frac{d\Omega}{dt} = P\exp\left(\frac{-\Delta E}{RT}\right)$$

which becomes:

$$\Omega = \int_0^t P\exp\left(\frac{-\Delta E}{RT}\right)dt$$

In order to integrate the function the trapezoidal rule is used. In generic form this is:

$$\int_0^t f(t) \approx \sum_{k=0}^{n} \frac{f(t_k) + f(t_{k+\Delta t})}{2}\Delta t \qquad \text{(Eq. 28)}$$

where $n = \frac{t}{\Delta t}$

If the value calculated for Ω is greater than 0.53 than a first degree burn has formed, if it is greater than 1.0 than a 2nd degree burn has formed.

3.2.7. Test Procedure

Two different testing procedures were employed to collect data using the mannequin. First a series of tests were conducted with the mannequin just outside the room with the sensors located on the front of the mannequin. Another series of tests was conducted with the mannequin moving through the room. Both of these procedures involved exposing the naked mannequin to the fire to record the incident heat flux on the surface of the mannequin. Then a series of tests were conducted with protective clothing on the mannequin. The mannequin is a size 40 male. Coveralls available at the time of testing were all size 44. This provided a very loose fit with large air gaps in certain regions. Currently there exists no accurate way to measure the air gaps between the sensors and the mannequin. They range from 0 (direct contact) to approximately 3 cm.

3.2.7.1. Radiant Exposure

For the radiant exposures with the mannequin outside of the room, distances of 8 and 9 feet from the burner centerline were selected for two sets of tests. The reason for these distances is that they are the closest that the mannequin could be positioned outside

of the room. Since the mannequin is in clear view of the room, a thermal shield was placed in front of it to block incident radiation while the fire was reaching steady state. A space between the mannequin and the doorway was needed to place the shield. At the time this test was conducted the ambient temperature was rather cold and maximum propane flow could not be achieved. The propane delivery system relies on four 100 lb tanks located outside of the building (fig 37). The propane from these tanks flows into a ThermoFlo® vaporizer (fig 38) and then through the HFC-308 mass flow controller (fig 39). During cold weather the pressure in the tanks is not sufficiently large to flow the propane required to produce large fires. During the first round of testing the largest flow rate that could be achieved was 30 g/s (1.32 MW).

Figure 37- Exterior Propane Tanks

Figure 38- LPG Vaporizer

Figure 39- Mass Flow Controller

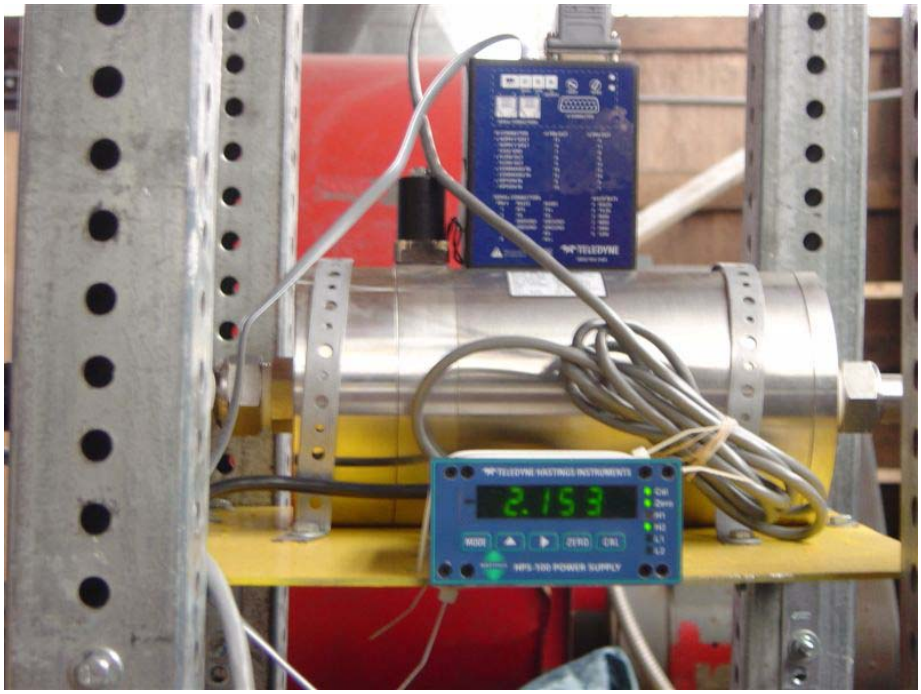

The test procedure was carried out as follows: A shield was placed in front of the mannequin to block the radiant heat. The data acquisition system was turned on and allowed to run for 1 minute to verify operation and record baseline temperatures. The fire was set to the desired HRR by means of the mass flow controller and allowed to stabilize. The shield was moved from in front of the mannequin exposing it to a radiant heat flux and then replaced after either 30 or 60 seconds. Six tests were conducted in this fashion. Measurements were taken with the mannequin completely bare, and with a fire resistant treated cotton suit. Tests with the FR cotton suit were carried out for 30 and 60 seconds. Measurements were taken at two distances from the fire: 8 and 9 feet from the burner centerline. The test summaries are given in table 9.

Table 9- Radiant Exposure Test Summary

Test #	Distance from Fire	Clothing	Duration
1R	8 ft	Bare	30 s
2R	8 ft	FR Cotton	30 s
3R	8 ft	FR Cotton	60 s
4R	9 ft	Bare	30 s
5R	9 ft	FR Cotton	30 s
6R	9 ft	FR Cotton	60 s

Between tests the mannequin was cleaned with a damp cloth and exposed to a fan until the sensors cooled below 25^{o}C.

3.2.7.2. Mannequin Moving Through Room

Before testing was begun in the room, the fire size from previous tests needed to be approximated. Previous measurements taken in the room were taken without the use of a flow controller Woodward showed that the fire could be reproduced fairly reliably (Woodward, 2003), but since there is no assurance that all tests were carried out at the same heat release rate some caution must be used when relating this data to his. The fire sizes were approximated by a group of students (Carnazza et al, 2003), but never measured. Heat flux measurements were taken in the doorway to the room and compared to previous data to approximate the fire size used for previous work by Woodward. Previous fires produced an incident heat flux of 17 kW/m^2 on a Gardon gauge mounted in the stomach of the mannequin. The mannequin was positioned 6 feet from the burner centerline for these tests. To get a rough idea of the fire size that was used to produce this exposure three fire sizes were investigated: 1.32, 1.4 and 1.5 MW. The ambient temperature on these days was substantially warmer than on previous test days. This

temperature combined with fresh propane tanks allowed higher propane flow rate to be achieved. The Gardon gauge was calibrated in the WPI Cone Calorimeter and as such has at least a 10% uncertainty associated with it. The calibration curve is given in figure 40.

Figure 40- Gardon Gauge Calibration

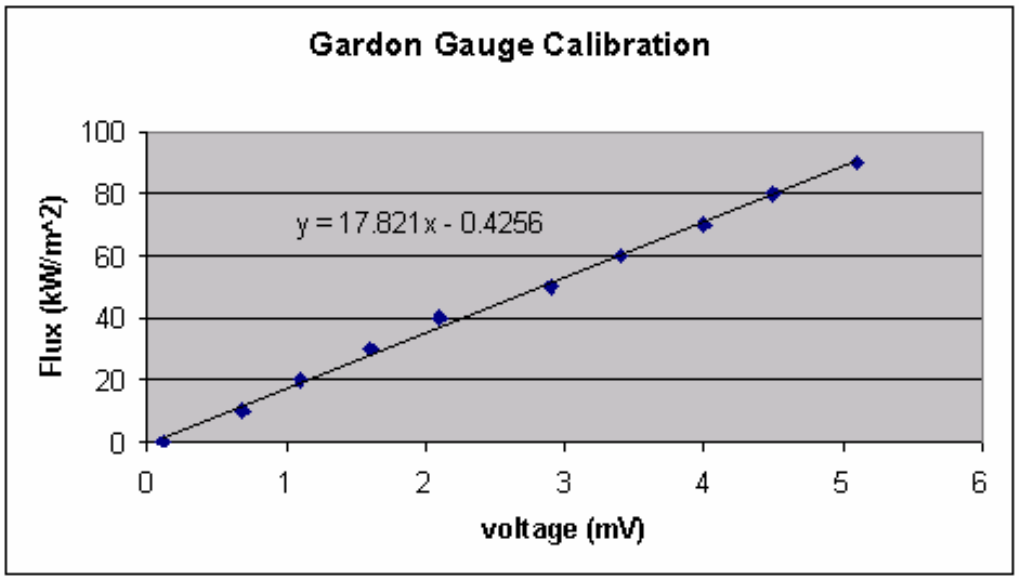

The mannequin was also instrumented with the copper disk sensors in the front side arrangement, so these doorway tests were also another opportunity to rate their performance. The test procedure went as follows: The mannequin was positioned behind a plywood shield and the fire was set to the specified HRR and allowed to level out for 30 seconds. The shield was moved and the mannequin was moved forward to a predetermined mark 6 feet from the burner centerline. The mannequin remained at this position in the doorway for 10 seconds and was then backed out of the room and the shield replaced as the fire was dialed down. The heat fluxes recorded by the Gardon gauge and the copper disk sensor in the lower abdomen that was closest to the Gardon gauge are shown in figures 41, 42, and 43. The copper disk sensor was inclined slightly

so the view factor would be expected to be slightly less than the Gardon gauge that pointed straight at the fire.

Figure 41- Mannequin Heat Flux- 6 feet from 1.32 MW fire

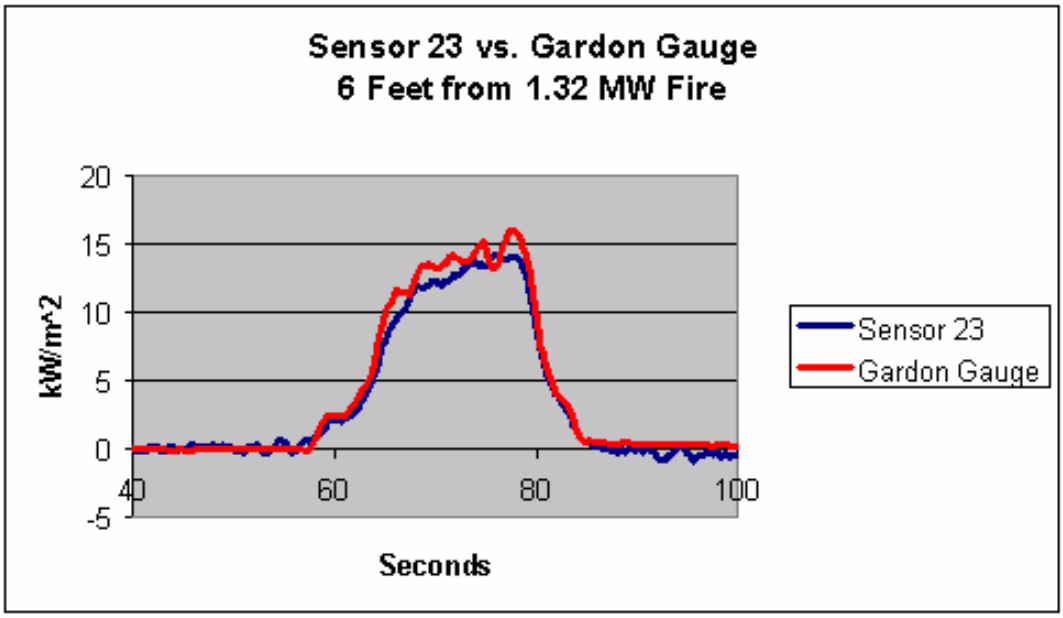

Figure 42- Mannequin Heat Flux- 6 feet from 1.4 MW fire

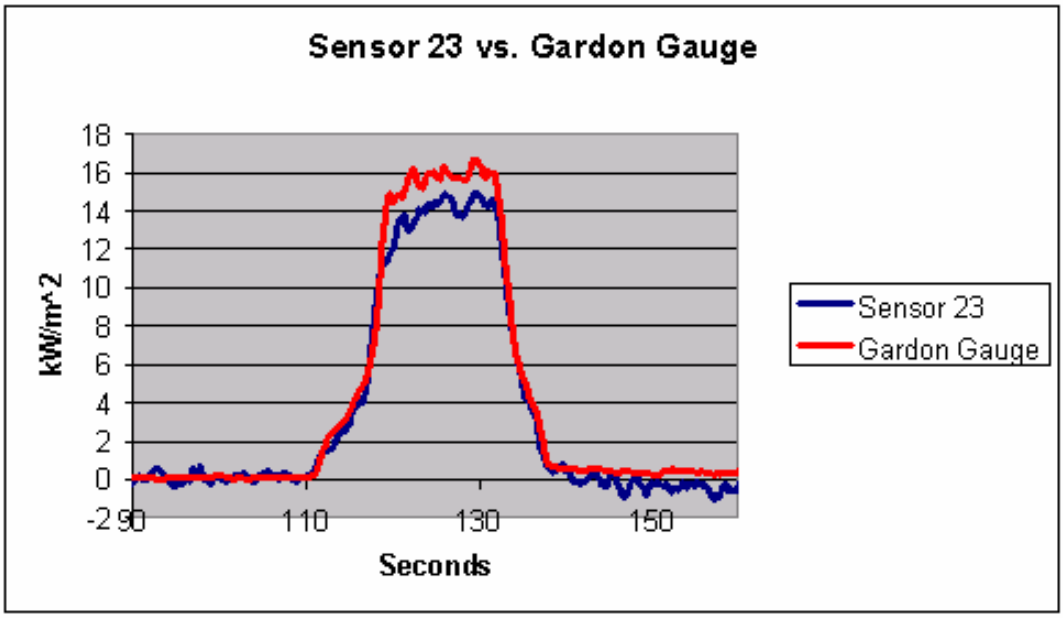

Figure 43- Mannequin Heat Flux- 6 feet from 1.5 MW fire

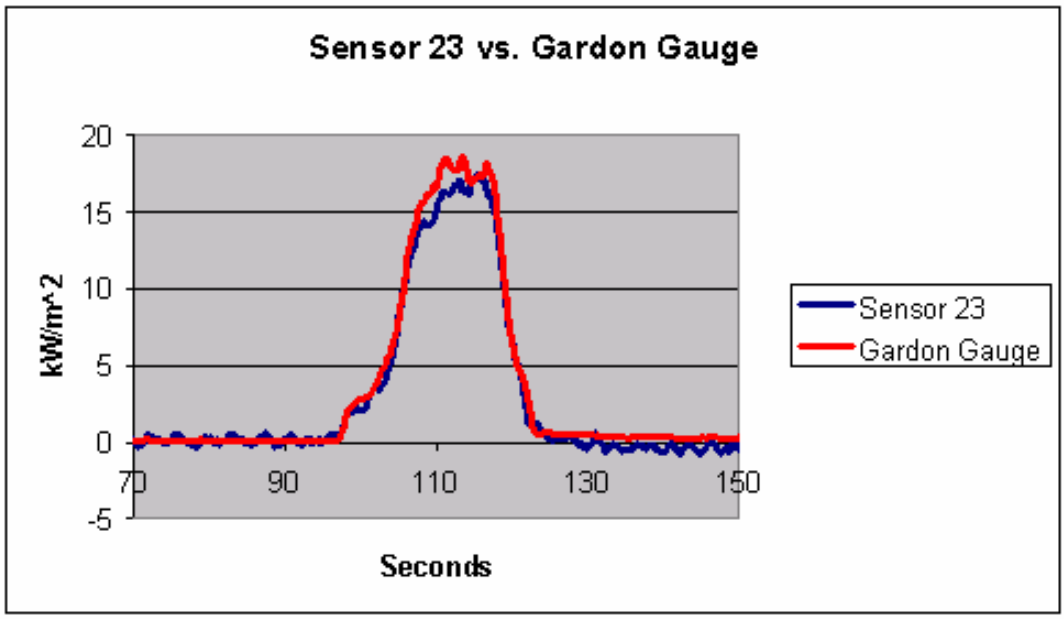

The copper disk sensor is shown here to follow the heat flux that is measured by the Gardon gauge as long as it is not changing too rapidly. The heat flux from the 1.5 MW test is the closest to the value of 17 kW/m^2 that was previously observed. This indicates that the previous fires tested were most likely very close to 1.5 MW. Visual observations from the two different tests support this, but further detailed testing that includes thermal profiling will be needed to know for sure. For now the data collected from Woodward will be assumed to apply to the current test conditions at 1.5 MW.

Once the 1.5 MW HRR was determined, a series of tests were carried out that involved transporting the mannequin through the room. Measurements were taken by the bare mannequin for a range of exposures, but for the more severe exposures fear of damaging the mannequin prevented our sending it through the room bare. There was not adequate funding in the budget to purchase a spare mannequin should the primary unit be

damaged. Subsequent tests used FR Cotton coveralls and PBI 7.5 oz/yard coveralls with moisture barriers and thermal insulation.

Table 10- Tests Through Room

Test	Clothing	Speed	
		Turns	Feet/sec
1T	Bare	4	2.2
2T	Bare	3	1.65
3T	Bare	2	1.1
4T	PBI (7.5 oz/yd)	5	2.75
5T	PBI (7.5 oz/yd)	3	1.65
6T	PBI (7.5 oz/yd)	2.6	1.43
7T	PBI (7.5 oz/yd)	2	1.1
8T	PBI (7.5 oz/yd)	1.3	0.715
9T	PBI (7.5 oz/yd)	1	0.55
10T	PBI (7.5 oz/yd)	0.8	0.44
11T	FR Cotton	5	2.75
12T	FR Cotton	4	2.2
13T	FR Cotton	3	1.65
14T	FR Cotton	2	1.1
15T	FR Cotton	1	0.55

Between tests the mannequin was cleaned with a damp cloth and exposed to a fan until the sensors returned to below 25^{o}C.

4. Testing Results

4.1. Radiant Exposure

For the radiant exposures with the mannequin in the doorway, the range of incident heat fluxes is shown in table 11. The maximum averages were calculated to be 6.3 kW/m^2 at a distance of 8 feet, and 4.5 kW/m^2 at a distance of 9 feet. The most intense exposures were recorded on the lower quadriceps. These incident heat fluxes are shown in figures 38 and 39. These values represent the low end of the range of expected heat fluxes from fires aboard Navy ships. This test configuration serves the purpose of testing the performance of clothing that is not intended for primary firefighting use. The low incident heat fluxes that are provided for the exposure simulate the radiant heat that would be received from a pool or jet fire at a distance. Higher heat fluxes could be attained with larger fires, which are easily within the capacity of the facility. Warmer ambient temperature and more efficient piping configurations could provide greater propane flow. The test arrangement also has the potential of testing fire fighter's primary protective clothing for long duration exposures. The maximum duration of the exposure is primarily governed by the capacity of the room. For intense fires of long duration (>5 min) the ceiling and upper walls become very hot and the gypsum lining begins to lose its integrity.

Table 11- Bare Mannequin 8 feet from 1.32 MW Fire- 30 Second Exposure

Sensor	Navy #	Description	Average Heat Flux
1	1	Left Shoulder	0.5
2	4	Left Bicep	1.2
3	6	Left Elbow	0.0
4	8	Left Forearm Facing Out	0.7
5	9	Left Forearm Facing In	3.7
6	15	Right Shoulder	1.3
7	16	Right Bicep	2.7
8	20	Right Elbow	0.1
9	21	Right Forearm Facing Out	0.6
10	24	Right Forearm Facing In	4.5
11	30	Left Quad	6.3
12	34	Left Knee	5.6
13	39	Left Upper Shin	2.2
14	40	Left Calf Facing Out	0.1
15	41	Left Calf Facing In	0.2
16	46	Right Quad	5.6
17	50	Right Knee	5.0
18	52	Right Back of Knee	0.1
19	60	Right Lower Calf	0.1
20	56	Right Upper Calf Facing Out	0.0
21	71	Left Abdomen	3.5
22	65	Right Thorasic Region	5.2
23	70	Right Stomach	3.1
24	63	Right Pectorial	5.5
25	78	Right Hip	0.6
26	82	Right Quad	3.2
27	88	Left Quad	0.1
28	90	Right Hip	0.6
29	68	Center Stomach	5.8
30	66	Left Lower Chest	5.7
31	74	Right Clavicle	3.7
32	94	Left Clavicle	4.6
33	62	Left Upper Chest	4.8
34	93	Left Side Chest	2.0
35	61	Right Upper Chest	5.6
36	79	Right Upper Side Abdomen	3.2
37	89	Left Hip Flexor	4.0
38	83	Right Quad	5.8
39	85	Left Quad	3.7
40	84	Lower Abdomen	5.9
Max			6.3
Avg			2.9

Table 12- Bare Mannequin 9 Feet from 1.32 MW Fire- 30 Second Exposure

Sensor	Navy #	Description	Average Heat Flux
1	1	Left Shoulder	0.2
2	4	Left Bicep	0.8
3	6	Left Elbow	0.0
4	8	Left Forearm Facing Out	0.5
5	9	Left Forearm Facing In	2.6
6	15	Right Shoulder	0.6
7	16	Right Bicep	1.6
8	20	Right Elbow	0.0
9	21	Right Forearm Facing Out	0.3
10	24	Right Forearm Facing In	3.1
11	30	Left Quad	4.5
12	34	Left Knee	3.9
13	39	Left Upper Shin	1.5
14	40	Left Calf Facing Out	0.1
15	41	Left Calf Facing In	0.1
16	46	Right Quad	4.0
17	50	Right Knee	3.6
18	52	Right Back of Knee	0.0
19	60	Right Lower Calf	0.0
20	56	Right Upper Calf Facing Out	0.0
21	71	Left Abdomen	2.4
22	65	Right Thorasic Region	3.1
23	70	Right Stomach	2.1
24	63	Right Pectorial	3.1
25	78	Right Hip	0.3
26	82	Right Quad	2.3
27	88	Left Quad	0.0
28	90	Right Hip	0.4
29	68	Center Stomach	3.7
30	66	Left Lower Chest	3.5
31	74	Right Clavicle	0.1
32	94	Left Clavicle	0.6
33	62	Left Upper Chest	2.6
34	93	Left Side Chest	1.0
35	61	Right Upper Chest	3.1
36	79	Right Upper Side Abdomen	1.8
37	89	Left Hip Flexor	2.9
38	83	Right Quad	4.0
39	85	Left Quad	2.6
40	84	Lower Abdomen	4.1
Max			4.5
Avg			1.8

Figure 44- Sensor #38 (Right Quad) - Incident Heat Flux from Tests 1R and 4R

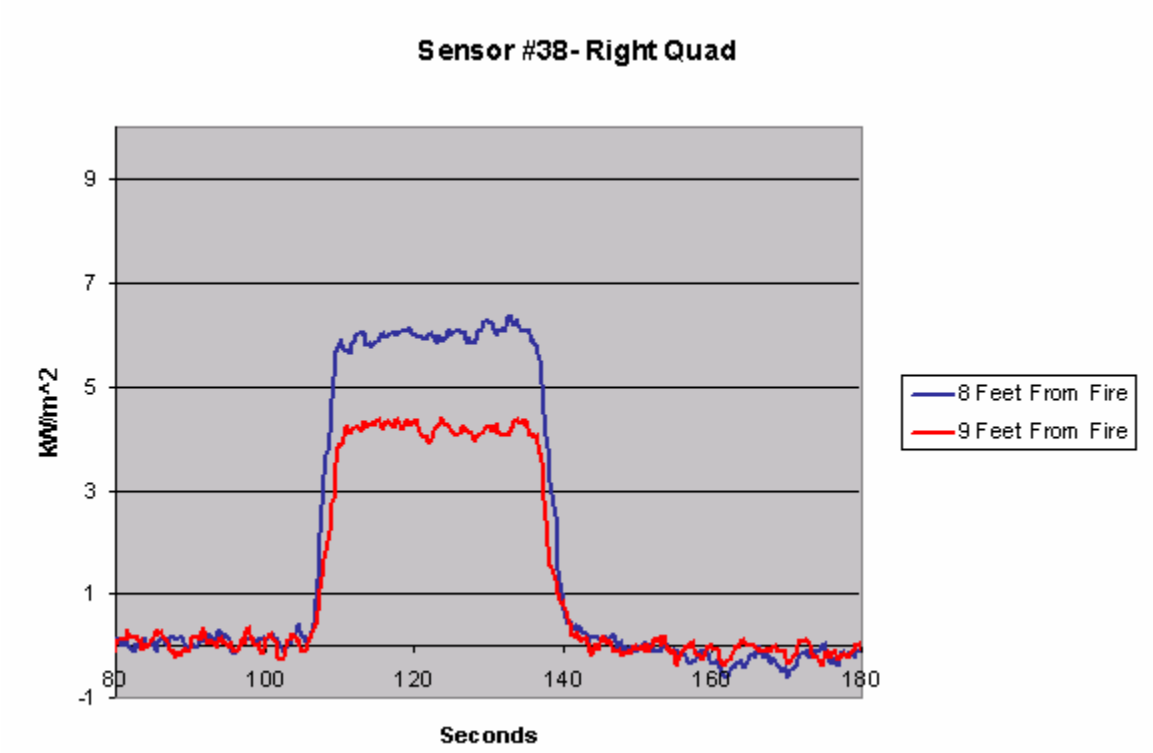

Figure 45- Sensor #11 (Left Quad) – Incident Heat Flux from Tests 1R and4R

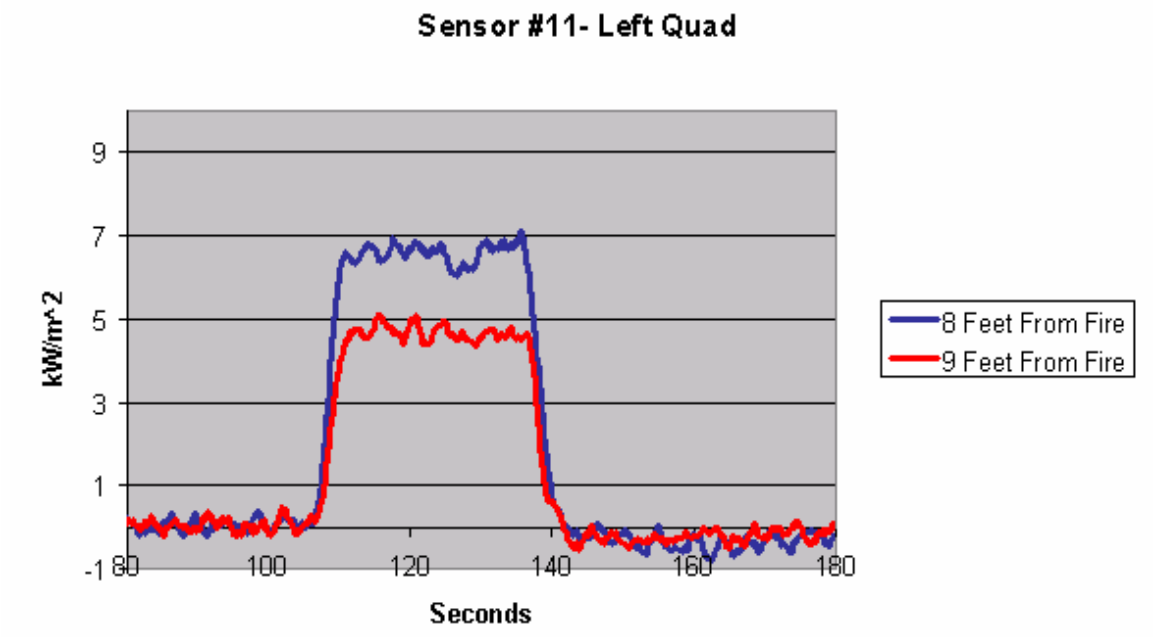

Using the skin burn prediction method outlined in section 3.2.6., the skin temperature and burn damage was calculated for each sensor in tests 2R, 3R, 5R, and 6R. These tests involved exposing the mannequin to radiant heat at distances of 8 and 9 feet from the burner centerline for exposure durations of 30 and 60 seconds. The test results for 2R and 3R are shown in tables 13 and 14. No 1^{st} and 2^{nd} degree burns were predicted, and only one sensor location predicted skin a temperature above 44^{o}C. The maximum temperatures for tests 2R and 3R are shown in tables 13 and 14. Figure 40 shows the measured heat flux at sensor #38 and the predicted skin response. The skin temperature only reaches 39^{o}C. This is below 44^{o}C, the minimum temperature for skin burn damage. Future work should focus on either more intense or longer duration exposures.

Table 13- Test 2R- 30 Second Radiant Exposure- 8 Feet From Burners

Sensor #	Navy #	Description	Burn Damage	Max Temp
1	1	Left Shoulder	0	33.6
2	4	Left Bicep	0	33.9
3	6	Left Elbow	0	32.8
4	8	Left Forearm Facing Out	0	33.1
5	9	Left Forearm Facing In	0	34.0
6	15	Right Shoulder	0	35.4
7	16	Right Bicep	0	36.3
8	20	Right Elbow	0	32.9
9	21	Right Forearm Facing Out	0	33.3
10	24	Right Forearm Facing In	0	34.8
11	30	Left Quad	0	40.9
12	34	Left Knee	0	38.6
13	39	Left Upper Shin	0	33.5
14	40	Left Calf Facing Out	0	33.1
15	41	Left Calf Facing In	0	32.9
16	46	Right Quad	0	36.2
17	50	Right Knee	0	35.2
18	52	Right Back of Knee	0	32.9
19	60	Right Lower Calf	0	32.7
20	56	Right Upper Calf Facing Out	0	32.8
21	71	Left Abdomen	0	35.2
22	65	Right Thorasic Region	0	35.9
23	70	Right Stomach	0	34.2
24	63	Right Pectorial	0	38.4
25	78	Right Hip	0	34.2
26	82	Right Quad	0	38.8
27	88	Left Quad	0	32.9
28	90	Right Hip	0	34.9
29	68	Center Stomach	0	33.7
30	66	Left Lower Chest	0	40.1
31	74	Right Clavicle	0	37.1
32	94	Left Clavicle	0	37.3
33	62	Left Upper Chest	0	36.5
34	93	Left Side Chest	0	34.2
35	61	Right Upper Chest	0	35.0
36	79	Right Upper Side Abdomen	0	33.7
37	89	Left Hip Flexor	0	35.4
38	83	Right Quad	0	37.3
39	85	Left Quad	0	40.6
40	84	Lower Abdomen	0	37.8

Table 14- Test 3R- 60 Second Radiant Exposure- 8 Feet From Burners

Sensor #	Navy #	Description	Burn Damage	Max Temp
1	1	Left Shoulder	0	36.5
2	4	Left Bicep	0	37.3
3	6	Left Elbow	0	32.8
4	8	Left Forearm Facing Out	0	33.8
5	9	Left Forearm Facing In	0	36.5
6	15	Right Shoulder	0	36.5
7	16	Right Bicep	0	37.3
8	20	Right Elbow	0	32.8
9	21	Right Forearm Facing Out	0	33.8
10	24	Right Forearm Facing In	0	36.5
11	30	Left Quad	0	45.9
12	34	Left Knee	0	39.7
13	39	Left Upper Shin	0	34.5
14	40	Left Calf Facing Out	0	33.6
15	41	Left Calf Facing In	0	33.5
16	46	Right Quad	0	39.3
17	50	Right Knee	0	37.9
18	52	Right Back of Knee	0	33.3
19	60	Right Lower Calf	0	32.8
20	56	Right Upper Calf Facing Out	0	33.1
21	71	Left Abdomen	0	35.9
22	65	Right Thorasic Region	0	37.9
23	70	Right Stomach	0	35.7
24	63	Right Pectorial	0	40.3
25	78	Right Hip	0	35.0
26	82	Right Quad	0	40.2
27	88	Left Quad	0	33.1
28	90	Right Hip	0	35.6
29	68	Center Stomach	0	34.7
30	66	Left Lower Chest	0	42.2
31	74	Right Clavicle	0	38.2
32	94	Left Clavicle	0	39.1
33	62	Left Upper Chest	0	38.5
34	93	Left Side Chest	0	35.4
35	61	Right Upper Chest	0	36.3
36	79	Right Upper Side Abdomen	0	34.5
37	89	Left Hip Flexor	0	37.8
38	83	Right Quad	0	39.4
39	85	Left Quad	0	43.6
40	84	Lower Abdomen	0	40.0

Figure 46- Measured Heat Flux at Sensor #38 and Predicted Skin Response- Test 3R

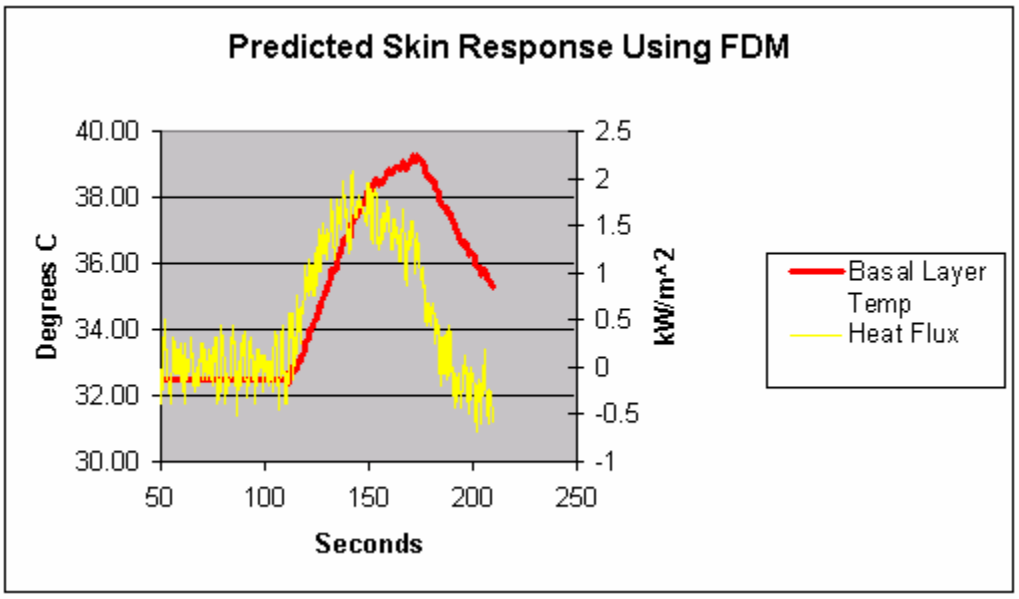

The maximum and average skin temperature rises are 8.4 ^{o}C and 3.0^{o}C respectively for test 2R, and 13.4 ^{o}C and 4.3^{o}C respectively for test 3R. If the incident heat flux from the bare test at 8 feet (1R) is compared to the predicted skin temperature rises at the corresponding sensors from the clothed tests, significant scatter is seen. Large air gaps at certain sensors are most likely the cause of this scatter. If the air gaps were uniform at every sensor, then a fairly linear relationship could be expected between incident heat flux and skin temperature rise. This general trend is seen, but there are very many outlying data points. The correlation between incident heat flux and temperature rise is seen in figures 41 and 42. Closer fitting coveralls for testing will most likely eliminate some of the scatter shown in these figures. The difficulty with tighter fitting coveralls is the dressing and undressing process. The size 44 coveralls were rather difficult to slip over the rigid mannequin, although slightly smaller sizes are probably possible.

Figure 47- Incident Heat Flux vs. Predicted Skin Response using FDM - Test 2R

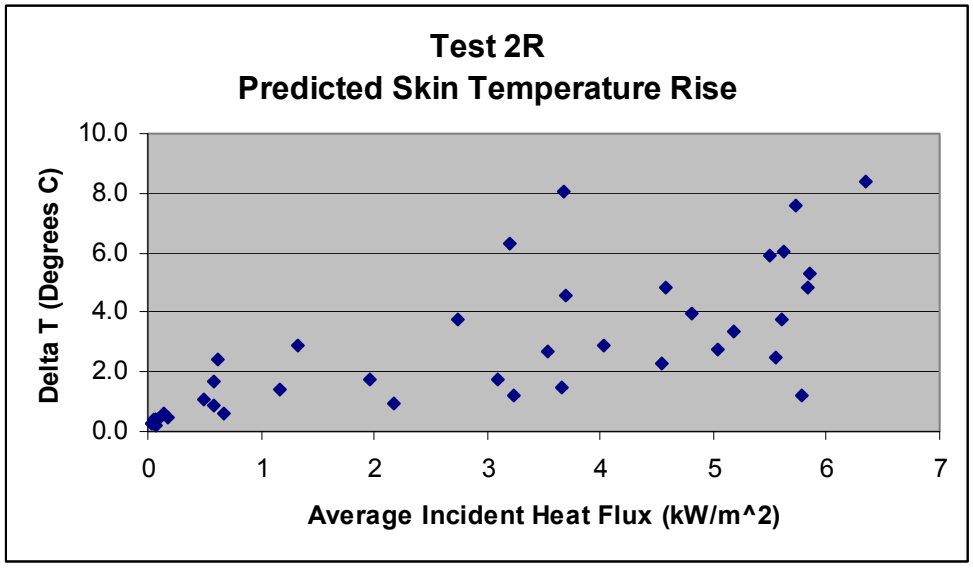

Figure 48- Incident Heat Flux vs. Predicted Skin Response - Test 3R

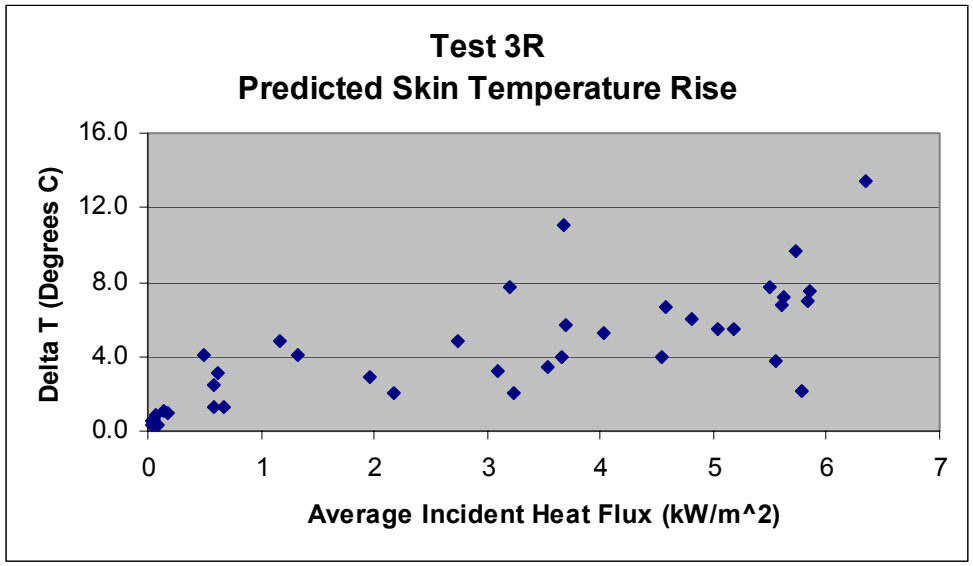

4.2. Through Room

Tests in which the mannequin was moved through the room are grouped into three types: Bare, covered with FR Cotton coveralls, and covered with PBI coveralls. The mannequin was only moved through the room at three speeds to prevent damaging it. The PBI coveralls were tested at the full range of speeds, and the FR Cotton coveralls were tested at all but the very slowest speed.

4.2.1. Bare Mannequin

The mannequin was exposed to the fire in the room for 5.5, 7.27, and 10.9 seconds by adjusting the motor speed (2.2, 1.65, and 1.1 ft/s). The average and maximum heat fluxes recorded by the mannequin are shown in tables 14, 15, and 16. If the heat flux is integrated over the exposure duration, this gives the total energy absorbed per unit area. The total energy absorbed, in kJ/m^2, is shown in tables 17.

Table 15- Test 1T- 2.2 ft/sec- Max and Average Heat Fluxes

Sensor #	Navy #	Location	Max kW/m^2	Avg kW/m^2
1	1	Left Shoulder	10	6
2	2	Left Bicep	13	7
3	6	Left Elbow	12	6
4	8	Left Forearm Facing Out	8	5
5	9	Left Inner Forearm Facing In	13	5
6	15	Right Shoulder	7	4
7	16	Right Bicep	11	6
8	20	Right Elbow	22	10
9	21	Right Forearm Facing Out	20	9
10	24	Right Forearm Facing In	18	8
11	30	Left Quad	25	9
12	34	Left Knee	23	9
13	39	Left Front Calf	24	9
14	40	Left Calf Facing Out	17	8
15	41	Left Calf Facing In	24	11
16	46	Right Quad	32	10
17	50	Right Knee	28	10
18	52	Right Rear Knee	30	13
19	60	Right Lower Calf	6	3
20	56	Right Upper Calf	19	10
21	63	Right Pectorial	13	6
22	64	Left Pectorial	10	5
23	68	Center Abdomin	15	6
24	73	Right Upper Shoulder	2	1
25	78	Right Hip	11	5
26	82	Right Upper Quad	23	8
27	89	Left Upper Quad	12	5
28	90	Left Hip	6	4
29	84	Lower Abdomen	13	7
30	95	Left Upper Shoulder	6	4
31	108	Left Back	17	10
32	97	Left Shoulder Blade	16	8
33	99	Right Shoulder Blade	13	7
34	101	Left Lower Shoulder Blade	14	8
35	105	Right Lower Shoulder Blade	18	10
36	107	Center of Back	16	8
37	112	Left Upper Butt	14	8
38	117	Right Butt	28	13
39	121	Left Rear Upper Thigh	18	9
40	124	Right Upper Thigh	22	11

Table 16- Test 2T- 1.65 ft/sec- Max and Average Heat Fluxes

Sensor #	Navy #	Location	Max kW/m^2	Avg kW/m^2
1	1	Left Shoulder	11	7
2	2	Left Bicep	16	13
3	6	Left Elbow	15	6
4	8	Left Forearm Facing Out	11	7
5	9	Left Inner Forearm Facing In	16	12
6	15	Right Shoulder	9	6
7	16	Right Bicep	14	10
8	20	Right Elbow	22	11
9	21	Right Forearm Facing Out	20	13
10	24	Right Forearm Facing In	22	16
11	30	Left Quad	34	21
12	34	Left Knee	32	19
13	39	Left Front Calf	35	18
14	40	Left Calf Facing Out	26	12
15	41	Left Calf Facing In	28	12
16	46	Right Quad	40	23
17	50	Right Knee	34	20
18	52	Right Rear Knee	29	12
19	60	Right Lower Calf	6	2
20	56	Right Upper Calf	19	8
21	63	Right Pectorial	20	13
22	64	Left Pectorial	12	10
23	68	Center Abdomin	22	15
24	73	Right Upper Shoulder	1	1
25	78	Right Hip	14	9
26	82	Right Upper Quad	26	16
27	89	Left Upper Quad	16	12
28	90	Left Hip	9	7
29	84	Lower Abdomen	18	12
30	95	Left Upper Shoulder	8	5
31	108	Left Back	20	9
32	97	Left Shoulder Blade	16	8
33	99	Right Shoulder Blade	12	5
34	101	Left Lower Shoulder Blade	16	7
35	105	Right Lower Shoulder Blade	18	8
36	107	Center of Back	16	9
37	112	Left Upper Butt	17	7
38	117	Right Butt	30	13
39	121	Left Rear Upper Thigh	26	12
40	124	Right Upper Thigh	22	10

Table 17- Test 3T- 1.1 ft/sec- Max and Average Heat Fluxes

Sensor #	Navy #	Location	Max kW/m^2	Avg kW/m^2
1	1	Left Shoulder	12	7
2	2	Left Bicep	14	10
3	6	Left Elbow	19	8
4	8	Left Forearm Facing Out	11	7
5	9	Left Inner Forearm Facing In	14	9
6	15	Right Shoulder	10	6
7	16	Right Bicep	15	9
8	20	Right Elbow	28	13
9	21	Right Forearm Facing Out	31	13
10	24	Right Forearm Facing In	26	13
11	30	Left Quad	37	15
12	34	Left Knee	36	15
13	39	Left Front Calf	34	12
14	40	Left Calf Facing Out	25	10
15	41	Left Calf Facing In	33	12
16	46	Right Quad	48	18
17	50	Right Knee	40	16
18	52	Right Rear Knee	44	15
19	60	Right Lower Calf	11	4
20	56	Right Upper Calf	29	12
21	63	Right Pectorial	17	10
22	64	Left Pectorial	13	8
23	68	Center Abdomin	20	11
24	73	Right Upper Shoulder	2	1
25	78	Right Hip	19	8
26	82	Right Upper Quad	37	14
27	89	Left Upper Quad	17	9
28	90	Left Hip	10	6
29	84	Lower Abdomen	20	11
30	95	Left Upper Shoulder	9	5
31	108	Left Back	26	11
32	97	Left Shoulder Blade	19	10
33	99	Right Shoulder Blade	16	8
34	101	Left Lower Shoulder Blade	19	9
35	105	Right Lower Shoulder Blade	24	10
36	107	Center of Back	24	10
37	112	Left Upper Butt	21	9
38	117	Right Butt	41	15
39	121	Left Rear Upper Thigh	28	11
40	124	Right Upper Thigh	35	14

The maximum heat fluxes measured by the copper disk calorimeters are between 40 and 50 kW/m^2. This is about half of the average heat flux used for Thermo®-Man and other instrumented mannequin tests. The sensors may not be measuring the maximum heat flux accurately since they have a lag time that prevents them from being able to measure heat fluxes that change rapidly. Since the average exposure intensity is more important than a peak value, this lag time is not significant. The total energy absorbed at each sensor location is a more complete assessment of the total exposure. This value is given in figure 17. There are some anomalies in the data, but these are caused by the unpredictable nature of the buoyancy driven turbulent diffusion flames produced by the sand burners. Generally there is an increasing trend in total energy absorbed as mannequin speed decreases. For the NFPA 1971 TPP test, a minimum of 1450 kJ/m^2 must be absorbed by the material before a burn is predicted using the Stoll and Chianta criterion (NFPA 1971, 2000). Instrumented mannequin tests will report on the %Total Body Area (TBA) that is burned for a given test. Typically Thermo®-Man tests are run for between 2 and 20 seconds. Typical tests for fire fighters protective clothing are 5 seconds in duration. This gives a total of 420 kJ/m^2 absorbed. Total energy absorbed during the bare mannequin tests range from very little on the shoulders to over 1300kJ/m^2 on the legs. When the total energy absorbed criteria is considered, the two tests look somewhat similar. The current test average for the entire mannequin, however, is about 2/3 the average value for Thermo®-Man. Tests conducted at slower or faster speeds than the three bare mannequin tests will have higher or lower values respectively for total energy absorbed.

Table 18- Total Energy Absorbed by Bare Mannequin

Sensor	Location	Energy Absorbed (kW/m^2)		
		Test 1T	Test 2T	Test 3T
1	Left Shoulder	83	54	50
2	Left Bicep	137	127	100
3	Left Elbow	11	21	8
4	Left Forearm Facing Out	164	112	69
5	Left Forearm Facing In	121	134	76
6	Right Shoulder	30	45	23
7	Right Bicep	94	80	43
8	Right Elbow	63	44	29
9	Right Forearm Facing Out	651	354	346
10	Right Forearm Facing In	567	300	269
11	Left Quad	479	315	195
12	Left Knee	579	480	262
13	Left Front Calf	419	364	180
14	Left Calf Facing Out	124	182	68
15	Left Calf Facing In	363	343	208
16	Right Quad	1314	941	644
17	Right Knee	947	609	385
18	Right Rear Knee	77	55	47
19	Right Lower Calf	175	57	52
20	Right Upper Calf	224	69	72
21	Right Pectoral	440	326	222
22	Left Pectoral	96	132	59
23	Center Abdomen	136	131	82
24	Right Upper Shoulder	6	10	2
25	Right Hip	21	11	11
26	Right Upper Quad	433	194	130
27	Left Upper Quad	455	233	188
28	Left Hip	54	54	29
29	Lower Abdomen	109	87	42
30	Left Upper Shoulder	72	51	26
31	Left Back	60	37	31
32	Left Shoulder Blade	321	197	151
33	Right Shoulder Blade	108	71	70
34	Left Lower Shoulder Blade	153	98	98
35	Right Lower Shoulder Blade	227	155	126
36	Center of Back	420	209	178
37	Left Upper Butt	137	84	90
38	Right Butt	476	281	217
39	Left Rear Upper Thigh	721	447	266
40	Right Upper Thigh	418	234	185
Average		287	193	133

4.2.2. PBI Coveralls

The next round of testing involved a set of coveralls with an outer shell constructed from 60% Kevlar and 40% Polybenzimidazole (PBI). PBI is the only commercial textile fiber that is nonflammable in air under normal conditions, and produces little smoke and virtually no toxic offgases up to a temperature of 560^{o}C (Jackson, 1978). Due to the high cost of PBI, it is typically woven with Kevlar in a 60/40 blend, but for this analysis the coveralls will be referred to a simply "PBI". The coveralls used in these tests showed very little sign of visible damage in the first 3 tests, so the same outfit was used for each test. After the last test at 0.5 ft/sec there was extensive visible damage including charring of the outer shell. Between tests the mannequin was cleaned with a damp cloth and cooled with a fan until all of the sensors were below 25^{o}C. The coveralls were size 44 and fit the mannequin very loosely. The wrists and ankles had Velcro straps that were tightened to prevent hot gases from entering. The wrists fit the mannequin snugly due to protective hand covers with holes for the thumb. The Ankle holes were loose and were taped tightly shut for each test with high temperature tape. The mannequins head was protected with a Nomex® hood for each test. Seven tests were run, each one at a slower speed than the previous. Speeds ranged from 2.75 ft/s to 0.44 ft/sec. None of the tests recorded any first or second degree burns. The maximum temperatures for tests 9T and 10T are shown in table 19. The Maximum Heat Fluxes recorded are shown in table 20.

Table 19- Skin Burns and Temps- Tests 9T and 10T

Sensor	Location	Test 9T		Test 10T	
		Ω	Max Skin Temp	Ω	Max Skin Temp
1	Left Shoulder	0.00	36.7	0.00	39.1
2	Left Bicep	0.00	35.4	0.00	37.3
3	Left Elbow	0.00	35.4	0.00	36.3
4	Left Forearm Facing Out	0.00	33.5	0.00	33.7
5	Left Inner Forearm Facing In	0.00	34.3	0.00	34.8
6	Right Shoulder	0.00	38.1	0.00	42.1
7	Right Bicep	0.00	35.5	0.00	38.2
8	Right Elbow	0.00	34.8	0.00	37.4
9	Right Forearm Facing Out	0.00	35.0	0.00	37.7
10	Right Forearm Facing In	0.00	34.2	0.00	35.6
11	Left Quad	0.00	36.2	0.00	42.2
12	Left Knee	0.00	35.6	0.00	39.1
13	Left Front Calf	0.00	33.5	0.00	34.1
14	Left Calf Facing Out	0.00	34.3	0.00	35.1
15	Left Calf Facing In	0.00	34.6	0.00	36.0
16	Right Quad	0.00	38.1	0.00	44.2
17	Right Knee	0.00	34.4	0.00	37.1
18	Right Rear Knee	0.00	34.4	0.00	36.2
19	Right Lower Calf	0.00	34.6	0.00	37.1
20	Right Upper Calf	0.00	34.1	0.00	34.9
21	Right Pectoral	0.00	37.1	0.00	40.4
22	Left Pectoral	0.00	38.8	0.00	43.1
23	Center Abdomen	0.00	33.2	0.00	34.2
24	Right Upper Shoulder	0.00	32.9	0.00	33.1
25	Right Hip	0.00	33.4	0.00	34.0
26	Right Upper Quad	0.00	39.0	0.00	44.8
27	Left Upper Quad	0.00	34.7	0.00	35.2
28	Left Hip	0.00	33.6	0.00	34.1
29	Lower Abdomen	0.00	33.3	0.00	33.5
30	Left Upper Shoulder	0.00	36.2	0.00	39.0
31	Left Back	0.00	34.4	0.00	36.3
32	Left Shoulder Blade	0.00	38.3	0.00	40.9
33	Right Shoulder Blade	0.00	36.5	0.00	39.5
34	Left Lower Shoulder Blade	0.00	36.1	0.00	37.7
35	Right Lower Shoulder Blade	0.00	35.4	0.00	38.0
36	Center of Back	0.00	33.9	0.00	35.1
37	Left Upper Butt	0.00	33.6	0.00	34.2
38	Right Butt	0.00	35.5	0.00	40.4
39	Left Rear Upper Thigh	0.00	34.0	0.00	34.6
40	Right Upper Thigh	0.00	34.3	0.00	36.5

Table 20- Maximum Heat Fluxes Recorded- Test 9T and 10T

Sensor	Location	9T	10T
1	Left Shoulder	1.9	2.6
2	Left Bicep	1.3	1.7
3	Left Elbow	1.4	1.7
4	Left Forearm Facing Out	0.8	0.9
5	Left Inner Forearm Facing In	1.1	1.2
6	Right Shoulder	2.4	3.7
7	Right Bicep	1.5	2.5
8	Right Elbow	1.1	2.0
9	Right Forearm Facing Out	1.2	2.1
10	Right Forearm Facing In	0.8	1.4
11	Left Quad	1.6	4.3
12	Left Knee	1.4	2.5
13	Left Front Calf	0.9	0.9
14	Left Calf Facing Out	0.9	1.1
15	Left Calf Facing In	1.1	1.6
16	Right Quad	2.6	4.8
17	Right Knee	0.9	1.8
18	Right Rear Knee	1.1	1.6
19	Right Lower Calf	1.0	1.9
20	Right Upper Calf	1.0	1.2
21	Right Pectoral	1.9	3.0
22	Left Pectoral	2.6	4.3
23	Center Abdomen	0.9	1.0
24	Right Upper Shoulder	0.8	0.7
25	Right Hip	0.7	0.8
26	Right Upper Quad	2.8	5.1
27	Left Upper Quad	1.1	1.2
28	Left Hip	0.8	1.0
29	Lower Abdomen	0.7	0.7
30	Left Upper Shoulder	1.6	2.4
31	Left Back	1.0	1.7
32	Left Shoulder Blade	2.5	3.1
33	Right Shoulder Blade	1.8	2.7
34	Left Lower Shoulder Blade	1.7	2.1
35	Right Lower Shoulder Blade	1.3	2.4
36	Center of Back	0.7	1.1
37	Left Upper Butt	0.7	0.8
38	Right Butt	1.1	3.1
39	Left Rear Upper Thigh	0.9	1.3
40	Right Upper Thigh	1.0	1.6

The average skin temperature rise for the two tests shown is 2.7^{o}C for test 9T, and 4.8 ^{o}C for test 10T. The test is not sufficiently intense, in terms of heat flux or duration to

cause skin burns through the PBI coveralls with the moisture barrier and thermal liner in place.

4.2.3. FR Cotton Coveralls

Five tests were conducted with fire retardant cotton coveralls on the mannequin. The tests were conducted with the fire size at 1.5 MW, and with mannequin speeds between 2.75 to 0.55 ft/sec. The FR Cotton coveralls showed no visible signs of damage at 2.75 ft/sec. A different pair of coveralls was used for each test, and the damage was compared side by side following the test. The material charred slightly at the ankle cuffs at 2.2 ft/sec, and charred more as the speed was decreased. The material released a pungent odor after charring. At 0.55 ft/sec the FR Cotton coveralls ignited and burned vigorously until the mannequin was completely out of the room. At that time the flames self extinguished. This test was the only exposure that recorded skin burns. The results from tests 14T and 15T (1.1, and 0.55 ft/sec) are shown in tables 21 and 22. The skin burn damage and the maximum skin temperatures reached are both shown. The significant figures in the burn damage for test 14T do not indicate the level of accuracy that is believed to be associated with the calculations but rather to illustrate which areas are predicted to have a very minimal amount of burn damage. If only two significant figures were used, all of the sensors would report zero. For locations where the burn damage is predicted to be very large, the only significance of the number is that it is greater than 1. The burn damage integral has no meaning after a value of 1 is reached.

Table 21- Test 14T- Skin Burn Damage and Maximum Skin Temperatures

Sensor	Location	Ω	Ist Deg Burn	2nd Deg Burn	Max Skin Temp
1	Left Shoulder	0.0000	-	-	36.9
2	Left Bicep	0.0000	-	-	38.8
3	Left Elbow	0.0000	-	-	37.0
4	Left Forearm Facing Out	0.0000	-	-	37.0
5	Left Inner Forearm Facing In	0.0000	-	-	36.6
6	Right Shoulder	0.0003	-	-	46.5
7	Right Bicep	0.0000	-	-	38.5
8	Right Elbow	0.0000	-	-	37.6
9	Right Forearm Facing Out	0.0000	-	-	40.3
10	Right Forearm Facing In	0.0000	-	-	35.8
11	Left Quad	0.0000	-	-	43.5
12	Left Knee	0.0000	-	-	42.8
13	Left Front Calf	0.0000	-	-	36.4
14	Left Calf Facing Out	0.0000	-	-	37.8
15	Left Calf Facing In	0.0000	-	-	39.0
16	Right Quad	0.0000	-	-	41.7
17	Right Knee	0.0000	-	-	39.4
18	Right Rear Knee	0.0000	-	-	40.8
19	Right Lower Calf	0.0000	-	-	39.1
20	Right Upper Calf	0.0000	-	-	38.4
21	Right Pectoral	0.0000	-	-	37.1
22	Left Pectoral	0.0000	-	-	37.3
23	Center Abdomen	0.0000	-	-	36.2
24	Right Upper Shoulder	0.0000	-	-	32.9
25	Right Hip	0.0000	-	-	36.0
26	Right Upper Quad	0.0032	-	-	50.2
27	Left Upper Quad	0.0000	-	-	38.5
28	Left Hip	0.0000	-	-	38.4
29	Lower Abdomen	0.0000	-	-	37.1
30	Left Upper Shoulder	0.0000	-	-	37.6
31	Left Back	0.0000	-	-	38.3
32	Left Shoulder Blade	0.0003	-	-	46.4
33	Right Shoulder Blade	0.0000	-	-	43.8
34	Left Lower Shoulder Blade	0.0000	-	-	42.0
35	Right Lower Shoulder Blade	0.0000	-	-	40.3
36	Center of Back	0.0000	-	-	37.5
37	Left Upper Butt	0.0007	-	-	48.0
38	Right Butt	0.0005	-	-	46.8
39	Left Rear Upper Thigh	0.0000	-	-	38.0
40	Right Upper Thigh	0.0000	-	-	40.0
		% TBA	0	0	

Table 22- Test 15T- Skin Burn Damage and Maximum Skin Temperatures

Sensor	Location	Ω	Ist Deg Burn	2nd Deg Burn	Max Skin Temp
1	Left Shoulder	0.00	-	-	49.9
2	Left Bicep	0.00	-	-	50.1
3	Left Elbow	0.02	-	-	52.3
4	Left Forearm Facing Out	0.00	-	-	44.3
5	Left Inner Forearm Facing In	0.01	-	-	48.0
6	Right Shoulder	0.89	BURN	-	59.2
7	Right Bicep	2.07E+06	BURN	BURN	86.0
8	Right Elbow	1.26E+09	BURN	BURN	99.2
9	Right Forearm Facing Out	1.55E+12	BURN	BURN	113.4
10	Right Forearm Facing In	3.05E+09	BURN	BURN	101.9
11	Left Quad	3.42E+11	BURN	BURN	110.8
12	Left Knee	1.89E+08	BURN	BURN	94.8
13	Left Front Calf	4.79	BURN	BURN	62.7
14	Left Calf Facing Out	2898.48	BURN	BURN	73.4
15	Left Calf Facing In	637.49	BURN	BURN	72.3
16	Right Quad	1.59E+09	BURN	BURN	98.9
17	Right Knee	3.62E+06	BURN	BURN	87.4
18	Right Rear Knee	7.93E+09	BURN	BURN	101.2
19	Right Lower Calf	8.70E+03	BURN	BURN	73.1
20	Right Upper Calf	5.29E+09	BURN	BURN	87.9
21	Right Pectoral	0.00	-	-	42.6
22	Left Pectoral	0.04	-	-	54.0
23	Center Abdomen	1.27	BURN	BURN	58.7
24	Right Upper Shoulder	0.00	-	-	35.8
25	Right Hip	21.64	BURN	BURN	67.6
26	Right Upper Quad	3.99E+13	BURN	BURN	121.7
27	Left Upper Quad	9.88E+06	BURN	BURN	89.3
28	Left Hip	0.00	-	-	40.5
29	Lower Abdomen	120.47	BURN	BURN	67.1
30	Left Upper Shoulder	406.96	BURN	BURN	72.2
31	Left Back	8.76E+04	BURN	BURN	79.6
32	Left Shoulder Blade	1014.50	BURN	BURN	71.4
33	Right Shoulder Blade	2.72E+05	BURN	BURN	82.5
34	Left Lower Shoulder Blade	5.42E+07	BURN	BURN	92.9
35	Right Lower Shoulder Blade	5.90E+08	BURN	BURN	99.3
36	Center of Back	2.35E+09	BURN	BURN	99.8
37	Left Upper Butt	15.34	BURN	BURN	63.9
38	Right Butt	4.65E+11	BURN	BURN	109.0
39	Left Rear Upper Thigh	1.53E+06	BURN	BURN	84.6
40	Right Upper Thigh	3.10E+11	BURN	BURN	90.0
		% TBA	77.5	75	

Table 23- Tests 14T and 15T- Maximum Measured Heat Flux

Sensor	Location	Heat Flux (kW/m^2)	
		Test 14T	Test 15T
1	Left Shoulder	3	9
2	Left Bicep	3	8
3	Left Elbow	3	10
4	Left Forearm Facing Out	3	5
5	Left Inner Forearm Facing In	3	11
6	Right Shoulder	10	15
7	Right Bicep	4	42
8	Right Elbow	3	61
9	Right Forearm Facing Out	5	71
10	Right Forearm Facing In	2	61
11	Left Quad	8	73
12	Left Knee	7	51
13	Left Front Calf	2	21
14	Left Calf Facing Out	3	29
15	Left Calf Facing In	4	32
16	Right Quad	6	63
17	Right Knee	5	54
18	Right Rear Knee	5	52
19	Right Lower Calf	4	21
20	Right Upper Calf	4	51
21	Right Pectoral	3	9
22	Left Pectoral	3	18
23	Center Abdomen	3	19
24	Right Upper Shoulder	1	2
25	Right Hip	2	30
26	Right Upper Quad	14	92
27	Left Upper Quad	4	55
28	Left Hip	4	4
29	Lower Abdomen	3	19
30	Left Upper Shoulder	3	29
31	Left Back	3	39
32	Left Shoulder Blade	10	24
33	Right Shoulder Blade	7	43
34	Left Lower Shoulder Blade	6	58
35	Right Lower Shoulder Blade	5	64
36	Center of Back	3	62
37	Left Upper Butt	10	20
38	Right Butt	11	65
39	Left Rear Upper Thigh	4	37
40	Right Upper Thigh	5	39

The ignition of the FR Cotton coveralls provided direct flame contact to the mannequin which resulted in very high heat fluxes and severe burns as a result. In some

cases the heat fluxes recorded are an order of magnitude larger than the test where ignition was not achieved. For test 15T a total of 77.5% of the body received 1st degree burns, and 75% received 2nd degree burns. Skin temperature calculations are shown in figures 49 and 50, and sample burn calculations are shown in figures 51 and 52.

Figure 49- Sensor #6 Right Shoulder- Test 15T- Predicted Skin Response

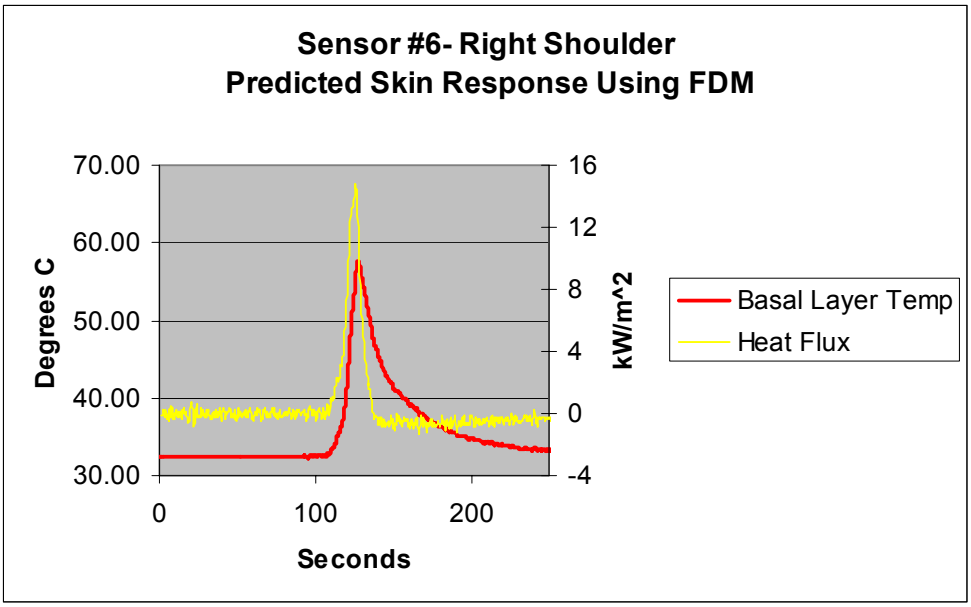

Figure 50- Sensor #23 Center Abdomen-Test 15T- Predicted Skin Response

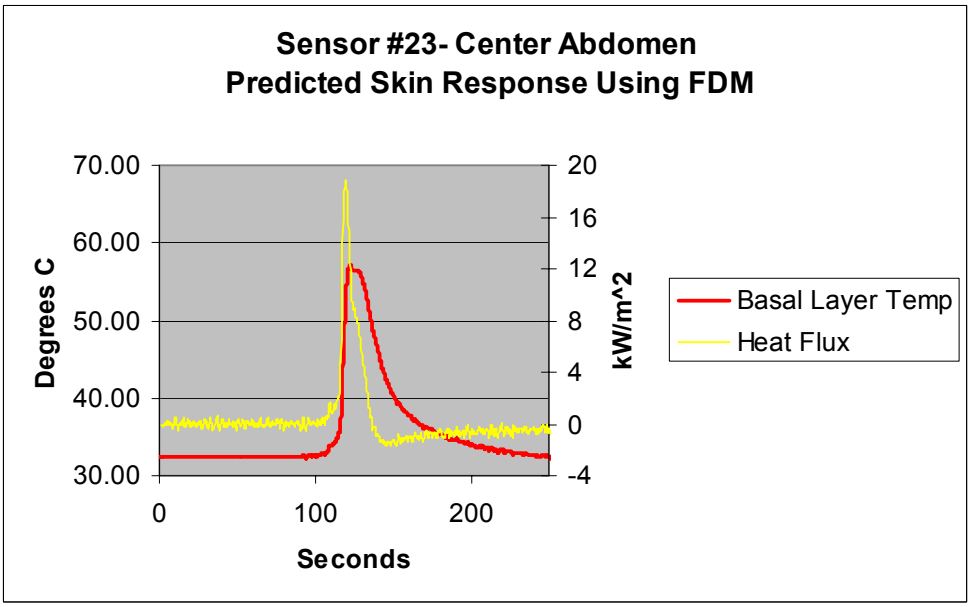

Figure 51- Sensor #6 Right Shoulder- Test 15T- Burn Damage

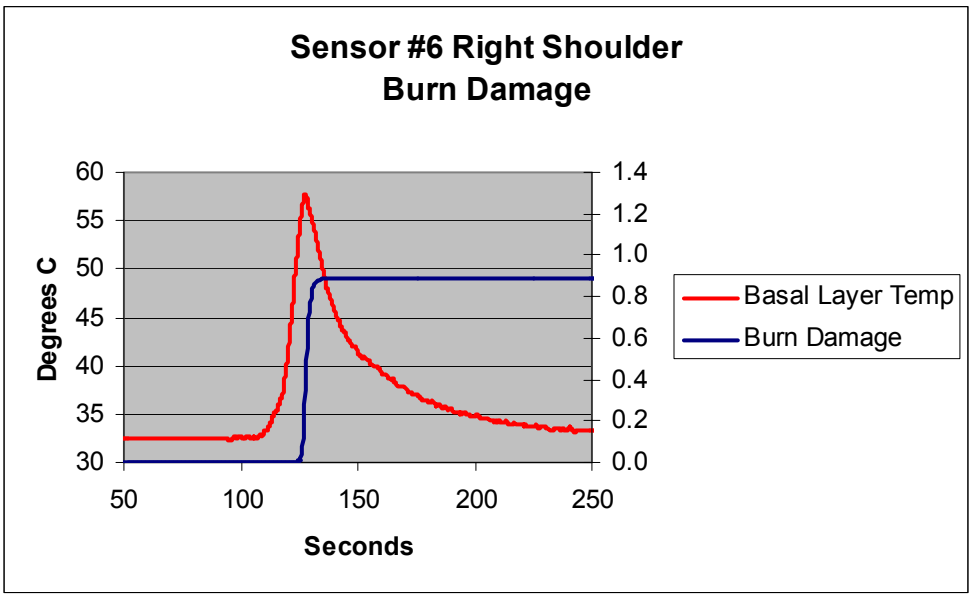

Figure 52- Sensor #23 Center Abdomen- Test 15T- Burn Damage

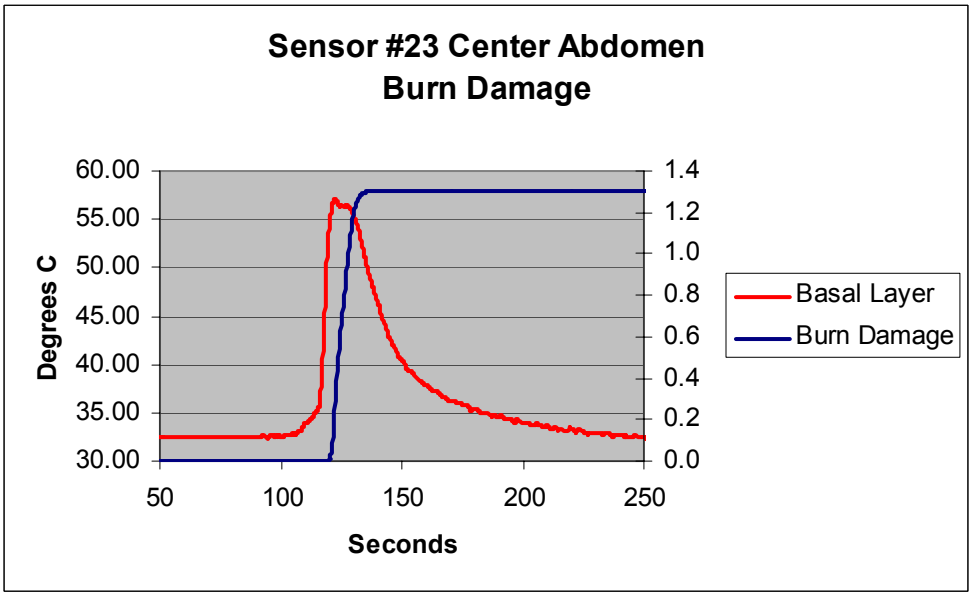

Sensor 6 predicts a first degree burn (Ω>0.53), and sensor 23 predicts a second degree burn (Ω>1.0).

These results show that the test apparatus is now capable of testing protective clothing and providing data for comparative rating purposes. The sensors give output that can be used in several ways to rate the level of protection provided by protective clothing.

Clothing can be compared by the heat flux transferred through to the sensors, or by the maximum temperature predicted by the finite difference model of skin, and also by the prediction of first and second degree burns. This provides the Navy with a tool to comparatively rate the protection that a particular set of clothing will provide for a set of scenarios that accurately replicate fires that are likely to occur on a Navy ship.

5. Sensitivity Analysis

Since both the heat flux calculations and skin burn predictions have a level of uncertainty associated with them, it is necessary to quantify this uncertainty. Heat fluxes will have an uncertainty based on uncertainties in the physical and thermal properties of the sensor itself. Skin burn predictions will then have an uncertainty as a result of the uncertainty in the heat flux into the skin.

5.1. Sensors

Many uncertainties are involved in the calculation of the heat flux reaching the sensors. This section will address the uncertainty of the incident heat flux calculation for the conditions under which the cone testing was performed. The ambient conditions and sensor properties for the test are taken from the end of the exposure at 10 kW/m^2. The conditions and associated uncertainties are assumed to be:

$\rho = 8910\ kg/m^3 \pm 100\ kg/m^3$

$c_p = 0.385\ kJ/kg^oC \pm 0.019\ kJ/kg^oC$

$l = 0.0016\ m \pm 0.000016\ m$

$\frac{dT}{dt} = 1.5\ \text{deg C/sec} \pm 0.07\ \text{deg C/sec}$

$h = 0.025\ kW/m^2C \pm 10\ W/m^2C$

$T = 343\ K \pm 3\ K$

$T_\infty = 288\ K \pm 3\ K$

$\varepsilon = 0.96 \pm 0.03$

The density and specific heat are assumed to be accurate values, although the specific heat is treated as a constant value in this analysis when it is actually temperature dependant. For this reason the uncertainties of specific heat and density for copper 110 are assumed to be 100 kg/m^3 (~1%) and 0.019 kJ/kg^{o}C (5%) respectively. The copper disk thickness is assumed to be accurate to within 0.016 mm. To determine the uncertainty of the rate of temperature change, experimental data was analyzed. For a 60 second sample of temperature recordings with no fire exposure, the "noise" in the data acquisition system produced a standard deviation of 0.07 deg C/sec in the dT/dt calculations. For the heat transfer coefficient, h, the value of 0.025 kW/m^{2}C is the maximum value for free convection for cooling of skin (SFPE Guide, 2000). When the disk is at lower temperatures this value will be lower, so an uncertainty of 0.010 kW/m^{2}C is assumed. Temperatures are measured with thermocouples that have an uncertainty of ± 3 deg C. The emissivity of the high temperature paint used for the sensors is listed in product literature as 0.96, although there could be some uncertainties caused by not properly cleaning the surface or small areas of paint chipping off. The uncertainty of emissivity is assumed to be 0.03. The uncertainty of the calculated heat flux can be expressed as a function of the uncertainties associated with the individual parameters (Taylor, 1997). Assuming all of the uncertainties are independent and random the probable uncertainty of the heat flux calculated can be expressed as:

$$\delta \dot{q}'' = \sqrt{\left(\frac{d\dot{q}''}{dx}\delta x\right)^2 + \ldots + \left(\frac{d\dot{q}''}{dz}\delta z\right)^2} \qquad \text{(Eq. 29)}$$

But the total uncertainty can never be larger than:

$$\delta\dot{q}'' \le \left|\frac{d\dot{q}''}{dx}\right|\delta x + \ldots + \left|\frac{d\dot{q}''}{dz}\right|\delta z \qquad \text{(Eq. 30)}$$

The individual uncertainties for the copper disk heat flux calculations are:

$$\frac{d\dot{q}''}{d\rho}\delta\rho = c_p l\frac{dT}{dt}\delta\rho = 0.092\ \frac{kW}{m^2} \qquad \text{(Eq. 31)}$$

$$\frac{d\dot{q}''}{dc_p}\delta c_p = \rho l\frac{dT}{dt}\delta c_p = 0.406\ \frac{kW}{m^2} \qquad \text{(Eq. 32)}$$

$$\frac{d\dot{q}''}{dl}\delta l = \rho c_p\frac{dT}{dt}\delta l = 0.082\ \frac{kW}{m^2} \qquad \text{(Eq. 33)}$$

$$\frac{d\dot{q}''}{d\dfrac{dT}{dt}}\delta\frac{dT}{dt} = \rho c_p l\delta\frac{dT}{dt} = 0.384\ \frac{kW}{m^2} \qquad \text{(Eq. 34)}$$

$$\frac{d\dot{q}''}{dh}\delta h = \Delta T\delta h = 0.55\ \frac{kW}{m^2} \qquad \text{(Eq. 35)}$$

$$\frac{d\dot{q}''}{dT}\delta T = -h\delta T = 0.075\ \frac{kW}{m^2} \qquad \text{(Eq. 36)}$$

$$\frac{d\dot{q}''}{dT_\infty} = h = 0.075\ \frac{kW}{m^2} \qquad \text{(Eq. 37)}$$

$$\frac{d\dot{q}''}{d\varepsilon}\delta\varepsilon = \sigma\left(T^4 - T_\infty^4\right)\delta\varepsilon = 0.012\ \frac{kW}{m^2} \qquad \text{(Eq. 38)}$$

The largest uncertainties in heat flux are traceable to the values of specific heat, rate of temperature change, and the heat transfer coefficient. For our calculations with clothing on the mannequin the convective cooling is not calculated. When clothing covers the sensor, conduction and radiation dominate the heat transfer process. This uncertainty is not a great concern. In order to decrease the uncertainty, a temperature

dependant specific heat could be used, and better data acquisition hardware could be used. For the current analysis however the uncertainties predicted by this method are acceptable. The total uncertainty assuming all uncertainties are independent and random is:

$$\delta\dot{q}'' = \sqrt{\left(\frac{d\dot{q}''}{dx}\delta x\right)^2 + \ldots + \left(\frac{d\dot{q}''}{dz}\delta z\right)^2} = 0.8 \text{ kW/m}^2$$

And is never greater than:

$$\delta\dot{q}'' \le \left|\frac{d\dot{q}''}{dx}\right|\delta x + \ldots + \left|\frac{d\dot{q}''}{dz}\right|\delta z = 1.68 \text{ kW/m}^2$$

5.2. Sensitivity Analysis of Burn Predictions

The uncertainty involved in the burn predictions can be calculated as:

$$\frac{d\left(\frac{d\Omega}{dt}\right)}{dT}\delta T = \left(P\exp\left(\frac{-\Delta E}{RT}\right)\right)\left(\frac{-\Delta E}{RT^2}\right) \qquad \text{(Eq. 39)}$$

This is the uncertainty in the rate at which the burn is progressing. In order to calculate the total uncertainty in the value of Ω the uncertainty at each time step must be summed numerically. Since dΩ/dt is an exponential function, a small uncertainty in temperature can have a large effect on the uncertainty in Ω. The band of uncertainty for a set of burn calculations is shown in figures 53 and 54. Figure 53 shows the temperatures calculated when the incident heat flux from figure 49 is adjusted ± 10%.

Figure 53- Uncertainty in Temperature calculations- Sensor #6- Test 15T

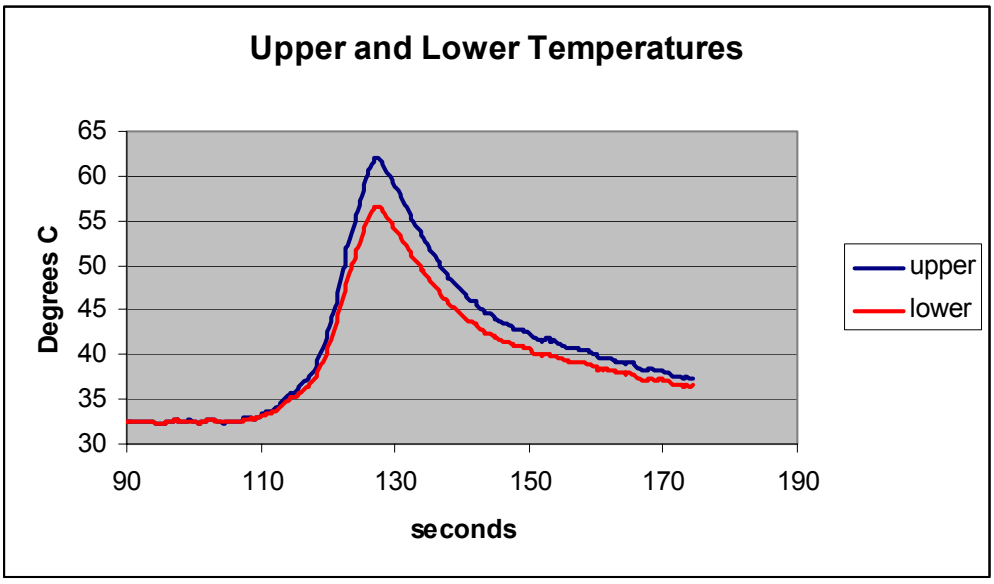

Figure 54- Uncertainty in Burn Calculation- Sensor #6- Test 15T

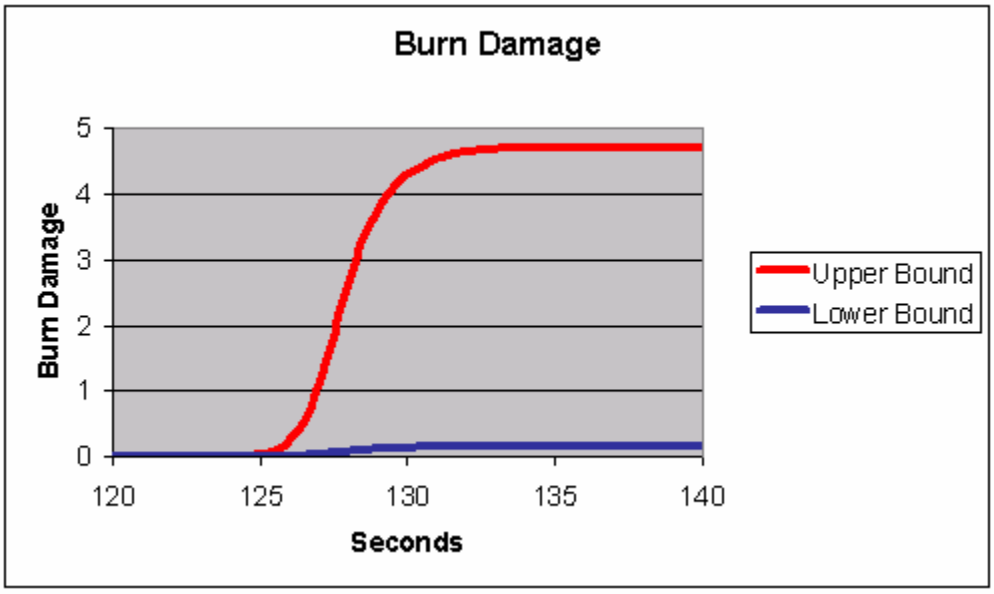

A relatively small uncertainty in the heat flux input (±10%) is shown here to have a very large effect on the uncertainty in the burn calculations. As this example shows, the uncertainty can be over 500%. The burn damage calculated for sensor #6 in test 15T is

0.88, but is actually somewhere in between 0.16 and 4.87. For this reason the values of Ω must be used with great caution for there is a large uncertainty involved.

6.0 Conclusions

The new test apparatus offers the ability to test varying types of protective clothing and can produce exposures that are much different than existing mannequin tests. While clothing not intended for primary firefighting use, such as the FR Cotton coveralls, may not pass an instrumented mannequin test that uses an 84 kW/m^2 exposure, it has been shown here to provide good protection for less intense exposures. The new test apparatus can also provide fully radiant exposures. To the best of this author's knowledge this is not a feature that is available anywhere else. The test apparatus can also simulate brief exposures to fires of varying sizes. This provides a more realistic test for clothing such as the FR Cotton coveralls. The likelihood of an exposure to a flash fire, such as the Thermo®-Man exposure, is less than the likelihood of an exposure predicted by LeBlanc. Clothing that is not intended for severe fire exposures is more likely to be exposed to a radiant heat flux from a nearby fire or a brief exposure to direct flame. Also the idea of designing everyday work clothing for Navy personnel that can withstand a Thermo®-Man exposure is not economical or even practical. This test apparatus offers the ability to expose this type of clothing to a fire scenario that it should be able to provide protection from.

The sensors have been shown to be accurate enough for the purposes of measuring heat flux for the exposures tested. Fear of damaging the mannequin outweighs fear of damaging the sensors. The thermocouple connectors allow for easy replacement of malfunctioning sensors. An additional 10 sensors were constructed for the purpose of having spare sensors available. If more funding were available, it would be beneficial to

add more sensor locations to the mannequin to get a more complete assessment of the burn damage, or lack thereof. The mannequin has 124 sockets for sensors, which is far beyond the current data acquisition capacity. If the test is eventually developed to become a standardized Navy test protocol, then it is recommended that commercially available sensors should be used. For experimental purposes such as this research, the current sensors are accurate enough.

Future testing should focus on longer radiant exposures outside of the room and possibly with larger heat release rates. Tests should be conducted with clothing that fits the mannequin more snugly to investigate the effect of air gaps. Clothing used for these tests were very loose on the mannequin and large air gaps were present.

References

1. ASTM D 4108-87, "Standard Test Method for Thermal Protective Performance of Materials for Clothing by Open Flame Method", American Society for Testing and Materials, Philadelphia, PA, 1987.

2. ASTM E 457-96, "Standard Test Method for Measuring Heat Transfer Rate Using a Thermal Capacitance (Slug) Calorimeter", American Society for Testing and Materials, Philadelphia, PA, 1996.

3. ASTM E 459-97, "Standard Test Method for Measuring Heat Transfer Rate Using a This Skin Calorimeter", American Society for Testing and Materials, Philadelphia, PA, 1997.

4. ASTM E1354, Test Method for Heat and Visible Smoke Release Rates for Materials and Products Using an Oxygen Consumption Calorimeter, American Society for Testing and Materials, Philadelphia, PA, 1999.

5. ASTM F 1930-00, "Standard Test Method for Evaluation of Flame Resistant Clothing for Protection Against Flash Fire Simulations Using an Instrumented Manikin", American Society for Testing and Materials, Philadelphia, PA, 2000.

6. Baker, D., "A Dynamic Method for Determining the Thermal Conductivity of Charring Materials", 8th Conference on Thermal Conductivity, Purdue University, 1969.

7. Barker, Roger L., "Modeling of Thermal Protection Outfits for Fire", National Textile Center Annual Report, 2002.

8. Barker, Roger L., Hamouda, Hechmi, Shalev, Itzhak, and Johnson, Jason, "Review and Evaluation of Thermal Sensors for Use in Testing Firefighters Protective Clothing", NIST GCR 99-772, March, 1999.

9. Behnke, W. P., "Predicting Flash Fire Protection of Clothing from Laboratory Tests Using Second-degree Burn to Rate Performance", Fire and Materials, Vol. 8, No. 2, pgs 57-63, 1984.

10. Behnke, W. P., Geshury, A. J., and Barker, R. L., "Thermo-Man® and Thermo-Leg: Large Scale Test Methods for Evaluating Thermal Protective Performance", Performance of Protective Clothing: Fourth Volume, ASTM STP 1133, American Society for Testing and Materials, West Conshohocken, PA, pgs 266-280, 1992.

11. Blake, G. K., Diller, K., and Hayes, L. C., "Analysis of Alternate Methods for Simulating Thermal Burns", Journal of Burn Care and Rehabilitation, Vol. 12, pgs 177-189, 1991.

12. Blevins, Linda G. and Pitts, William M., "Modeling of Bare and Aspirated Thermocouples in Compartment Fires", Fire Safety Journal 33, pgs 239-259, 1999.

13. Brown, J. R. and Ennis, B. C., "Thermal Analysis of Nomex and Kevlar Fibers", Textile Research Journal, Vol. 47, pgs 62-66, 1977.

14. Carnazza, Brian, Forrester, Anthony, and Shook, Jason, The Development of an Accurate and Reproducible Full Scale Clothing Flammability Test, Senior Project (MQP), Worcester Polytechnic Institute, 2003.

15. Dale, J. D., Crown, E. M., Ackerman, M. Y., Leung, E., and Rigakis, K. B., "Instrumented Mannequin Evaluation of Thermal Protective Clothing", Performance of Protective Clothing: Fourth Volume, ASTM STP 1133, American Society for Testing and Materials, West Conshohocken, PA, pgs 717-733, 1992.

16. Diller, T. E., "Methods of Determining Heat Flux from Temperature Measurements", Proceedings of the 42nd International Instrumentation Symposium, Aerospace Industries Division and Test Measurement Division of ISA, 1996.

17. Drysdale, Dougal, "An Introduction to Fire Dynamics", 2nd Edition, John Wiley and Sons, Chichester, UK, 1998.

18. Fay, Terry S., "Development of an Improved Fabric Flammability Test", M.S. Thesis, Worcester Polytechnic Institute, 2002.

19. FEMA, Firefighter Fatalities in the United States in 2001, US Fire Administration, August 2002.

20. Gagnon, Brian D., "Evaluation of New Test Methods for Fire Fighting Clothing", M.S. Thesis, Worcester Polytechnic Institute, 2000.

21. Gardon, Robert, "An Instrument for the Measurement of Intense Thermal Radiation", The Review of Scientific Instruments, Vol. 24, No. 5, May 1953.

22. Henriques, F. C., "Studies of Thermal Injury V. The Predictability and the Significance of Thermally Induced Rate Processes Leading to Irreversible Epidermal Injury", Archives of Pathology, Vol 43, pgs 489-502, 1947.

23. Henry, Norman W., "How Protective is Protective Clothing?", Performance of Protective Clothing", ASTM STP 900, American Society of Testing and Materials, Philadelphia, 1986, pgs 51-58.

24. Hoschke, B. N., "Standards and Specifications for Firefighters' Clothing", Fire Safety Journal, Vol. 4, pgs 125-137, 1981.

25. Hoschke, B. N., Holcombe, B. V., and Plante, A. M., "A Critical Appraisal of Test Methods for Thermal Protective Clothing Fabrics", Performance of Protective Clothing, ASTM STP 900, American Society for Testing and Materials, Philadelphia, PA, pgs 311-326, 1986.

26. Jackson, R., "PBI Fiber and Fabric- Properties and Performance", Textile Research Journal, Vol 48, pgs 314-319, 1978.

27. Lawson, J. Randall, "Fire Fighter's Protective Clothing and Thermal Environments of Structural Fire Fighting", National Institute of Standards and Technology, NISTIR 5804, August, 1996.

28. Lawson, J. Randall and Mell, William E., "A Heat Transfer Model for Firefighters Protective Clothing", National Institute of Standards and Technology, NISTIR 6299, January, 1999.

29. Lawson, J. Randall and Pinder, Terhia A., "Estimates of Thermal Conductivity for Materials Used in Firefighters Clothing", National Institute of Standards and Technology, NISTIR 6512, May, 2000.

30. Lawson, J. Randall and Twilley, William H., "Development of a Dynamic Compression Test for Measuring Thermal Performance of Fire Fighters' Protective Clothing", National Institute of Standards and Technology, NISTIR 502, April 2000.

31. Lawson, J. Randall and Twilley, William H., "Development of an Apparatus for Measuring the Thermal Performance of Firefighters Protective Clothing", National Institute of Standards and Technology, NISTIR 6400, October, 1999.

32. Luo, Mingchun, "Effects of Radiation on Temperature Measurement in a Fire Environment", Journal of Fire Sciences, Vol 15, pgs, 443-459, November/December, 1997

33. Lynch, James A., "Thermal Properties Evaluation for Protective Clothing Fabrics", WPI Center for Firesafety Studies report submitted to US Army Soldier and Biological Chemical Command, May, 2001.

34. Mehta, Arun K. and Wong, Franklin, "Measurement of Flammability and Burn Potential of Fabrics", MIT Fuels Research Laboratory, Cambridge MA, 1973.

35. NFPA 1971- Protective Ensemble for Structural Fire Fighting, 2000 Edition, National Fire Protection Association, Quincy, MA.

36. NFPA 1977- Protective Clothing and Equipment for Wildland Firefighting, 1998 Edition, National Fire Protection Association, Quincy, MA.

37. Norton, M. J. T., Kandolph, S. J., Johnson, R. F., and Jordan, K. A., "Design Construction and Use of Minnesota Woman, A Thermally Instrumented Mannequin", Textile Research Journal, Vol. 55, pgs 5-12, 1985

38. Shalev, I. and Barker, R. L., "Predicting the Thermal Protective Performance of Heat Protective Fabrics from Basic Properties", Performance of Protective Clothing: First Volume ASTM STP 900, American Society for Testing and Materials, West Conshohocken PA, pgs 358-375, 1984.

39. Stoll, Alice., "The Thermal Protection Capacity of Aviators Textiles", Aerospace Medicine, Vol. 33, pgs 846-850, 1962.

40. Stoll, Alice. M. and Chianta, M. A., "Heat Transfer Through Fabrics as Related to Thermal Injury", Transactions of the New York Academy of Sciences, Vol. 33, pgs 649-669, 1971.

41. Stoll, Alice. M. and Chianta, M. A., "Method and Rating System for Evaluation of Thermal Protection", Aerospace Medicine, November, 1969.

42. Stoll, Alice. M., and Greene, Leon C., "Relationship Between Pain and Tissue Damage due to Thermal Radiation", Journal of Applied Physiology, Vol. 14, No. 3, pgs 373-382, 1959.

43. Stoll, A. M. and Weaver, J. A., "Mathematical Model of Skin Exposed to Thermal Radiation", Aerospace Medicine, Vol. 40, pgs 24-30, 1969.

44. Stroup, David W., Twilly, William H., and Vettori, Robert, "Measurement Techniques for Low Heat Flux Exposures to Firefighters Protective Clothing", National Institute of Standards and Technology, NISTIR 6750, October, 1999.

45. Takata, Arthur, "Development of Criterion for Skin Burns", Aerospace Medicine, Vol. 45, No. 6, pgs 634-637. June, 1974.

46. Taylor, Barry N. and Kuyatt, Chris E., "Guidelines for Evaluating and Expressing the Uncertainty of NIST Measurement Results", National Institute of Standards and Technology, NIST Technical Note 1297, 1994.

47. Taylor, John R., "An Introduction to Error Analysis: The Study of Uncertainties in Physical Measurements, Second Ed" 1997 University Science Books, Sausalito, CA ISBN: 0-935702-75-X

48. Torvi, David A., "Heat Transfer in Thin Fibrous Materials Under High Heat Flux Conditions", PhD Thesis, University of Alberta, Edmonton, Alberta, 1997.

49. Torvi, David A. and Hadjisophocleous, “Research Needs in Protective Clothing for Fire Fighters”, National Research Council Canada, 1997.

50. Trent, L. C., Resch III, W. A., Coppari, L. A., and Finley, D. L., “Design and construction of a Thermally Instrumented Mannequin for Measuring the Burn Injury Potential of Wearing Apparel”, Textile Research Journal, pgs 639-647, November, 1979.

51. Quintiere, James, “Radiative Characteristics of Firefighters Coat Fabrics” Fire Technology, Vol. 10, No. 2, pgs 153-161, May 1974.

52. Woodward, Andrew B., “Fire Scenarios for an Improved Fabric Flammability Test”, M.S. Thesis, Worcester Polytechnic Institute, 2003.